ABSTRACT

ADDINGTON, JR., DAVID ALLEN. Experimental Investigation of Temperature Effects on Radiation Portal Monitor Performance. (Under the direction of Dr. Man-Sung Yim.)

Radiation portal monitor (RPM) systems are currently deployed in many countries around the world. Because deployed RPMs are placed in natural environments along borders and other remote locations, they are exposed to and must tolerate a wide range of ambient temperatures. Therefore, understanding the temperature dependent behavior in RPM type detectors is increasingly important. The research presented in this thesis seeks to augment the current understanding of temperature effects on the performances of RPMs, to determine the causes of temperature dependent RPM behavior, and to present solutions to degradations in RPMs' performances due to these temperature dependencies.

In order to better understand the temperature dependence of RPM systems' performance, a series of experimental investigations was performed on the systems. For this research work, climate chambers at Oak Ridge National Laboratory (ORNL) were used to control the ambient temperature of two separate RPM systems. The experiments performed include efficiency measurements, spectrum analysis, and the monitoring of the average background count rate during temperature cycles typical of American National Standards Institute (ANSI) testing.

The experimental results of this study identify several temperature dependencies in the tested RPMs' performances. Specifically, this study demonstrates that the average background count rates reported by the RPMs depend significantly on environmental temperature. The background gamma count rates increase significantly at high temperatures,

decreasing the RPMs' detection capability. This research also pinpoints the root cause of this count rate increase to be a mechanism consistent with thermionic emission in the photomultiplier tube (PMT).

In addition, the results of this research indentify changes in the gain of the gamma detectors over temperatures ranging from -30°C to 60°C and confirm studies in existing literature which stated that the gain of detectors similar to those found in RPM systems is affected by the temperature dependence of the scintillators and the PMTs used by these detectors. Furthermore, the results demonstrate that the temperature dependence of the gain decreases the RPMs' low-energy gamma detection efficiency—particularly the ^{57}Co efficiency—at high temperatures.

A model specific to the detectors tested in this research is included in this work and quantifies the change in gain as a function of temperature. While this model is not applicable to deployed RPM systems in general, it provides justification for future tests that explore the gain change in a larger sample of gamma detectors in order to generalize the model to similar RPM detectors. By modeling the gain as a function of temperature, advanced solutions which compensate for the gain change can be developed to ensure that the RPMs maintain the same sensitivity over the entire range of temperatures.

 By demonstrating that high temperature climates result in potential RPM performance vulnerabilities, this research identifies the need for solutions which limit the effect that high temperature has on RPM performance. This research work was unable to remedy the temperature dependence of the RPM detectors; however, it suggests solutions which minimize the maximum temperature of the detectors by providing shade to the RPM

system or by utilizing active cooling in the systems. These tests also justify future work exploring the potential for advanced solutions which compensate for the temperature dependence of the detectors' gain. These potential solutions, as well as detailed experimental results and recommendations for future testing, are presented in this research work.

Experimental Investigation of Temperature Effects on
Radiation Portal Monitor Performance

by
David Allen Addington, Jr.

A thesis submitted to the Graduate Faculty of
North Carolina State University
in partial fulfillment of the
requirements for the degree of
Master of Science

Nuclear Engineering

Raleigh, North Carolina

2011

APPROVED BY:

_____   _____
Dr. Man-Sung Yim   Dr. David McNelis
Committee Chair

_____
Dr. Sharon Lubkin

DEDICATION

To my parents, Jimmy and Susi, and to my wife, Leigh.

BIOGRAPHY

David (DJ) Addington was born in Spartanburg, South Carolina on May 29, 1986. He attended Dorman High School and graduated in 2004. DJ continued his education at Furman University in Greenville, SC, majoring in both physics and political science before graduating in May 2008. Following graduation from Furman University with a Bachelor of Science, he began pursuit of a graduate degree in Nuclear Engineering from North Carolina State University.

While at NC State, DJ has worked under the direction of Dr. Man-Sung Yim. He has also participated in two summer internships at Oak Ridge National Laboratory, the second of which was under the mentorship of Dr. Kenneth Baird. Following the second internship, Dr. Yim and Dr. Baird provided the opportunity for continuing the research performed during the summer internship, which is the foundation of the work presented in this thesis.

ACKNOWLEDGMENTS

TABLE OF CONTENTS

LIST OF TABLES

LIST OF FIGURES

Chapter 1: Introduction

Radiation portal monitor (RPM) systems have been utilized in nuclear security

applications for many years. However, in the light of the events of September 11, 2001, the

deployment of RPMs to prevent the diversion and spread of radioactive materials has become

increasingly important (Ely et al., 2006; R. T. Kouzes, Siciliano, Ely, Keller, & McConn,

2008; Wahl, Alderson, & Pibida, 2007). The goal is to detect potential threats that include

not only completed weapons of mass destruction (WMDs) and special nuclear material

(SNM), but also industrial and medical radioactive sources which can be used to fashion

improvised nuclear devices (INDs) or radiological dispersal devices (RDDs) (R. T. Kouzes et

al., 2008).

There are a variety of applications for RPM systems, and different systems vary in

size and capability. Some radiation portal monitors are deployed to monitor pedestrian

traffic in and out of areas where SNM is present. These RPM systems are often referred to as

pedestrian RPMs and are typically smaller than RPM systems used in commercial

transportation monitoring. The larger RPMs are used to monitor vehicle traffic ranging from

cars to semi-trailer trucks and are thus referred to as vehicle RPMs. The monitoring of rail

traffic is performed by an even larger version of the RPM: the rail RPM.

In addition to the differences in size of the RPMs, their capabilities also vary. While a

few RPMs use gamma detectors made of thallium-doped crystalline sodium iodide (NaI(Tl)),

which allows for spectroscopic identification of some radionuclides, the most common

commercial RPMs use plastic scintillators such as polyvinyltoluene, or PVT (Siciliano et al.,

2005). Detectors based on PVT scintillators are the most common type of gamma detector utilized in RPM systems because of the relatively low cost and excellent light transmission properties of PVT scintillators. In addition, plastic scintillators are easily shaped and fabricated to provide large detection areas (Knoll, 2000). One final characteristic of the PVT scintillators which makes them ideal for deployment in RPMs is that they are more resistant to the environmental conditions in which RPMs are often deployed than other scintillation materials (Ely et al., 2006). The experiments discussed in this research work will focus only on RPM systems which utilize these PVT scintillators, each of which is coupled to a photomultiplier tube (PMT), as their gamma detectors.

A common design of radiation portal monitors employs two large metal columnar detection systems, often called pillars, which are a sufficient distance apart so that the monitored traffic can pass between them. This distance between the two pillars can range from around 3 feet for the pedestrian model, to 10 or 15 feet for vehicle portal monitors, and up to even greater distances for the rail RPMs. These RPM systems can be found at ports of entry in many countries around the world, and have become a common feature in seaports and at border crossings. An example of deployed RPMs is shown in Figure 1.1. The size of the RPM pillars also varies depending on the

Figure 1.1: An example of deployed RPM systems. Image taken from <http://rdnsgroup.pnnl.gov/projects.stm>.

model since the size of the scintillators found inside the columns directly determines the size of the detection area of the RPMs. Large detection areas are very important because RPMs are often used to monitor commercial traffic. Since the flow of commerce must not be unduly hampered, a large detection area is necessary to ensure that sufficient detection capability can be maintained without each vehicle passage requiring a long count time. Typically the traffic is required to pass at a relatively low speed through the detection area and is only stopped for further examination if the RPM's alarms are triggered. If an alarm occurs, the person, vehicle, or train can be pulled out of the flow of traffic and examined using more sophisticated detection equipment to determine if any threatening material is present. Thus, the RPM serves as the primary screening mechanism that determines any need for the more intrusive and extensive secondary screening (R. T. Kouzes et al., 2005).

Because RPMs are not operated in a controlled environment, the sensitive electronics and detectors must be protected from environmental conditions. Therefore, all the detector components are placed inside the two metal pillars which are typically constructed of aluminum. Rubber gaskets create a moisture tight seal when the pillar doors are closed. In this manner, some protection from the environment is provided, but as this study will show, the temperature of the environment can still affect the detectors' performance despite the protection of the sealed columns. For the RPM systems considered in this study, the components typically found inside the master pillar include two gamma detectors, a single-channel analyzer (SCA), and the RPM controller. The slave pillar includes many of the same components, including the two gamma detectors and the SCA board, but it does not contain a separate controller. Therefore, the master pillar's controller supports the slave pillar's

detectors, summing and analyzing the detectors' counts in both the master and slave pillar. In addition, many RPM systems, including the pedestrian RPM tested in this study, also utilize helium-3 neutron detectors. However, this study focuses only on the gamma detectors; therefore, no discussion of neutron detectors is included in this research.

The two gamma detectors in each RPM pillar are rectangular and are both oriented vertically, one in the bottom half of the pillar and one in the top half. These gamma detectors are the focus of this study and will be discussed in detail later in this research work. The SCA board in each pillar supplies the high-voltage bias to the two gamma detectors located in the same pillar and also provides amplification of and discrimination of the voltage peaks from the same two detectors. The controller in the master pillar serves as the data acquisition system for all the RPM's detectors, analyzes the data, and provides the communication system used for reporting the counts and any alarms which occur. For the gross-count RPMs examined in this study, an alarm occurs if the count rate when the RPM is occupied is greater than a threshold count rate based on the average background count rate when the detector is not occupied. This study is not primarily concerned with specific alarm algorithms used in RPMs but rather on the overall behavior of the gamma detectors.

Because RPM systems are deployed in remote locations around the world and are unprotected from their environments, it is critical to understand the effects that environmental factors can have on the performance of RPMs. In particular, RPMs are subjected to conditions including extreme temperature variations, as well as rain, humidity, and other sources of moisture. However, because the RPMs' detectors and sensitive electronics are encased in sealed metallic pillars, they are well protected from rain and

humidity. When properly maintained and operated, the pillar's seals prevent all moisture

from reaching the sensitive RPM components, limiting any performance issues due to

moisture. Therefore, this research will focus on temperature as the primary environmental

factor affecting RPM performance.

The components of these systems must withstand extreme variations in ambient

temperature without compromise to, or degradation of, detection capability (Siciliano et al.,

2005). Therefore, it is desirable to understand how RPMs respond to the harsh climates to

which they are subjected. A better understanding of the RPM's response could help identify

any potential shortcomings in the RPM's performance due to temperature, aid in the

prediction of detector vulnerabilities, and provide recommendations for circumventing these

vulnerabilities.

For all of the reasons discussed so far, RPM systems were the focus of the

experiments performed during this study. Furthermore, access to these RPM systems and the

climate chambers used to test temperature effects on the systems' performance was made

possible by collaboration with Oak Ridge National Laboratory (ORNL). The experiments

performed during this study utilized temperature cycles typical of American National

Standards Institute (ANSI) testing and included the monitoring of the RPMs' background

count rates, efficiency measurements, and spectral analyses. The measurements that

occurred during the temperature cycles sought to reveal any temperature dependence in the

performance of the RPMs and also to identify specific system components responsible for the

temperature dependence. This study will use results from the experiments involving these

RPMs to augment the existing understanding of performance degradation in radiation detectors due to temperature.

The purpose of this research work is to provide important insight for the deployment of RPM-type detectors in nuclear security applications. Specifically, this research work will demonstrate that the performance of RPM-type detectors is temperature dependent, search for operational solutions to the temperature dependent behavior of the detectors, and identify the root cause of the temperature dependence. The first hypothesis tested was that the detectors were temperature dependent, especially at high temperature. The second hypothesis was that the magnitude of the temperature dependence could be decreased using operational solutions. And the third hypothesis was that the PMT was the root cause of the temperature dependent behavior of the detectors.

In order to show that the detectors' performance is dependent on ambient temperature, a pedestrian RPM system and two gamma detectors from a rail RPM system were exposed to the temperature cycle mentioned previously. These two systems were tested during separate rounds of experiments. During the testing of the pedestrian RPM system, the measurements described earlier were performed at 10°C intervals during the test, and the differences between the measurements were examined to reveal the temperature dependence of the system's performance. During the testing of the two rail RPM gamma detectors, less emphasis was placed on intermediate temperatures and more was placed on the background count rate variation over the entire range of temperature as well as the difference in the detectors' behavior at the minimum and maximum temperatures.

A search for an operational solution was performed during the investigation of the two rail RPM gamma detectors. This search involved varying the high-voltage bias of the detectors and changing the detectors' supporting electronics. More details of the experiments performed during this portion of testing will be outlined in a later chapter of this research work.

The search for an operational solution also set the stage for determining the system components responsible for the temperature dependent behavior of the RPM detectors. By varying the high-voltage setting and replacing the supporting electronics, the source of the detectors' temperature dependent behavior was determined to exist in the gamma detectors of the RPM system. This determination identified the PMT and PVT scintillator as the two potential root causes of the temperature dependent behavior. An additional experiment, which separated one of the PMTs from its PVT scintillator, demonstrated that the PMT was the system component which was most likely the cause of the temperature dependence.

A brief review of existing literature is presented in chapter 2 of this thesis. The literature review will highlight the fundamentals of radiation detection using PVT based detectors in RPM systems and describe the typical operation of RPM systems as it pertains to the experiments performed for this thesis. In addition, existing literature relating to the temperature dependence of both PVT scintillators and PMTs will be discussed in the review.

Chapter 3 outlines the setup and procedures used during the two rounds of temperature testing performed for this investigation of RPMs. Details of the systems used during the experiments will be presented. The explanation of each experiment's setup describes all relevant settings and arrangements utilized during each test. In addition, the

measurements performed and the procedures followed during each experiment are also presented in chapter 3.

The results for the experiments performed during this investigation are presented in chapter 4 of this thesis. These results are broken into sections based on the type of measurements performed and the system components examined. Brief discussions are also included in each section which identify any important discoveries made in the experiments. Because of the large number of tests performed, the end of the chapter 4 presents a summary of the results from both rounds of temperature tests.

The final chapter, chapter 6, concludes the thesis and presents suggestions for future work. The conclusions section presents the final thoughts on the results and includes temporary solutions to the vulnerabilities discovered.

Chapter 2: Literature Review

In recent years, especially following the events of September 11, 2001, an emphasis has been placed on increasing the deployment of radiation portal monitors (RPMs) at international border crossings. These increased deployments are a result of several initiatives of the United States under programs such as the Department of Homeland Security and the National Nuclear Security Administration (NNSA). As mentioned in the Introduction chapter of this research work, the purpose of these RPM deployments is not only to detect completed nuclear weapons but also to monitor the flow of special nuclear material (SNM) which could be used to develop nuclear weapons as well as industrial and medical sources which could be used in radiological dispersal devices (RDDs) (Wahl et al., 2007).

Although presently RPMs are increasingly deployed in order to monitor the flow of commerce across international borders, historically, these systems have been used for both safeguard applications near SNM processing and storage facilities and for the detection of radioactive sources in material entering scrap metal processing facilities (R. T. Kouzes et al., 2008). This change in the focus of RPM deployments introduces a new set of challenges. For example, because they are increasingly deployed in remote locations around the world, RPMs are exposed to more environmental challenges including extreme variations in ambient temperature. Furthermore, the large volumes of traffic associated with monitoring the flow of commerce and an increased global nuclear threat demand that the RPM's response to environmental changes must be thoroughly examined and understood.

As stated in the Introduction, the RPMs examined in this study utilize PVT scintillator based gamma detectors, each having a PVT scintillator coupled to a PMT. The

use of PVT scintillators has many advantages which were discussed in the Introduction. However, it is well known that both the scintillator and the PMT are essentially temperature dependent devices (Pausch, Stein, & Teofilov, 2005). Therefore, before any discussion of the experiments performed in this study, it is beneficial to discuss the existing research outlining the temperature dependence of both PVT scintillators and PMTs. In addition, it is important to first describe the fundamentals of gamma detection based on PVT scintillation.

There are three gamma interaction mechanisms which are important in radiation measurements: photoelectric absorption, Compton scattering, and pair production (Knoll, 2000). These mechanisms represent processes through which the gamma ray deposits part or all of its energy in the scintillator. For detectors utilizing a PVT scintillator and for the gamma energies of interest in most RPM applications, however, the dominant mechanism is Compton scattering. Because of the energy dependence of the PVT cross-sections for gamma interactions in PVT scintillators, Compton scattering is the most likely interaction for incident gamma energies greater than 20 keV and dominates other interaction mechanisms for incident gamma energies greater than 80 keV (Siciliano et al., 2005). Since Compton scattering is by far the dominant gamma interaction type for the detectors examined in this study, it is the only mechanism addressed in this discussion.

When gamma photons undergo a Compton scattering interaction, the energy of the incident gamma is distributed between a scattered gamma photon and a recoil electron. It is the recoil electron which creates pulses of light in the scintillator as it deposits its energy in the scintillator. In turn, the light from the scintillator is collected by the PMT and converted to a voltage pulse. The distribution of the energy between the scattered gamma photon and

the recoil electron is dependent on the scattering angle. Glenn Knoll (2000) provided an equation to determine the energy of the scattered photon in *Radiation Detection and Measurements* that is reproduced in Equation (2.1) (Knoll, 2000).

$$hv' = \frac{hv}{1 + (hv/m_0c^2)(1 - \cos\theta)} \quad \text{where:}$$
$$hv = \text{incident photon energy}$$
$$hv' = \text{scattered photon energy} \tag{2.1}$$
$$m_0c^2 = \text{rest mass energy of electron (0.511 MeV)}$$
$$\theta = \text{photon scattering angle}$$

Since the energy of the incident gamma is distributed between the scattered gamma and the recoil electron, the kinetic energy of the recoil electron is given by the following equation:

$$E_{e^-} = hv - hv' = hv\left[\frac{(hv/m_0c^2)(1 - \cos\theta)}{1 + (hv/m_0c^2)(1 - \cos\theta)}\right] \quad \text{where:} \tag{2.2}$$
$$E_{e^-} = \text{energy of recoil electron}$$

All scattering angles will typically occur in the detector; however, there are two particular scattering angles which are of special importance: 0° and 180°. The scattering angle approximately equal to 0° represents a glancing interaction and results in the minimum amount of energy (approximately 0 keV) being transferred to the recoil electron. A scattering angle of 180° occurs following a head-on collision in which the incident gamma ray is backscattered 180° and the recoil electron travels in the direction of incidence. It is during this head-on collision that the recoil electron is imparted with the maximum energy which can be transferred during a single Compton scattering interaction. This maximum recoil electron energy is called the Compton edge and can be determined from the following equation presented by Knoll (Knoll, 2000):

$$E_{e^-}\big|_{\theta=\pi} = hv\left(\frac{2\,hv/m_0c^2}{1+2\,hv/m_0c^2}\right) \text{ where:}$$

$E_{e^-}\big|_{\theta=\pi} = $ maximum energy of recoil electron   (2.3)

$hv = $ incident photon energy

$m_0c^2 = $ rest mass energy of electron (0.511 MeV)

Because all scattering angles can be expected under normal conditions, PVT scintillators and other detectors dominated by Compton scattering will produce a signal with energy ranging from zero to the energy of the Compton edge. The resulting range of signal energies is called the Compton continuum. Due to the poor intrinsic resolution of the PVT scintillator, the Compton edge in spectra collected from PVT detectors will be smeared over a range of energy channels resulting in a downward sloped edge rather than a sharp edge (Ely et al., 2006). The result is a spectrum with a less defined structure than that associated with higher resolution sodium iodide (NaI(Tl)) detectors. A comparison of spectra taken using a PVT scintillation detector and spectra taken using a NaI(Tl) detector is shown in Figure 2.1. Both images in the figure were originally presented by Siciliano et al. in "Comparison of PVT and NaI(Tl) scintillators for vehicle portal monitor" (Siciliano et al., 2005).
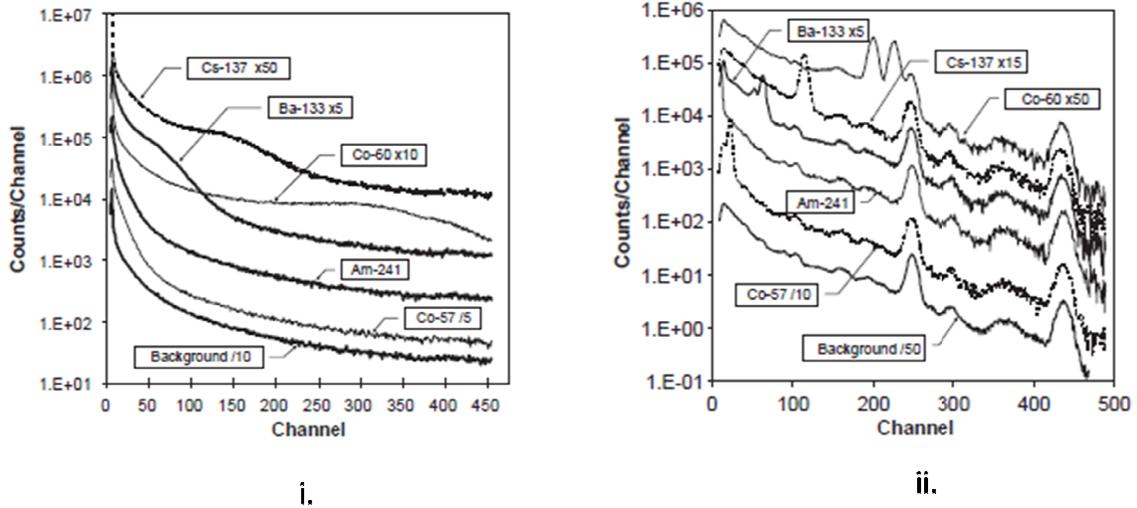
Figure 2.1: Spectra from a PVT detector (i) compared to spectra from a NaI(Tl) detector (ii.)
(Siciliano et al., 2005).

It is clear that the PVT based detector systems do not have the same inherent

spectroscopic capabilities as higher resolution detectors, such as NaI(Tl) detectors, and thus

cannot provide any detailed spectroscopic information. However, Figure 2.1 demonstrates

that the PVT detector's spectroscopic response is somewhat dependent on the energy of the

incident gamma rays. Thus, some crude information, including a rough differentiation

between high- and low-energy sources, can be gleaned from spectra collected from PVT

scintillation detectors using a multi-channel analyzer (MCA) (Ely et al., 2006). Experiments

in this study, which will be discussed in the Results chapter, used spectra collected to

examine changes in the gain of the detectors as a function of temperature. The spectra

collected for this study serve as supplemental data, helping to further the understanding of

several RPM detectors' responses to temperature.

13

In most RPM field applications, including the RPMs tested during this study, the signal from the PVT based detectors is not collected using an MCA. Instead, the signal is passed through a pre-amplifier and amplifier scheme before being examined by a differential discriminator. If the peak pulse height of the detector's amplified signal is between the lower-level discriminator (LLD) setting and the upper-level discriminator (ULD) setting, a logic pulse is sent to the controller. These logic pulses represent one gamma interaction count and are counted by the controller to produce the count rates used in alarm algorithms.

While this study does not focus on specific alarm algorithms or counting schemes employed by RPM systems, a brief overview of the RPM's general counting method is necessary to understand how the system calculates the gamma count rates reported by its controller. The RPMs examined in this study operate in one of two modes: background mode and occupied mode. In normal operation, RPMs switch between the two modes based on whether or not occupancy is sensed by the detector. Typically these RPM systems have an occupancy sensor which detects when a vehicle or pedestrian is passing between the two pillars and switches the RPM from background mode to occupied mode. After the sensors no longer detect occupancy, the detector reverts to background mode. During testing however, the RPM can be forced into occupied mode by manually programming the controller or bypassing the sensors. In both modes, the RPM counts the logic pulse from the discriminator. However, the difference between the two modes of operation is how the logic pulses from the discriminator are processed.

While in background mode, the RPM controller uses a moving average of the logic pulse counts to calculate the average background count rate. This average background count

rate is recorded every five seconds and is typically reported with units of counts per second (CPS). However, in occupied mode, the RPM controller records the number of logic pulse counts every 200 milliseconds. These recorded counts represent the number of gamma interactions detected during 200-millisecond time intervals. A one-second count rate, in counts per second, is calculated using a moving sum of five sequential 200-millisecond count records. Thus, both background and occupied mode can be used to calculate count rate data. During normal operation, the RPM uses an alarm algorithm to compare the count rate calculated when the detector is in occupied mode to the average count rate calculated when the detector was last in background mode to determine if a gross count alarm should occur. However, during this study, the count rates from the two different modes will only be used for measurements requiring a count rate. Background mode will be used when the experiments seek to examine a more average response of the detector over long time periods, while occupied mode will be used when the experiments seek to examine a detailed response of the detector over short time spans.

Several of the experiments performed in this study include efficiency measurements for the gamma detectors. A detector's absolute efficiency refers to the ratio of detected particles or photons to the number of particles or photons emitted by the source. For charged particles, it is often easy to arrange the detectors in a configuration that provides 100% counting efficiency. However, gamma detectors often exhibit counting efficiencies well below 100% because uncharged radiation—like the gamma photons which are the primary concern of this study—can travel very large distances between interactions and is only detected when interactions occur inside the detector. Therefore, it is often convenient to

describe two efficiency measurements: absolute and intrinsic. The absolute efficiency for gamma photons can be calculated as follows:

$$\varepsilon_{abs} = \frac{\#\ \text{of interactions reported by detector}}{\#\ \text{of gammas emitted by source}} \qquad (2.4)$$

However, because gammas are emitted in all direction by gamma sources, the absolute efficiency is dependent on geometric details of the detector setup, namely the distance between the source and the detector. If the source is assumed to be isotropic, meaning that the probability of a photon traveling in any direction is equal to the probability that it will travel in any other direction, the geometry of the system can be taken into account by considering the solid angle of the detector. Specifically, the solid angle is used to determine the number of radiation quanta that will be incident on the detector by the following:

$$N_{incident} = \frac{\Omega}{4\pi} N_{emitted} \ \text{where:}$$
$$N_{incident} = \text{Number of radiation quanta incident on the detector} \qquad (2.5)$$
$$N_{emitted} = \text{Number of radiation quanta emitted by the source}$$
$$\Omega = \text{Solid angle of the detector in steradians}$$

The incident number of gamma rays can be used to calculate the intrinsic efficiency using the following equation:

$$\varepsilon_{int} = \frac{\#\ \text{of interactions reported by detector}}{\#\ \text{of gammas incident on the detector}} \qquad (2.6)$$

The intrinsic efficiency (ε_{int}) is most often used because the geometric dependence of the efficiency is milder than in the case of the absolute efficiency. All the efficiency

measurements discussed in this study are intrinsic efficiencies calculated using Equation

(2.6).

The calculation of the solid angle is performed using an integral over the detector

surface which faces the source. Because the distribution of the gamma source used in this

study was unknown, and because the area of the gamma source was much smaller than the

area of the detector, the gamma source was assumed to behave as a isotropic point source. A

diagram of the setup for which a solid angle calculation would be necessary is shown in

Figure 2.2.
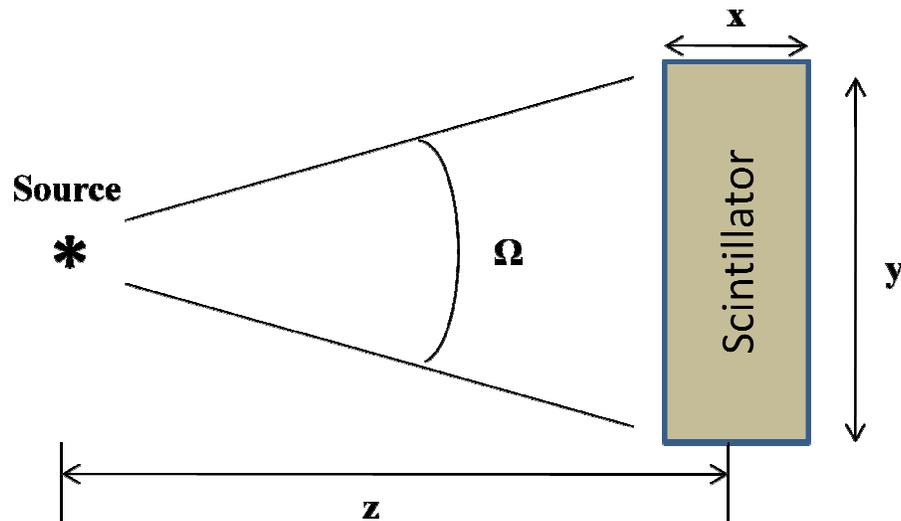
Figure 2.2: Diagram of setup where a solid angle calculation is necessary.

Using the assumption that the source behaves as an isotropic point source, the solid angle for

Cartesian geometry (because the detectors are rectangular) is determined by the following:

$$\Omega = \iint_{A} \frac{z\,dxdy}{\left(x^2 + y^2 + z^2\right)^{3/2}}$$

where:

Ω = the solid angle of the detector

x = the width of the detector (2.7)

y = the length of the detector

z = the distance between the source and the detector

A = the detector surface in the x-y plane facing the source

Equation (2.7) is used to determine the solid angle for the efficiency measurements when the

source is not placed on the detectors face. In cases where the source is placed on the face of

the detector and in the center of the PVT scintillator, the distance between the source and the

detector is approximately zero, and the resulting solid angle is approximately 2π. Thus, the

efficiency measurements when the source can be placed on the face of the detector and in the

center of the scintillator were determined by the following:

$$\varepsilon_{int} = \frac{1}{2}\left[\frac{\#\ \text{of interactions reported by detector}}{\#\ \text{of gammas emitted by source}}\right]$$ (2.8)

In addition to outlining the typical behaviors of the PVT based detectors used in the

RPMs tested during this study, it is also informative to discuss the known temperature

dependencies of the PVT scintillators and coupled PMTs. While PVT scintillators do exhibit

some temperature dependent behavior, it is the PMT that exhibits the behavior most

important to this study and most consistent with the results of the experiments presented in this research work. Therefore, a brief overview of scintillators will be presented first, and the remainder of this literature review will focus on important phenomena that occur in the PMT with changing temperature.

A study by Yasushi Kawada, Jun Ito, and Qiu-Wei Wang (2004) examined the pulse-height and time spectra of after-pulses at various temperatures for an NE102A scintillator and sandwiched ^{60}Co source. The NE102A scintillator is composed of material similar to the PVT scintillators used in many RPMs. The study by Kawada, Ito, and Wang (2004) showed that as temperature increased, time-dependent after-pulses from the plastic scintillator decreased. The effect of the decrease in these time-dependent after-pulses was a decrease in the intensity of pulse height as the temperature rose to 50°C (Kawada, Ito, & Wang, 2004). Once the temperature exceeded 50°C, Kawada, Ito, and Wang (2004) showed that the temperature dependence of the PMT resulted in a random component of the spurious pulses causing the pulse heights to increase (Kawada et al., 2004).

The results presented by Kawada, Ito, and Wang (2004) were consistent with other studies showing that the light output of the scintillator decreases with increasing temperature. One such study, presented by Guntram Pausch (2005), stated that the amount of light in the form of photons emitted per unit of energy deposited in the scintillator, called the scintillation light output, is dependent on the temperature of the scintillator (Pausch et al., 2005). Furthermore, Pausch (2005) cited material presented by William R. Leo (1994) showing that the light output can vary by 10% to 20% over the temperature range of -15°C to 55°C for common scintillator materials (Leo, 1994). This decrease in light output is

consistent with results presented by Frank E. Kinard (1957), as well as discussions by William P. Ball, Rex Booth, and Malcolm MacGregor (Ball, Booth, & Macgregor, 1957; Kinard, 1957). However, Kinard noted in his study that the temperature dependence of the scintillator could be minimized by adjusting the decay time of the amplifier, suggesting that proper electronic design could result in compensation for the temperature dependence of the scintillator.

The decrease in light output from the scintillator can affect the overall gain of the detector. Since the photons from the scintillator are collected by the PMT and used to create voltage pulses, a decrease in the light output can lead to a lower voltage pulse coming out of the PMT. Therefore, since the pulse height is a direct indication of the detector's gain, the end result of the decrease in light output from the scintillator is a decrease in the gain with increasing temperature. However, the aforementioned studies presented concerning the temperature dependence of the scintillator also point heavily toward the PMT as yet another, more dominant cause of gain shifts.

The temperature dependence of the PMT is more documented that that of the PVT. There are two important behaviors of PMTs at high temperature that are must be addressed in order to understand the study presented in this thesis. The first is the temperature dependence of the photomultiplier gain, and the second is the temperature dependence of noise in the PMT.

A study on the temperature dependence of the photomultiplier was performed by Kinard (1957). This study examined the contribution of specific components associated with scintillation detectors by varying the ambient temperature of each component individually.

The results showed that the pulse height of a ^{137}Cs gamma source collected from the detectors varied with temperature when the PMT was exposed to a temperature controlled air bath. Recalling that pulse height is a direct indication of gain, this result indicated that the gain of the system is temperature dependent. Specifically, when the air bath temperature was -15°C, the gain was approximately 40% higher than when the air bath temperature was 50°C. Furthermore, this study by Kinard (1957) demonstrated that the temperature dependence of the gain is associated with the temperature experienced by the dynode structure inside the PMT rather than the photocathode (Kinard, 1957). Kinard's (1957) study was consistent with a separate study by Singh and Wright (1987) that also stated that for detector applications such as scintillation counting and spectrometry, the detectors are sensitive to the temperature dependent gain shifts of their photomultiplier (Singh & Wright, 1987). These studies, along with the study by Ball, Booth, and MacGregor (1957), demonstrated that the pulse height collected from detectors similar to the ones used in the RPMs examined in this study, is sensitive to the temperature dependence of the PMTs, and this sensitivity is dependent on the PMT design.

The temperature dependence of the noise created by the PMT is also known to be a significant issue in the detectors used in common RPMs. Furthermore, high PMT temperatures can result in an increase in the amplitude of the noise and can also move that noise into the signal window; however, controlling the temperature of a PMT with inherently low dark current can reduce this effect (Fehlau, 1987). Dark current, or dark noise, refers to pulses created in the PMT which are not the result of interactions within the scintillator. According to Knoll (2000), thermionic electrons spontaneously emitted by the photocathode

are the most significant source of noise in PMTs (Knoll, 2000). The emission of thermionic

electrons results when the thermal kinetic energy of the normal conduction electrons found in

photocathode material is able to overcome the surface potential barrier of the photocathode,

and the electron is close enough to the surface that it can escape (Knoll, 2000). In addition,

Knoll (2000) stated that in applications where very-low-energy radiation is measured, pulses

due to actual signal events may be indistinguishable from pulses due to thermionic emissions

(Knoll, 2000). Since RPMs are often optimized for low-energy gamma detection, it can

reasonably be assumed that the dark pulses from thermionic emissions could have significant

impact on the detector's performance at high temperatures.

The amount of noise created by thermionic emissions in the PMT should, in theory,

increase exponentially with increasing photocathode temperature (Knoll, 2000). Richard's

equation for thermionic emissions, as presented in the Hamamatsu PMT handbook (2006),

can typically be used to account for the noise associated with thermionic emissions and is

given by the following equation:

$$i_{DC} = AT^{5/4} e^{\left(-e\psi / KT \right)} \text{ where:}$$

i_{DC} = dark current due to thermionic emissions
A = constant
T = temperature (Kelvin)   (2.9)
e = electron charge
ψ = work function
K = Boltzmann constant

Based on the information presented in the existing literature, it is expected that the

RPMs discussed in this research work will exhibit strong temperature dependency.

Specifically, the detectors which consist of a PVT scintillator and coupled PMT are expected to experience shifts in the gain as the temperature changes and an increase in the system noise at high temperatures. The remainder of this research work will focus on an experimental investigation of the effect that the phenomena discussed above have on the performance of a pedestrian RPM system as well as on gamma detectors taken from a deployed rail RPM system.

Chapter 3: Experimental Setup and Procedures

While all the experiments performed focused on the gamma detectors of common

RPMs, there were variations in the experiment details. For this reason, it is important to

discuss each test's setup and procedures separately. Several of the system components

during both rounds of temperature testing are the same however, and will be discussed in

section 3.1. A few of the test procedures were also used during both rounds of testing and

are discussed in section 3.2. The same gamma sources were used during each testing period.

The creation date and strengths of both the ^{57}Co and ^{137}Cs sources are shown in Table 3.1.

Table 3.1: Source activity for the gamma sources used during both testing periods.

Isotope	Creation Date	Initial Activity	Half-Life
^{57}Co	05/01/2005	93 µCi (3.44 E+06 Bq)	271.79 days
^{137}Cs	12/20/1995	7 µCi (2.59 E+05 Bq)	30.07 years

3.1 Common System Components

Each gamma detector examined during the experiments presented in this research

consisted of a photomultiplier tube (PMT) and coupled polyvinyltoluene (PVT) organic

plastic scintillator. The detectors used during the experiments were identical models from

the same manufacturer. The gamma detectors were connected to the manufacturer's specific single-channel analyzer (SCA) via one BNC cable and one MHV cable. As discussed in the Literature Review chapter of this research work, the gamma interaction in the PVT scintillator produced light pulses which were collected by the PMT and transformed into voltage pulses of particular amplitudes depending on the energy deposited in the scintillator by the gamma ray.

The manufacturer's SCA provided the high-voltage (HV) bias to each detector's PMT via the MHV cable, as well as amplification and discrimination of voltage pulses coming from the detectors. This HV bias could be adjusted manually and controlled the shape and height of the voltage pulse coming out of the PMT during operation. The voltage pulse from the PMT was fed into a fixed gain first stage amplifier (pre-amp) located on the SCA's rabbit board. After the first stage amplifier, the pulse was again amplified by a fixed gain second stage amplifier attenuated in order to provide the correct shape. At this stage, the pulse shape and amplitude is set, and the pulse is processed by the SCA's differential discriminator. If the peak pulse amplitude is between the lower-level discriminator (LLD) voltage and upper-level discriminator (ULD) voltage, then a logic pulse is sent from the SCA to the manufacturer-specific RPM controller.

The RPM's controller acts as a counter and records the gamma count rate from each detector in counts per second format. For these tests, the controller was operated in one of two modes: "background" or "occupied". When operated in background mode, the controller averaged the counts over five-second intervals and output the data as a five-second average count rate in counts per second (CPS). When operated in occupied mode, the controller

instead used 200-millisecond intervals and reported the data as a 200-millisecond sum of the

gamma interactions detected five times per second. A cumulative summation of five

consecutive 200-millisecond sums yields the count rate in counts per second. In addition to

reporting the count rates, the controller also allows for fixed increment adjustments of the

LLD and ULD voltages.

A simplified detector setup is shown in Figure 3.1 and includes an alternate setup in

which a Tukan 8k MCA with 1024-channel resolution served as the MCA for spectrum

collection. The Tukan MCA could be connected by BNC cables to built-in test points inside

the SCA which allowed for spectral analysis of the voltage peak after the first or second stage

amplifier for each individual detector.
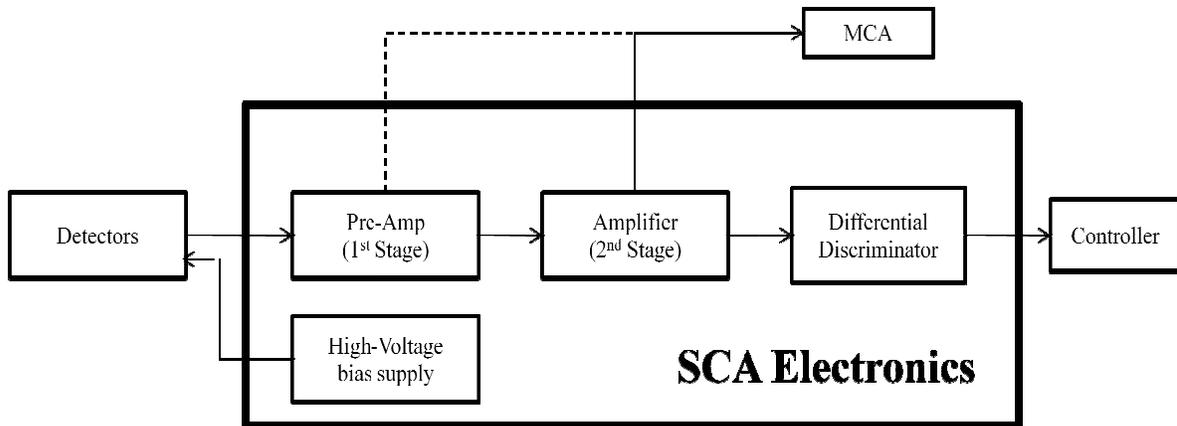
Figure 3.1: Simplified signal chain for the gamma detectors used during these experiments.

3.2 Common Procedures

3.2.1 Calibration Procedure

For both the first and second set of temperature tests, the gamma detectors had to be calibrated before any testing was performed. In addition, a significant portion of the second round of experiments focused on changes to the calibration. Therefore, it is important to discuss the procedure for calibrating the gamma detectors. For this discussion, only the manufacturer's recommended alignment will be discussed. Variations to this alignment in the second round of testing will be discussed in section 3.4.

For each factory recommended (nominal) calibration, the HV setting was adjusted to ensure that the peak pulse amplitude after the first stage of amplification was 0.75±0.05 V with a ^{137}Cs source placed on the face of each detector. The pulse was measured using a standard oscilloscope connected by BNC cable to the same built-in test points for the first stage which were used by the MCA during testing. While the recommended calibration does not state a specific value for the HV in order to ensure the proper pulse height, a numeric value of the HV can be measured by disconnecting the MHV cable supplying the high-voltage bias to the PMT and measuring the voltage with a generic high-voltage probe and multi-meter. The typical high-voltage setting which resulted in the desired 0.75 V peak pulse amplitude during both sets of testing was 1070±10 V.

Once the high voltage was set, the second stage amplifier was adjusted so that the second stage peak pulse amplitude of ^{137}Cs provided the 2.0 V pulse height which ensured that the proper energy-to-voltage ratio of 480 keV to 2.0 V was maintained. This energy

ratio guarantees that the sensitivity of the detectors is focused in the low-gamma-energy region associated with highly-enriched uranium (HEU). If the second stage peak pulse amplitude of ^{137}Cs is properly set to 2.0 V, the LLD and ULD default voltages of 0.069 V and 0.435 V correspond roughly to an energy window spanning from 22 keV to 144 keV. The second stage amplification is independent for each detector; therefore each detector's channel must be calibrated individually. The second stage amplifier is a fixed gain amplifier, but the level of pulse attenuation can be adjusted manually on the SCA's rabbit board to ensure that the peak pulse amplitude of ^{137}Cs after the second stage is equal to 2.0 V. This peak pulse amplitude is measured using a generic oscilloscope connected by a BNC cable to the built-in test points for the second stage, which are found on the SCA rabbit board for each detector's channel. No numerical values can be measured for the second stage amplifier; therefore, all adjustments are made by "eyeballing" the pulse shape as measured by the oscilloscope. Unfortunately, this alignment procedure allowed for a great deal of variation in the second stage alignment.

Because of the inherent variations in the calibration, the ^{57}Co efficiency of each detector must be measured to ensure that the alignment provides adequate sensitivity to this low-energy gamma source (^{57}Co) which is used as an ANSI surrogate for HEU. These efficiency measurements are performed using the count rates reported by the RPM's controller assuming a 100% live time. The method for calculating the efficiency is discussed in the Literature Review, while the specific efficiency calculations will be discussed in the set-up of each round of testing.

3.2.2 Recording the Count Rate and Spectra

During both rounds of testing, the count rate reported from the RPM's controller was recorded and analyzed. The count rate data from the RPM's controller was recorded by a generic laptop computer using a simple Perl script. The RPM's controller is designed for this type of data streaming and has a LAN port that allows for communication between the controller and the recording computer. While the RPM was operated in background mode, the count rate from the controller was directly recorded by the Perl script since the reported count rate was a five-second average in counts per second every five seconds and also included a time stamp. However, when the RPM was operated in occupied mode, the count rate was more difficult to extract from the controller's data. When operated in occupied mode, the controller reported a sum of the number of gamma interactions detected over 200-millisecond intervals. This sum was reported five times per second, and each sum included a time stamp. Another Perl script was used to convert these 200-millisecond sums into count rates by summing five consecutive 200-millisecond counts. These calculated count rates were then assigned the time stamp corresponding to the five counts which were summed. In this manner, the count rate reported by the RPM's controller was stored in data files by the laptop running the Perl scripts.

When necessary, another Perl script was used to average the count rates from the controller. By automating the averaging process, the average count rate over any period of time could be calculated. Furthermore, the averages could be processed in batches and output to single file, condensing the information from several files containing the raw count

rates into a single file containing the averaged count rates along with a time stamp corresponding to the average of the time stamps for the original counts.

The collection and analysis of the spectra was also consistent during both testing periods. The same Tukan MCA was used to collect each spectrum, which could be saved as data files. Each data file contained the number of counts occurring in each of the 1024 channels of the MCA. Analysis of the spectra was performed by importing the data files into Excel, allowing for calculation using the spectra and the recreation of each spectrum's curve.

3.2.3 Efficiency Calculations

The efficiency calculation was also consistent during all experiments performed. For each measurement, data from two measurements was needed: one measurement with the gamma source present and one measurement with no sources present. For each of these measurements the controller was placed in occupied mode, meaning that the number of gammas detected (gamma counts) was reported every 200 milliseconds. The sum of the counts from the measurement recorded when a gamma source was present represented the total number of gamma interactions detected and by nature included gamma interactions that were due not only to the source but also to natural background radiation. The sum of the counts from the measurement with no sources present represented the gamma interactions detected due only to background gamma radiation. The difference between these two sums represented the number of gamma interactions detected which are attributable to the gamma source. Furthermore, the expected number gamma interactions due to the gamma source can be determined from the activity of the source, the measurement time, and the solid angle of

the detector, which can be calculated using Equation (2.7) presented in the Literature

Review. The efficiency can then be counted using Equation (2.6) presented in the literature

review.

3.3 First Round of Testing

3.3.1 First Round Set-up

A pedestrian RPM was used for testing which contains the same major components as

the larger vehicle and rail RPMs designed by the same manufacturer, with the exception of

the size of the PVT scintillators. Originally this round of testing was to be performed on a

vehicle RPM, however, because of the size of the chamber, a pedestrian RPM was tested

instead. The motivation for the test stemmed from an increased interest in deploying RPM

systems from the same manufacturer in very hot climates.   For this reason and because

commercial off-the-shelf (COTS) heaters are often provided by the manufacturer when

deployed in cold climates, a focus was placed on the high-temperature response of the

detectors. Since the purpose of this experiment was to test the response of RPMs to

temperatures exceeding the RPMs rated maximum of 50°C, the entire pedestrian RPM was

placed inside the temperature chamber. Therefore, all the system components (detectors,

power supply, amplifiers, controllers, etc.) were inside sealed self-contained weather resistant

metallic pillars during the test. There were two of these pillars, connected via metal conduit,

which were mounted to a quarter-inch steel plate on wheels.

A Tenney Model 27STR environmental chamber was used provide a controlled

temperature environment. The interior dimensions of the chamber were approximately 9' x

8' x 6' and allowed for the pedestrian monitor to be placed in a normal upright configuration.

Thermocouples and voltage probe cables, along with several BNC cables connected to the

RPM's SCA unit, were passed through a wall penetration in the side of the chamber to a

measurement station outside the chamber. A picture of the RPM placed inside the chamber

is included in Figure 3.2.

Figure 3.2: Pedestrian RPM placed inside the Tenney Environmental Chamber.

Because this study focuses on the gamma detectors of the RPM, only the components

essential to the performance of the gamma detectors will be discussed. Each pillar of the

pedestrian RPM contained two gamma detectors each consisting of a polyvinyltoluene (PVT)

organic plastic scintillator coupled to a photomultiplier tube (PMT). The gamma detectors

are connected to the manufacturer's unique single-channel analyzer (SCA) unit, of which

there is one in each pillar. The outputs of the SCA in both pillars are sent to a common

controller which is located in the pillar on the left in Figure 3.2. This left pillar is called the

master pillar, and its detectors are named detectors 1 and 2, with detector 1 being in the

bottom half of the pillar and detector 2 being in the top half of the pillar. Similarly, the

bottom and top detectors in the right, or slave, pillar are called detectors 3 and 4 respectively.

The details of the interactions and functionality of the SCA, controller, and gamma detectors

are discussed in section 3.1 of this work.

3.3.2 First Round Experimental Procedure

After the RPM was placed inside the chamber and allowed to stabilize, the four

gamma detectors were aligned using the factory-specified procedures outlined previously in

section 3.2.1. Following the calibration, the gamma sensitivities for ^{57}Co were measured and

are presented in Table 3.2. According to experts at ORNL, the efficiencies shown are

acceptable and indicative that the RPM was properly calibrated.

Table 3.2: Gamma detector efficiencies at 22°C following initial set-up and calibration for the first round of testing.

[57]Co Source Activity		
3.44 E+06 Bq (93 MicroCuries)		Creation Date: 5/1/2005
2.96 E+04 Bq (0.8 MicroCuries)		Test Date: 6/8/2010
Pre-Test Gamma Detector Efficiency Calculations		
Detector	Net Gamma CPS (counts per second)	Detector Efficiency
1	3313	22.4%
2	3265	22.0%
3	3165	21.4%
4	3063	20.7%

Once the initial set-up and calibration was completed, the temperature profile to be used during this round of tests was programmed into the Tenney environmental chamber, and the chamber temperature was set to cycle through temperatures ranging from -30°C to 60°C. The temperature inside the chamber was controlled using a dedicated computer connected to the Tenney system. The approximate temperature profile used was as follows:

i. Hold at room temperature (22°C) for 2 hours

ii. Lower by 10°C/hr to -20°C and hold for 4 hours

iii. Lower by 10°C/hr to -30°C and hold for 24 hours

iv. Raise by 10°C/hr to -20°C and hold for 4 hours

v. Raise by 10°C/hr to 0°C and hold for 4 hours

vi. Raise by 10°C/hr to 20°C and hold for 4 hours

      vii.   Raise by 10°C/hr to 30°C and hold for 24 hours

     viii.   Raise by 10°C/hr to 40°C and hold for 24 hours

       ix.   Raise by 10°C/hr to 50°C and hold for 24 hours

       x.   Raise by 10°C/hr to 60°C and hold for 24 hours

      xi.   Lower by 10°C/hr to room temperature (22°C) and hold for 2 hours

The programmed temperature profile was adjusted so that each temperature hold ended during normal ORNL operating hours so that measurements could be taken after each hold; therefore the hold times listed above represent the minimum amount of time that the program held at each temperature. It should be noted that the humidity of the chamber was not controlled during these tests; however, because the RPM remained sealed during the tests, no moisture reached the inside of the columns. Therefore, no electrical components were affected by moisture created during the condensing atmosphere which formed as the temperature moved from extremely low temperature back to warmer temperatures.

      The temperature rate of change (10°C/hr) was set in accordance with ANSI N42.35, Section 7.1 (*American national standard for evaluation and performance of radiation detection portal monitors for use in homeland security* 2004). This standard outlines a typical testing method used to characterize RPM systems. However, this method was modified for this set of experiments to include extended hold times at each 10°C increment in order to ensure that the excessive mass of the RPM and the ambient temperature inside the chamber reached thermal equilibrium. In addition, temperature data from the slave pillar of the RPM was collected during the test using thermocouples and probes to ensure that the

components reached the desired temperature by the end of each temperature hold. The long holds, especially the 24-hour holds, are inconsistent with the normal operating environment of these RPMs, but it was hoped that a conservative approach would enable the detector's response to be more thoroughly examined for temperature dependent behavior.

Background gamma count rates were recorded in the manner discussed previously during the temperature cycle. These count rates were reported by the RPM controller and were continuously collected. The RPM was placed in occupied mode so that the data was collected at 200-millisecond intervals for each gamma detector. This information was later averaged using the Perl script discussed previously.

The responses of detectors 1 and 2 to gamma sources were measured at the end of each temperature hold. Using the ^{57}Co and ^{137}Cs sources listed in Table 3.1, the efficiency was measured by placing each source individually on the outside of the aluminum door of the master pillar. For each measurement, the source was placed at the location corresponding to the center each individual detector. A three minute measurement time was used to collect the 200-millisecond counts reported from the RPM's controller while operating in occupied mode. The three minute count time was used because the source was approximately 14 cm from the face of the scintillators which created a non-ideal solid-angle and also because some gamma rays were attenuated by the aluminum door. These two factors decreased the expected number of gamma interactions, and therefore dictated a relatively long count time to ensure Poisson counting statistics.

In addition to streaming the count rates from the detectors and performing efficiency calculations, spectra were collected for each detector using the Tukan MCA for the ambient

background and the two gamma sources during a subset of temperature intervals including: -30°C, 30°C, 40°C, 50°C, 60°C, and 22°C. The source was again placed on the aluminum door, and therefore the MCA utilized a 300 second live count time for each spectrum to ensure sufficient counts were collected.

3.4 Second Round of Testing

3.4.1 Second Round Set-up

For this round of testing, two PVT scintillators and their coupled PMTs were taken from a currently deployed rail RPM system and shipped to ORNL for investigation. Data collected from these detectors while they were deployed displayed background count rate oscillations, and thus ORNL was asked to examine them. These scintillators are the same type of PVT organic scintillators used in the pedestrian RPM but are much larger. Because only the detectors were shipped, spare RPM electronics, specifically the manufacturer's unique SCA and RPM controller which had previously been used at ORNL for various experiments and scientific studies, were used during these experiments. While not the specific units, the SCA and controller were the same models used for the first round of temperature tests since there is no variation in the RPM electronics used in the pedestrian, vehicle, and rail RPM from this manufacturer.

The gamma detectors were placed horizontally on an ad hoc stand. The detector on the bottom of the stand was connected to channel 1 of the SCA, while the top detector was connected to channel 2 of the SCA. For these tests, the electronics and gamma detectors

were not shielded from the environmental conditions by the RPM columns but were operated as a "skeleton" RPM system.

The temperature tests for this round were conducted in a Russell's model RD-125-605-605-AC environmental chamber at ORNL. The interior dimensions of the chamber are 5' x 5' x 5', which allowed for the horizontal configuration of the gamma detectors placed on the stand. A penetration in the chamber's wall was used to pass BNC and MHV cables from the detectors to the SCA for the experiments conducted with the electronics outside the chamber. The same penetration was used to pass data collection cables from the RPM controller to a generic laptop outside the chamber for experiments where the electronics were also placed in the chamber.

For this setup, any components placed outside the chamber were maintained at room temperature regardless of the chamber's internal temperature. All components inside the chamber experienced the ambient temperature determined by the chamber's temperature profile. Since the RPM components were exposed to the ambient temperature, no thermal couples were used other than those utilized by the Russell's climate control system. No condensing environments were created during these experiments, meaning that the detectors were not exposed to moisture build up during the cycles.

3.4.2 Second Round Experimental Procedure

Before discussing the procedures of the second round of testing, it is important to mention that many different types of experiments were performed during this round of testing over a two-week period, and the testing schedule was designed to maximize the

number of experiments and hypotheses which could be tested. Therefore, the experiments were not performed in a manner conducive to chronological explanation. Instead, the procedure—and later the results—will be discussed in a non-chronological order that best outlines the important discoveries made in each experiment.

At the beginning of the testing, the two detectors—each having a PVT scintillator and coupled PMT—were placed inside the environmental chamber. All other electronics were left outside of the chamber, and both detectors were calibrated at 22°C using the factory-specified procedure. The ^{57}Co efficiencies for both detectors after the initial calibration are shown in Table 3.3.

Table 3.3: Gamma detector efficiencies at 22°C following initial set-up and calibration for the second round of testing.

57Co Source Activity		
3.44 E+06 Bq (93 MicroCuries)		Creation Date: 5/1/2005
1.48 E+04 Bq (0.4 MicroCuries)		Test Date: 3/9/2011
Pre-Test Gamma Detector Efficiency Calculations		
Detector	Net Gamma CPS	Detector Efficiency
1	2201	29.8%
2	2056	27.8%

Following the initial calibration, the environmental chamber was programmed to cycle through temperatures ranging from 22°C to 50°C. No temperatures lower than room temperature (22°C) were examined because results from the first round of testing showed relatively insignificant degradation in the low-temperature performance of the gamma detectors and commercial off-the-shelf (COTS) heaters are available for deployments in cold climates. The initial temperature cycle, and each subsequent cycle, was based on the following schedule:

    i.   Hold at room temperature (22°C) for 2 hours

    ii.   Raise by 10°C/hr to +30°C and hold for 1 hour

iii.   Raise by 10°C/hr to +40°C and hold for 1 hour

iv.   Raise by 10°C/hr to +50°C and hold for 2 hours

v.   Lower by 10°C/hr to +40°C and hold for 1 hour

vi.   Lower by 10°C/hr to +30°C and hold for 1 hour

vii.   Lower by 10°C/hr to +22°C and hold indefinitely

As in the previous round of testing the temperature's rate of change was specified by ANSI 42.35 section 7.1 (*American national standard for evaluation and performance of radiation detection portal monitors for use in homeland security* 2004). For this round of testing, the temperature holds were not initially set for more than 2 hours because the PVT scintillators and PMTs were exposed to the ambient chamber temperature and were not inside a sealed column. In addition, during a subset of the experiments for this round, the end of this profile was modified to include a ramp to 50°C followed by a hold at 50°C. This change enabled measurements to be retaken while the temperature was holding at 50°C.

The fifth temperature cycle, which occurred over a weekend, used a modified schedule that allowed for slower cycles and longer holds at each 10°C interval. The modified schedule started with a slow cycle through the range of 22°C to 50°C, returning to 22°C before increasing back to 50°C with five-hour holds at each 10°C interval. For the slow cycling part of the schedule, the chamber temperature slowly increased from 22°C to 50°C at an average rate of 1°C per hour, and then decreased back to 22°C at the same average rate. The end of this schedule returned to the 10°C per hour rate of increase but included five-hour holds at each 10°C interval rather than 2 hour holds. The purpose of this test was to examine the detectors' responses to temperature in more detail and to determine whether or not the

42

count rate was still increasing at the end of the two-hour hold at 50°C that had been employed in the first four temperature cycles.

Following the fifth temperature cycle, all subsequent cycles used a modified form of the initial schedule that included a five-hour hold at 50°C instead of a two-hour hold. However, the holds at all other temperature intervals and the rate of temperature change were left unaltered from the original cycle.

The gamma background count rate reported from the RPM controller was recorded during each temperature cycle in order to expose any temperature dependence in the detectors' reported background measurements. For these experiments, the RPM controller was left in background mode, meaning that the count rate was reported as a five-second average by the controller.

3.4.2.1 Exploration of Potential Solutions to the Count Rate Oscillations

Following the initial temperature test which explored whether or not the background count rate oscillations observed in the field were temperature dependent, the next set of experiments performed in the second round sought to find an alternative detector calibration that lessened the magnitude of the oscillations. The hypothesis that the magnitude of the count rate oscillations was dependent on the high-voltage (HV) setting for the detectors was based on circumstantial evidence, the expert opinion of the technical staff of ORNL, and existing literature (Hamamatsu, 2006). Therefore, the initial temperature cycle was repeated five times while changing the PMT HV setting with the hope that an operational value of the HV could be discovered which would result in a decrease in the magnitude of the count rate

oscillations. Recall that cycle five did not explore an alternative HV setting; therefore, these alternative HV settings were explored in cycles two, three, four, six, and seven. The specific settings for these cycles are shown in Table 3.4, presented later in this section.

All of the alternative HV settings that were tested were between 870 V and 1300 V. For every alternative voltage setting other than 1300 V, the second stage amplifier was adjusted to ensure a 2.0 V second stage pulse height for ^{137}Cs on the face of the detector, which provides the desired energy-to-voltage ratio as discussed in the Calibration Procedure section. However, because the 1300 V high-voltage setting resulted in a 3.0 V first stage peak pulse height, the second stage amplifier was set so that the second stage pulse height was 3.0 V instead of 2.0 V. This corresponds to unity amplification of the first stage pulse height. To compensate for the 50% increase in the voltage height, the LLD and ULD voltages were also increased by 50% in order to maintain the low-energy sensitivity range to gamma rays.

Once the range of HV settings was explored and no setting was found which decreased the magnitude of the count rate oscillations, a second hypothesis was tested which focused on variations in the manufacturer's SCA. This hypothesis sought to demonstrate that the background count rate oscillations observed in the first seven cycles were not unique to the specific SCA unit used during those tests. Therefore, a recently purchased SCA unit replaced the unit used during the initial cycle and also the cycles exploring the alternative HV settings.

In addition, the decision was made to place the "New SCA" inside the temperature chamber. By placing the new SCA inside the chamber, the effect that the temperature of the

SCA had on the count rate oscillations was examined as well during this experiment. Ideally, this test would have been executed as two separate steps: First, examine the effect of replacing the SCA while leaving it outside the chamber, and then examine the effect of placing the new SCA inside the chamber. However, these two steps were condensed into one experiment due to time constraints during testing.

During both the search for an alternative HV setting and the cycle utilizing the new SCA, the background count rates from the RPM's controller were recorded. In addition, before each cycle began, a sensitivity measurement for ^{57}Co was performed on each detector at 22°C, and for a subset of the cycles, the measurement was repeated at 50°C.

The relevant settings for each cycle performed, along with the resulting ^{57}Co efficiencies calculated are presented in Table 3.4. Each calibration was performed in a manner similar to the factory recommended calibration—placing the same ^{137}Cs source on the center face of each detector and measuring the first stage pulse height with an oscilloscope. The value of the pulse height was decreased by 0.25 V for the second cycle and was increased by 0.25 V for the third cycle. The fourth cycle's calibration decreased the HV setting of the second cycle by 100 V. The fifth cycle was a return to the nominal calibration, while the sixth and seventh cycles were set to specific HV settings. All the remaining calibrations were performed using the nominal procedure of setting the first stage peak pulse amplitude to 0.75 V.

In addition to the settings discussed, the eighth temperature cycle is also mentioned in Table 3.4. Before the eight cycle, the system's HV was increased to 1500 V (the maximum rated voltage of the PMTs), and the system was left to sit overnight at room temperature

(22°C). No calibration was performed on the detectors, and no data was collected during this time. Anecdotal evidence suggested that increasing the HV to the PMT's maximum rated high voltage would have a "cleaning" effect on the PMT's photocathode. The hypothesis for this test predicted that after the overnight soak at the 1500 V, if the detectors were recalibrated to the nominal alignment and subjected to the cycling temperatures again, the count rate oscillations might decrease or disappear.

Therefore, after soaking at 1500 V overnight, the detectors were recalibrated to factory recommended settings, and the temperature was cycled from 22°C to 50°C using the same temperature schedule as the initial cycle. The background count rate was recorded during this cycle in order to observe any effect the 1500 V soak had on the count rate oscillations. Once the chamber temperature reached 50°C, the detectors were allowed to soak for 3 hours. Following the three hour soak, the rest of the cycle was aborted because it was clear that the count rate had still increased as the chamber temperature increased.

Table 3.4: Relevant settings for each temperature cycle performed in the second round of testing.

Electronic Alignment Data for Each Cycle (HV setting, 1st and 2nd stage peaks, LLD and ULD values – All Units are Volts)						[57]Co Efficiency for Each Cycle			
						22°C		50°C	
Temperature Cycle	HV:	1st Stage Voltage Peak	2nd Stage Voltage Peak	LLD	ULD	Bottom	Top	Bottom	Top
Original	1083	0.75	2.00	0.069	0.435	29.8%	27.8%	No Data	
Second	970	0.50	2.00	0.069	0.435	29.1%	28.5%		
Third	1101	1.00	2.00	0.069	0.435	28.5%	27.9%		
Fourth	870	0.20	2.00	0.069	0.435	28.5%	25.0%	26.5%	23.1%
Fifth	1070	0.75	2.00	0.069	0.435	30.3%	28.6%	25.2%	26.2%
Sixth	1300	3.00	3.00	0.099	0.6525	32.9%	30.0%	30.6%	27.4%
Seventh	900	0.25	2.00	0.069	0.435	29.1%	27.4%	27.2%	24.6%
Soak overnight with HV=1500 V to both detectors									
Eighth	1060	0.75	2.00	0.069	0.435	30.2%	28.0%	27.5%	25.1%
Placed SCA and Controller Inside Chamber									
New SCA Inside	1060	0.75	2.00	0.069	0.435	28.1%	28.4%	No Data	

3.4.2.2 Exploration of the Root Cause of the Count Rate Oscillations

The next step in the testing procedure was a departure from the typical experiments already performed. The system was recalibrated to the factory recommend alignment, after which no further adjustments were made to the HV setting or to the second stage amplifier. While leaving the system powered, the top detector, corresponding to channel 2 of the SCA, was disconnected, and the PVT scintillator was separated from its coupled PMT. The cut-off PMT was then placed in a light-tight covering and reconnected to channel 2. The bottom detector was left alone. By not powering the system off the system should have maintained the factory recommended alignment during this procedure.

After the cut-off PMT was reconnected, the system was allowed to re-stabilize. After the system was stable, the intact gamma detector and the cut-off PMT were examined during an additional temperature cycle based on the initial profile discussed previously. The count rates, as reported by the RPM's controller for both the intact detector and the cut-off PMT, were recorded in order to examine any similarities in the temperature response of the intact detector and the PMT sans scintillator. In addition, a spectrum was collected every 30 minutes from the second stage output for the cut-off PMT.

Using the intact detector, one final experiment was performed in order to rule out that the RPM's electronics had any impact on the temperature sensitivity of the RPM detectors. In order to rule out that a poor design of the manufacturer's standard SCA amplifier chain exacerbated the temperature sensitivity of the RPM detectors, the detector was disconnected from the SCA completely. The detector was then connected to an ORTEC 113 Preamp &

ORTEC 672 Spectroscopy Amplifier, both of which are Nuclear Instrumentation Module (NIM) standard equipment. The signal from the intact detector's PMT was sent directly to the pre-amp. In addition, a high-voltage bias of 900 V was supplied to the PMT by the NIM standard equipment, completely bypassing the signal chain shown in Figure 3.1. During a temperature cycle similar to that of the initial cycle, the detector's background spectrum—after both stages of NIM amplification—was collected every 30 minutes by the Tukan MCA utilizing a 100-second live time acquisition. Unfortunately, the standard post-calibration ^{57}Co efficiency measurements were not performed using this NIM equipment. Therefore, it is difficult to conclude with certainty that this setup allowed the detectors to operate in a manner consistent with their behavior during the other experiments performed during these temperature tests.

Chapter 4: Results

4.1 First Round of Testing

The first round of testing performed at Oak Ridge National Laboratory (ORNL) focused on identifying the changes in a pedestrian RPM's behavior at temperatures between -30°C and 60°C. An emphasis was placed on the measurements performed at temperatures above 22°C because—according to experts at ORNL—commercial-off-the-shelf (COTS) heaters are often provided by the vendor when these systems are deployed in locations where low temperatures are common. For this round of testing, the entire RPM was placed inside the temperature chamber, meaning that no definite conclusions can be drawn from the results as to which system components are responsible for the temperature dependent behaviors exhibited during the testing. These results instead examine the entire system's general behavior over the temperature range. A comparison of the results of this test to the existing literature did, however, provide the foundation for the hypotheses tested during the second round of temperature tests. The results of the second set of temperature tests will be discussed in a later section of this research work.

Before results pertaining to the RPM system's performance are presented, it is necessary to show that the controlled chamber temperature actually affected the temperature that the RPM system components experienced. Much like the larger vehicle and train RPMs, the components of the pedestrian RPM are shielded from the environment by a sealed weather-tight metal enclosure. Therefore, the temperature inside the metal columns was not

directly controlled during the temperature cycle but was indirectly controlled due to heat transfer mechanisms such as conduction and convection. In order to demonstrate that at the time of each measurement the temperature inside the column was approximately equal to the chamber temperature, it is necessary to examine how long it takes the internal temperature to come within 1°C of thermal equilibrium with the chamber temperature.

Figure 4.1 shows an example of the internal temperature change in one of the RPM columns as the environmental chamber temperature stepped from 22°C to 30°C. From the figure, it can be seen that the temperature of the chamber stabilized at approximately 29°C after the first two hours. However, the temperature inside the RPM column does not approach equilibrium as quickly. Note that at zero time the RPM column's internal temperature is not equal to the chamber temperature; this difference is because the chamber had been at very-low temperatures before zero time in the figure, and the system had not reached thermal equilibrium before the temperature began changing.

As seen in the figure the difference between the internal column temperature and the chamber temperature increases as the chamber temperature begins to rise and does not begin to decrease again until the chamber temperature begins to stabilize at 30°C. The internal temperature is within 1°C of equilibrium with the chamber temperature until approximately five hours after the ramp begins. Remembering that the temperature ramps occurred over one-hour periods, this means that at the end of a four-hour soak, the internal temperature is within 1°C of the chamber temperature. Therefore, since each measurement occurred at the end of either a 4-hour soak or a 24-hour soak, it can be assumed that the temperature inside the weather-tight columns—and thus the ambient temperature enveloping the system

components—can be approximated to be equal to the chamber's temperature at the time of each measurement.
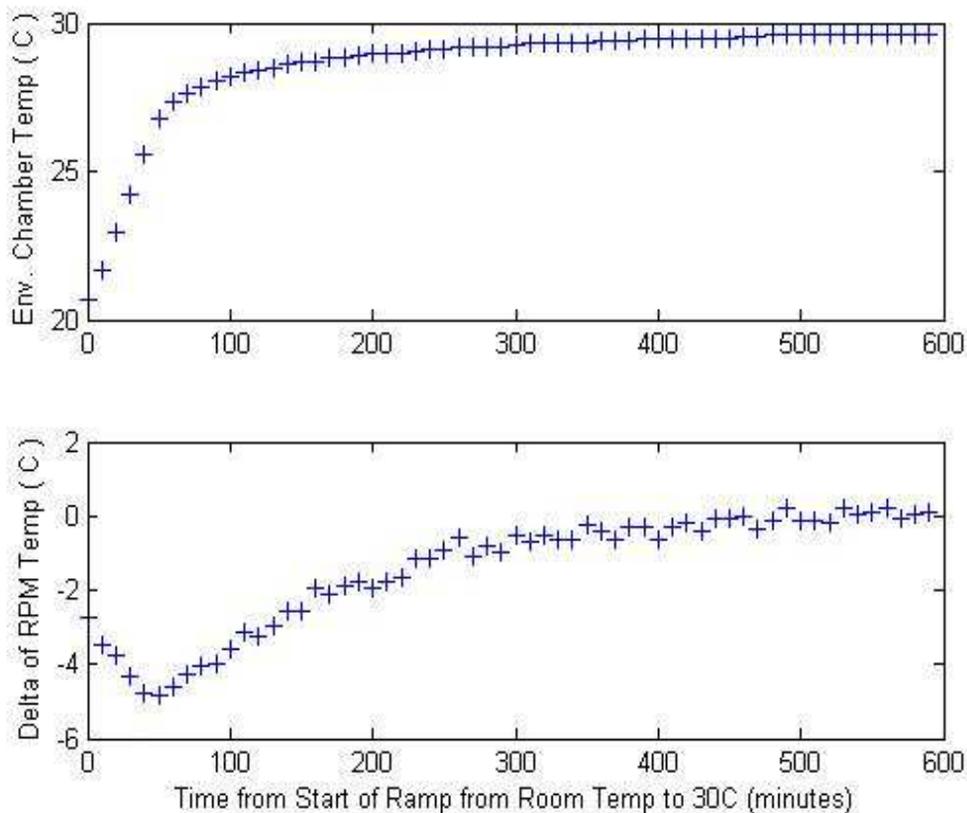
Figure 4.1: The temperature of the environmental chamber during a ramp from 22°C to 30°C, and the difference between this temperature and the internal temperature of the RPM's slave column. Figure is from previous report (Addington, Baird, & Chiaro,).

4.1.1 Temperature Dependence of Gamma Background Count Rate

The average background gamma count rates in counts per second (CPS) during the temperature cycle are shown in Figure 4.2 below. The average rates shown in the figure were calculated by averaging the count rate recorded by the controller every 200

milliseconds over successive five-minute periods. Average count rates are shown for all four

gamma detectors in the RPM and are referenced to the left vertical axis. In addition, a step-

like curve showing the ambient chamber temperature during the cycle is included and

referenced to the right axis. These two curves are time-synced, meaning that at each five

minute increment, the temperature corresponding to the count rates can be determined from

the step-like curve in the figure. It is clear from the figure that while the background count

rates do not vary significantly for low temperatures, they do vary at high temperatures,

sometimes very significantly. In three of the four detectors monitored, the backgrounds

increased dramatically as the temperature was increased from 50°C to 60°C. In addition, the

data for detector 3 fluctuates a great deal during each soak in spite of the fact that each data

point represents a five-minute average. Dramatic fluctuations in the recorded background

data, such as those seen here, could lead to an increase in false alarms when deployed in

operational environments.

There are two anomalies worth noting in the data presented in Figure 4.2 below that

are not a true reflection of the RPM's behavior during the test. The most noticeable is that the

average counts for detector 4 drop to zero counts per second in the final temperature soak at

22°C. This drop is because that particular detector was taken off-line in order to monitor the

high-voltage bias for that detector's PMT as the temperature cycled from the 60°C to 22°C.

The purpose of monitoring the high voltage was to determine if the dramatic increase in the

count rate was due to variance in the high-voltage detector bias as the temperature changed.

However, it will be shown in section 4.1.3 that there was no significant change in the

recorded voltage during the cooling off from 60°C to 22°C. The second anomaly is that there

is a visible gap in the data from the detectors during the temperature hold at -30°C. This gap corresponds to an overnight temperature hold during which the detector unexpectedly switched out of occupancy mode and began recording background scans, resulting in an inconsistency in how the count rate was reported.
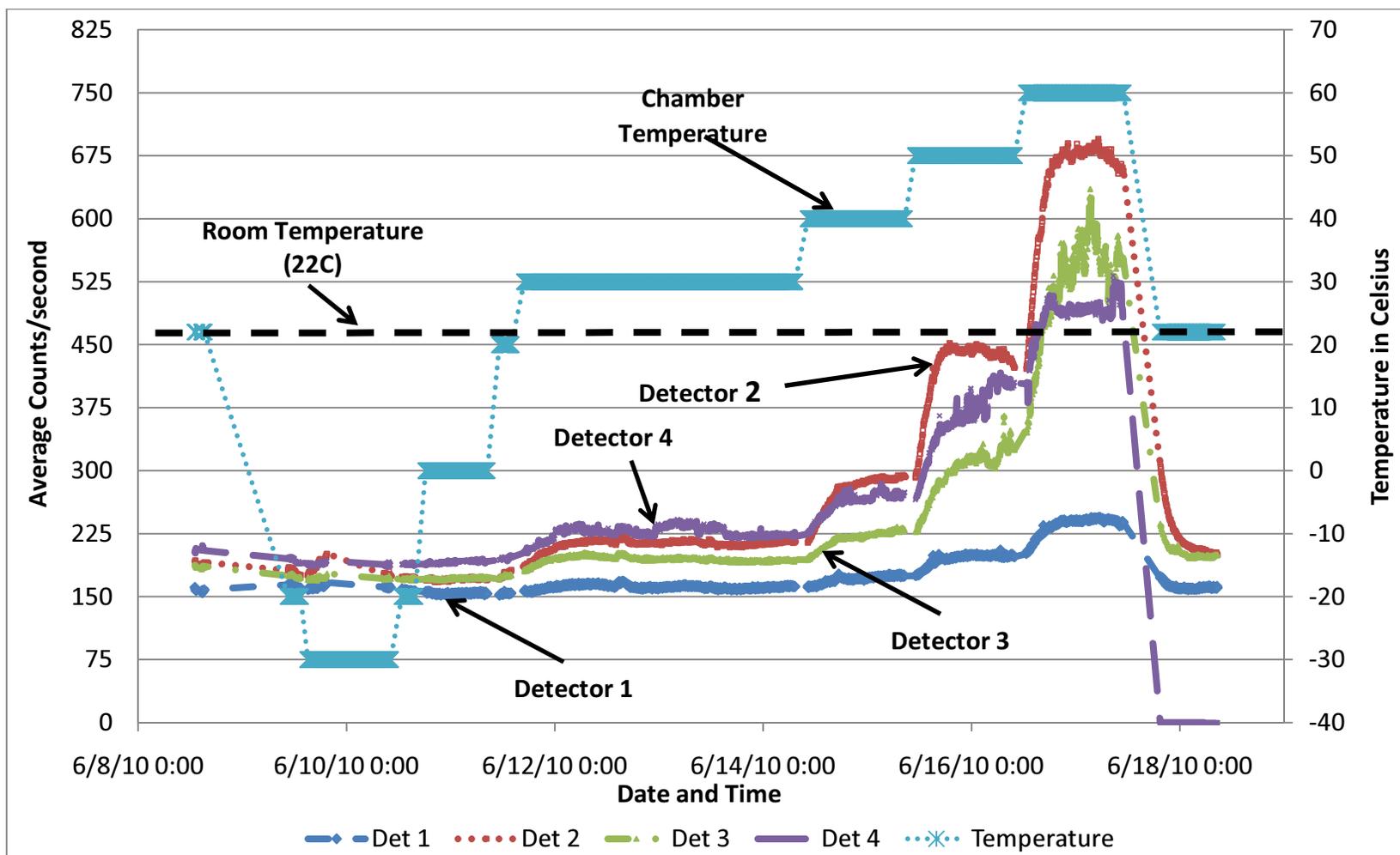
Figure 4.2: Average background gamma count rates of the pedestrian RPM during the temperature cycle.

The average background count rates at each temperature for detectors 1 and 2 are also shown in Table 4.1 below. Detectors 1 and 2 were chosen for closer examination because they were both located in the same RPM column, meaning that not only did they experience the same ambient temperature inside the column, but they also faced the same direction. Because the detectors faced the same direction, it can be reasonably assumed that the background radiation for both detectors should be consistent. Furthermore, because these detectors were in the same RPM column, they shared the same high-voltage supply and SCA board, thus eliminating any effect that differences in the RPM's electronics may have had on the count rates. Coincidentally, detectors 1 and 2 also represented the detectors with the smallest and largest increase in count rates respectively as the temperature reached 60°C.

Table 4.1: Average background levels for the least- and most-sensitive detectors as a function of temperature.

Chamber Temperature (°C)	Detector 1 Average Background (CPS)	Detector 2 Average Background (CPS)
22 (start)	160±10	190±10
-20	160±10	180±10
-30	160±10	180±10
-20	160±10	170±10
0	150±10	170±10
20	150±10	180±10
30	160±10	220±10
40	180±10	290±20
50	200±10	430±20
60	240±20	660±30
22	160±10	200±10

The statistical significance of the data presented in Figure 4.1 and Table 4.1 was tested using a two-way ANOVA test and showed with high confidence that the individual detector's count rates were dependent on both the detector characteristics and the temperature of the chamber. Thus, the results show that the gamma count rate of the RPM is temperature dependent.

4.1.2 Temperature Dependence of ^{57}Co and ^{137}Cs Efficiencies

In addition to recording the background count rates during the temperature cycle, the RPM's sensitivity to specific gamma sources was examined at each 10°C interval. This examination included the measurement of the ^{57}Co efficiency for detectors 1 and 2 at the end of each temperature soak. The numerical values of the ^{57}Co efficiencies for detectors 1 and 2 as a function of temperature are shown in Table 4.2 and Table 4.3 respectively. The table values for both detectors are summarized and presented in Figure 4.3. In each table, the first column represents the chamber temperature, the second column represents the average background count rate with no source in range of the detector, and the third column represents the count rate with the source placed on the door of the pillar in a location corresponding to the center of each individual detector's scintillator. The last two columns in each table represent two efficiencies calculated for each detector: the first is the calculation of the efficiency using the count rate data collected with the source on the door of the pillar, while the second is calculated using a correction factor to determine the expected equivalent efficiency if the source had been placed on the face of the scintillator. The correction factor accounts for solid angle differences and attenuation of the gamma rays by the aluminum door.

Table 4.2: Detector 1 Efficiency for ^{57}Co as a function of temperature.

Detector 1				
Chamber Temperature (°C)	Average Background (CPS)	Average Signal w/ Source (includes background) (CPS)	Estimated Efficiency (Solid Angle Corrected) (%)	Equivalent On-Contact Efficiency (%)
22 (start)	160±10	1090±30	19	22.3
-20	160±10	1340±40	23.9	27.2
-30	160±10	1370±40	24.5	27.8
-20	160±10	1330±40	23.7	27.1
0	150±10	1190±30	21	24.3
20	150±10	1130±30	19.6	23
30	160±10	1020±30	17.4	20.7
40	170±10	950±30	15.7	19
50	200±10	910±30	14.5	17.8
60	240±20	830±30	12.1	15.4
22	160±10	1070±30	18.5	21.8

Table 4.3: Detector 2 Efficiency for ^{57}Co as a function of temperature.

	Detector 2			
Chamber Temperature (°C)	Average Background (CPS)	Average Signal w/ Source (includes background) (CPS)	Estimated Efficiency (Solid Angle Corrected) (%)	Equivalent On-Contact Efficiency (%)
22 (start)	190±10	1090±30	18.1	22
-20	170±10	1280±40	22.3	26.2
-30	180±10	1290±40	22.5	26.4
-20	170±10	1240±40	21.6	25.5
0	170±10	1180±30	20.4	24.2
20	180±10	1110±30	18.8	22.7
30	220±10	1030±30	16.5	20.4
40	290±20	1050±30	15.2	19.1
50	430±20	1110±30	13.9	17.7
60	660±30	1250±40	12	15.9
22	200±10	1070±30	17.5	21.4
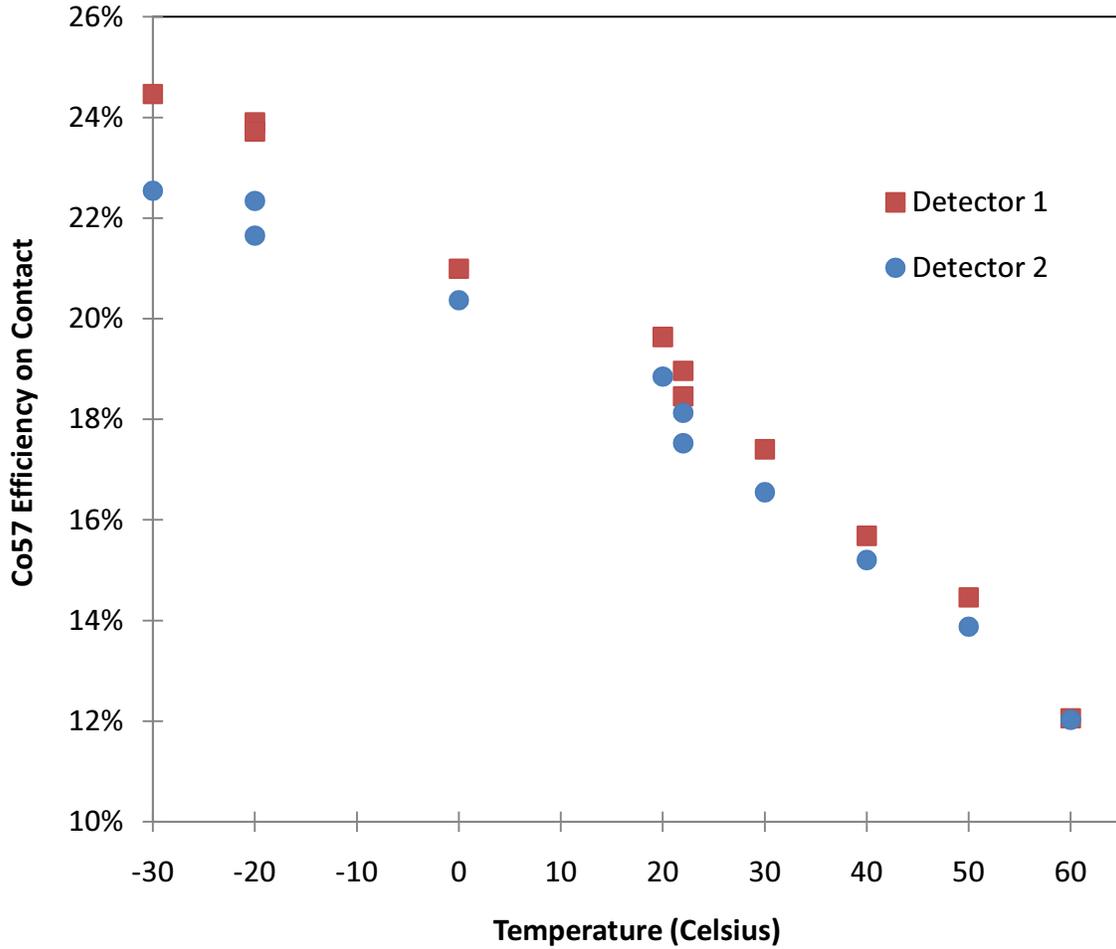
Figure 4.3: ^{57}Co efficiency as a function of temperature for detectors 1 and 2.

It is clear from Figure 4.3 that the measured ^{57}Co efficiency for both detectors decreases with temperature with an almost linear trend. A regression analysis was performed on the ^{57}Co efficiency, revealing that a second order term is statistically significant. However, a linear regression is more suitable for in-the-field calculations, and a linear

regression analysis revealed a significant fit with an adjusted R^2 value of 0.9449. Therefore, a linear fit to the data was chosen, and the resulting equation for estimating the efficiency of this RPM system over the temperature range of -30°C to 60°C is presented in Equation (4.1).

$$\eta(\%) = (20.538 \pm 0.212) - (0.124 \pm 6.5 \times 10^{-3}) * T$$

where:

$\eta = $ Efficiency in %

$T = $ Temperature in Celsius

(4.1)

In addition to [57]Co, the sensitivity of the gamma detectors was also examined for a ^{137}Cs source during a subset of the temperature holds. The measured efficiencies for ^{137}Cs shown in Table 4.4 and Table 4.5 are much lower than the [57]Co efficiencies presented early in Table 4.2 and Table 4.3. The lower efficiency is because the count rates used to calculate the efficiencies were taken from the RPM's default electronics. These electronics, specifically the SCA used to determine the range of gamma energies counted, are calibrated in order to maximize sensitivity to [57]Co. Thus, the higher energy ^{137}Cs gammas created pulse heights which were out of the SCA's discriminated region, resulting in a lower ratio of the number of detected gammas to the number of expected gammas.

Table 4.4: Detector 1 estimated solid angle corrected detection efficiency for ^{137}Cs as a function of temperature.

		Detector 1	
Chamber Temperature (°C)	**Average Background (CPS)**	**Average Signal w/ Source (includes background) (CPS)**	**Estimated Efficiency (Solid Angle Corrected) (%)**
-30	160±10	1370±40	5.7%
20	150±10	1130±30	6.1%
30	160±10	1020±30	6.3%
40	170±10	950±30	6.5%
50	200±10	910±30	6.8%
60	240±20	830±30	7.1%
22	160±10	1070±30	6.3%

Table 4.5: Detector 2 estimated solid angle corrected detection efficiency for ^{137}Cs as a function of temperature.

		Detector 2	
Chamber Temperature (°C)	**Average Background (CPS)**	**Average Signal w/ Source (includes background) (CPS)**	**Estimated Efficiency (Solid Angle Corrected) (%)**
-30	180±10	1290±40	5.4%
20	180±10	1110±30	5.6%
30	220±10	1030±30	5.7%
40	290±20	1050±30	5.9%
50	430±20	1110±30	6.3%
60	660±30	1250±40	6.4%
22	200±10	1070±30	6.0%

Table 4.4 and Table 4.5 also reveal that the ^{137}Cs detection efficiency for both detectors increases as temperature increases. This trend is the opposite of the trend seen in the previous examination of the ^{57}Co detection efficiency for both detectors. The explanation of the different effect that temperature has on the ^{57}Co and ^{137}Cs efficiency will be discussed in sections 0 and 4.1.1. The table values of the ^{137}Cs efficiency for both detectors is summarized and presented in Figure 4.4 below. Notice that compared to the curve representing the ^{57}Co efficiency in Figure 4.3 above, the curve representing the ^{137}Cs efficiency is relatively flat. This suggests that the detectors' sensitivity to higher energy gamma rays is not as temperature dependent as the sensitivity to low energy gammas like ^{57}Co. In addition, the trend of increasing ^{137}Cs efficiency with increasing temperature is clear in Figure 4.4 and contrasts with the opposite trend seen in Figure 4.3 for ^{57}Cs efficiency.
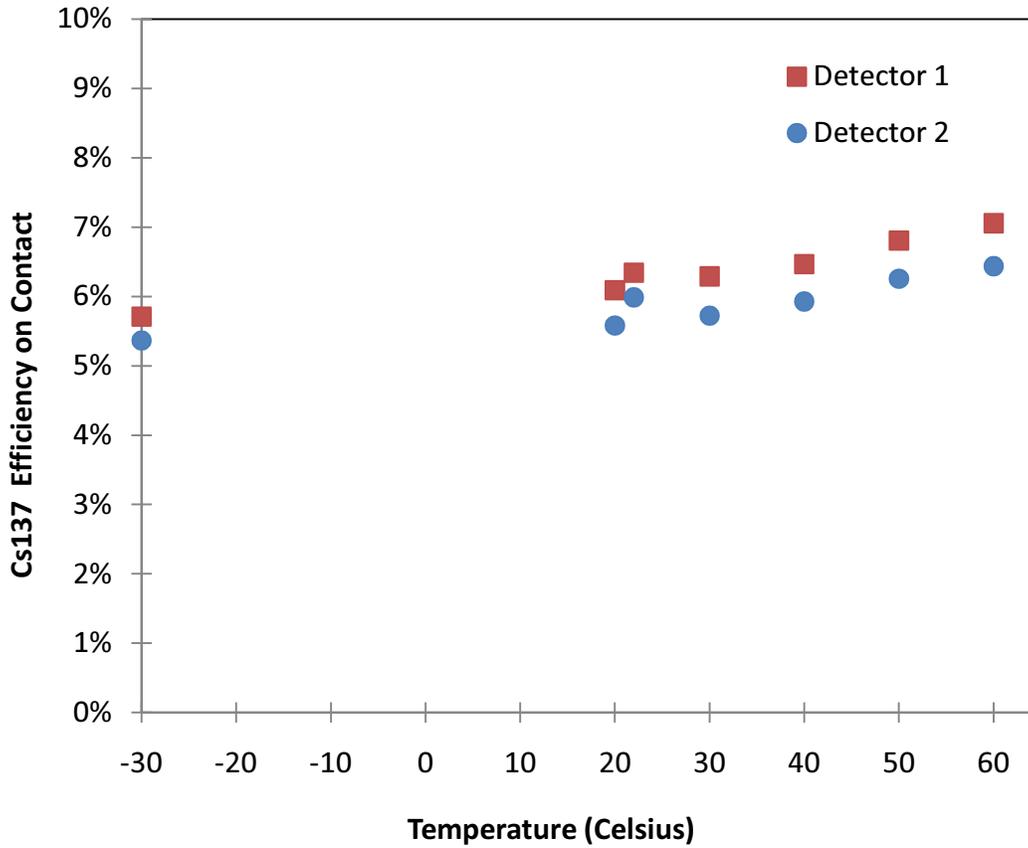
Figure 4.4: ^{137}Cs efficiency as a function of temperature for detectors 1 and 2.

4.1.3 Temperature Dependence of the Compton Edge Position

In addition to measurements utilizing the count rate from the RPM's built-in electronics, spectra were acquired at selected temperatures using a Tukan-8K multi-channel analyzer (MCA). Spectra for the background and for ^{137}Cs were acquired for detectors 1 and 2. The spectra were collected from the output of the second stage amplifier with the Tukan MCA set for a 300-s live acquisition time. The resulting background-subtracted spectra, or

net spectra, are shown for detector 1 in Figure 4.5 and for detector 2 in Figure 4.6. By examining the net spectra, the response of the detector to the gamma source can be distinguished better than it can be from gross spectra which include the counts from both the gamma source and natural background radiation. It is often useful in PVT scintillator based detectors such as these to discuss the location of the Compton edge of the ^{137}Cs signal. The meaning of the Compton edge is discussed in the Literature Review of this work, and while it is difficult to pinpoint the exact location of the Compton edge in the spectra shown in Figure 4.5 and Figure 4.6, it can be approximated as the location to the right of the "hump" of each spectrum at two-thirds of the maximum height of the "hump." It is clear from the figure that the position of the Compton edge moves with the entire continuum as it shifts with temperature.

Figure 4.5 and Figure 4.6 show that, while there are slight differences between the behaviors of the two detectors, a trend in the overall response to temperature is consistent for both detectors. Using the spectra collected at 22°C as a reference, it is clear that the spectra compress as the temperature increases above 22°C, shifting the entire Compton continuum of each detector to the left. Furthermore, the spectra collected at -30°C show that at low temperatures, the Compton continuum is smeared over a broader channel range than that of the spectra collected at 22°C.
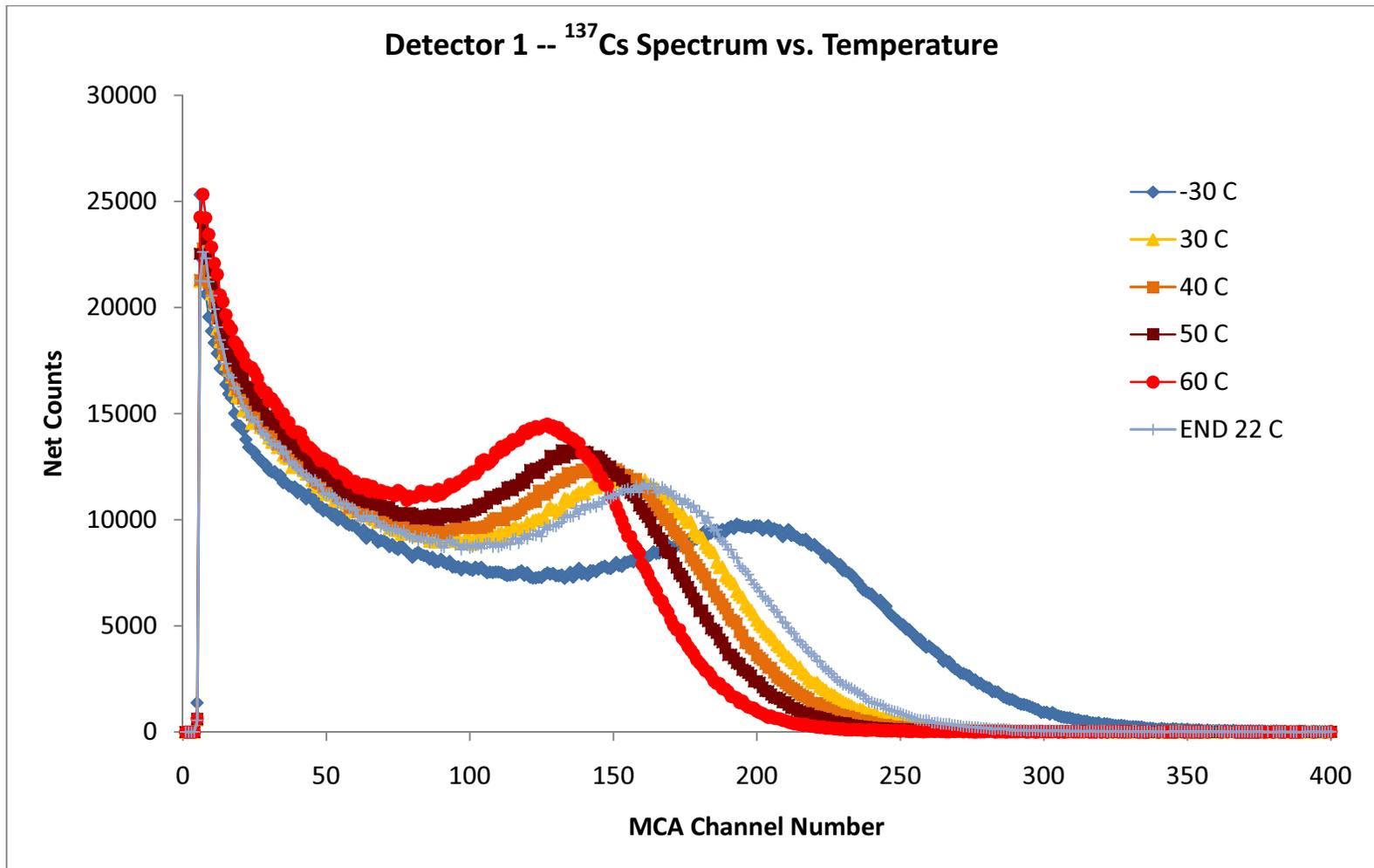
Figure 4.5: Net ^{137}Cs spectrum as function of temperature for detector 1.
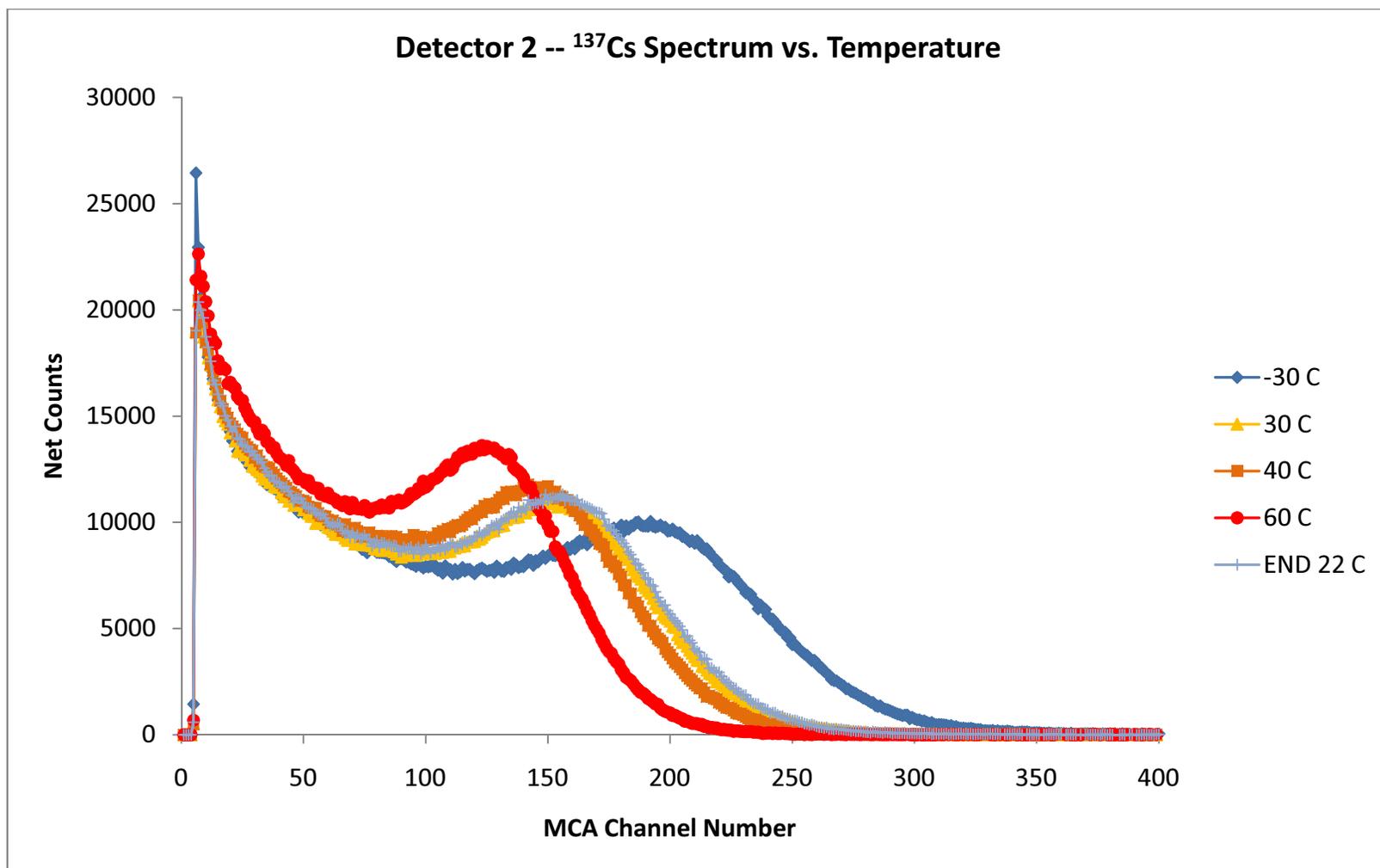
Figure 4.6: Net ^{137}Cs spectrum as function of temperature for detector 2.

Table 4.6 and Figure 4.7 below quantify the change in position of the Compton edge as a function of temperature. The table and figure add clarity to the discussion of the spectra's temperature dependent shifts shown in Figure 4.5 and Figure 4.6, and reiterate that the Compton edge shifts left with increasing temperature and shifts right with decreasing temperature. Since the position of the Compton edge is an indication of the gain of the system, these shifts imply that the gain decreased as the temperature increased, and increased as the temperature decreased.

Table 4.6: Tukan MCA channel position of the Compton edge of the ^{137}Cs Spectra as a function of temperature.

Temperature (°C)	-30	22	30	40	50	60
Detector 1	238	193	185	176	166	153
Detector 2	230	188	187	177	N/A	152
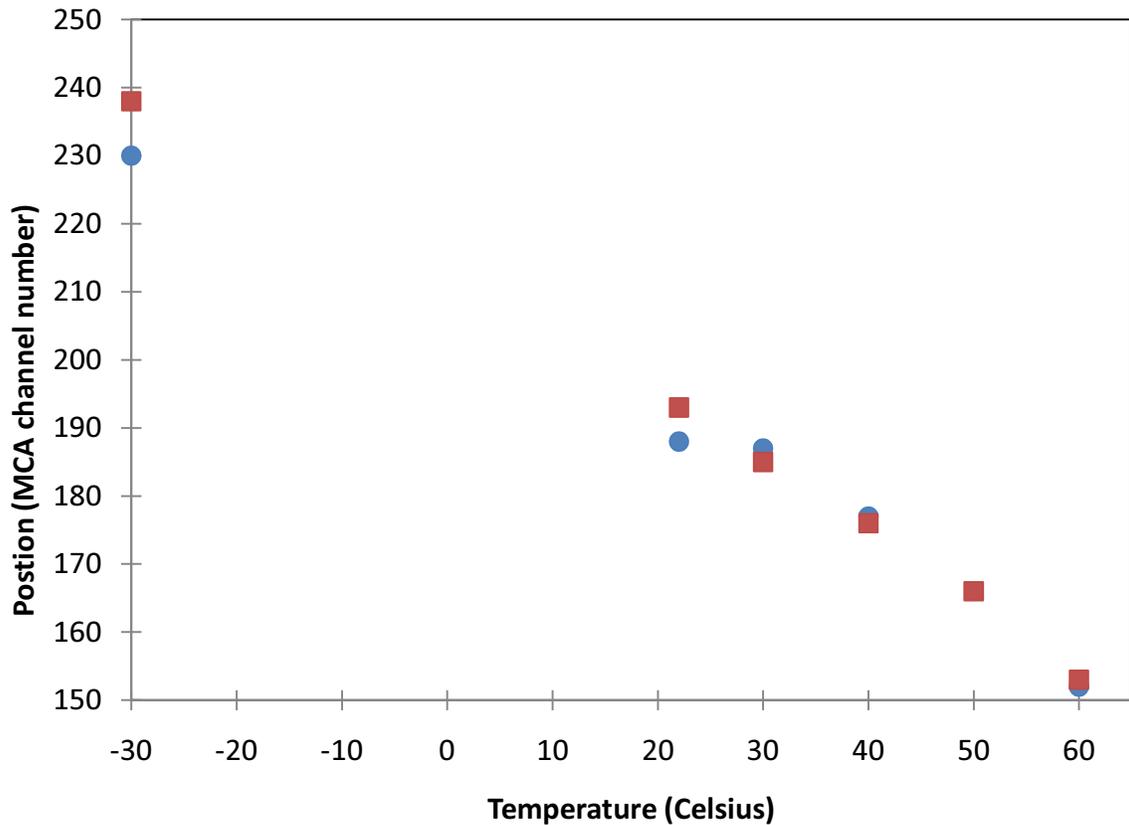
Figure 4.7: Compton edge of ^{137}Cs as a function of temperature.

This behavior in the peak shift has been observed in previous studies outlined in the
Literature Review of this work (Ball et al., 1957; Kinard, 1957; Singh & Wright, 1987).
These studies demonstrated that the pulse height collected from a detector very similar to the
one used in this RPM, decreased with increasing temperature, and suggested that, while the
PVT scintillator plays some role, the PMT is most likely responsible for this behavior.

It is worth noting in Figure 4.7 that even though these two detectors represented the two extremes in temperature sensitivity of the background count rate, the changes in the Compton edges as a function of temperature, and thus the gains, were very similar. In fact, both detectors appear to have a linearly decreasing trend with increasing temperature. A two-way ANOVA test confirmed that the Compton edge position was temperature dependent with a P-value of less than 0.0001, but the position did not significantly vary between detectors, yielding a P-value of 0.3551 for the relationship between the individual detector and the Compton edge position. This indicates that other RPM systems which use the same type of PVT based detectors would likely exhibit the same behavior.

Furthermore, a regression analysis of the Compton edge data confirmed that the position of the Compton edge, and thus the system's gain, does vary linearly with temperature. The calculated regression equation had an adjusted R^2 value of 0.9894 and is shown in Equation (4.2) below.

$$CE = (216 \pm 4.2) - (1 \pm 2.6) * T$$
where:
CE = Compton Edge Channel Number
T = Temperature in Celsius

(4.2)

While only valid for this particular RPM system and the specific Tukan MCA used, the regression analysis for this data suggests a method for determining the magnitude of the temperature dependent gain shifts in detectors similar to the coupled PVT scintillator and PMT type detectors used in this system. By providing a model for the temperature dependence of the gain, the possibility exists for advanced electronics which compensate for these shifts through changes in high-voltage bias or discriminator voltages. If the appropriate

71

adjustments could be made as the temperature varied, it is reasonable to assume that an improvement in the stability of the efficiencies could be attained.

As alluded to in section 4.1.2, the temperature dependence of the gain explains the temperature dependence of the efficiencies, particularly that of ^{57}Co. Since the gain of the system determines the energy-to-voltage calibration of the detector, any change in the gain means that for fixed upper-level discriminator (ULD) and lower-level discriminator (LLD) voltages the energy window of the discriminator is changed. As the energy window moves, the range of gamma energies to which the detector is most sensitive changes as well.

An example of this relationship between sensitivity and gain can be shown using the ^{137}Cs Compton edge channel values presented in Table 4.6. Recalling that the alignment procedure at the beginning of testing set the Compton edge of ^{137}Cs to 2.0 V, and that the energy of the Compton edge of ^{137}Cs is 480 keV, the voltage per channel and energy per channel for the MCA can be determined. Using the average channel value of 191 for the Compton edge of ^{137}Cs at 22°C and equating this channel position to 2.0 V and 480 keV, the channel-to-voltage conversion ratio is determined to be 10.5 mV per channel, while the channel-to-energy ratio is determined to be 2.51 keV per channel. Based on this, the LLD of 0.063 V corresponds to channel 6 in the MCA spectra and approximately 15 keV of gamma energy deposited in the scintillator. Similarly, the ULD of 0.455 V corresponds to channel 43 and approximately 108 keV. By repeating this calculation for each temperature interval, the gamma energy range to which the detector is most sensitive was calculated. The results are show in Table 4.7.

Table 4.7: Temperature dependence of the energy range corresponding to the SCA discriminator region.

Temperature (°C)	Compton Edge Position (Average Channel)	LLD Energy (keV)	ULD Energy (keV)
-30	234	12.308	88.205
22	191	15.118	108.346
30	186	15.484	110.968
40	177	16.317	116.941
50	166	17.349	124.337
60	153	18.885	135.344

Because of the design of the RPM, the count rate reported from the RPM's electronics represents only the counts resulting from gamma interactions within the scintillator which deposit energy amounts within the energy range of the SCA's discriminator. Therefore, because the efficiencies were calculated using the RPM's reported count rate, as the energy moved, the calculated efficiencies changed. For the higher-energy ^{137}Cs gamma rays, the efficiency of the detectors increased as the energy window moved to higher energies with increasing temperature, but the efficiency of the detectors decreased for the low-energy ^{57}Co gamma rays as the temperature increased. The effect that this change had on the ^{57}Co efficiency is discussed in more detail in section 4.1.1.

4.1.1 Temperature Dependence of ^{57}Co Spectra

In the same manner which the 137Cs spectra were collected, 57Co spectra were collected at each temperature interval as well. The same resolution issues exist in these spectra that exist for the 137Cs spectra, namely that the spectra represent the Compton continuum where the Compton edge is smeared over a range of channels. The Compton edge of 57Co is approximately equal to 40 keV; therefore, the Compton continuum is located in lower-energy channels. The 57Co spectra in these channels of interest are shown in Figure 4.8 and Figure 4.9.

The magnitude of the spectra reveals that there was not a significant difference for either detector in the number of ^{57}Co gamma rays detected at each temperature. Recalling that the counts recorded by the MCA are not limited by the SCA's discriminator, this consistency in the magnitude of the spectra rules out the possibility that the difference in the ^{57}Co efficiencies measured at different temperatures is related to a physical difference in the number of gamma rays which interact in the scintillator. Furthermore, the vertical scale of the two are the same, which is consistent with the results discussed previously for Table 4.2 and Table 4.3 which showed there was very little difference in the efficiencies of the individual detectors when both were at the same temperature.

Also, it is clear from the spectra in Figure 4.8 and Figure 4.9 that the ^{57}Co spectra exhibit temperature dependence similar to the ^{137}Cs spectra: As the temperature increases, the Compton continuum is compressed to fewer low-energy channels. Again, because the discriminator region remains fixed by the voltage of the LLD and ULD, only the counts which fall between channels 6 and 43 of the spectra collected by the MCA are counted by the

system. It is clear that as the ^{57}Co spectrum is shifted to the right at low temperatures, more of the spectrum falls in the MCA window between channels 6 and 43 which correspond to the voltage range used by the RPM's discriminator (0.063 V to 0.455 V). Conversely, as the spectrum is shifted to the left, fewer counts fall in this MCA window. This accounts for the change in the ^{57}Co efficiency discussed in section 4.1.2.
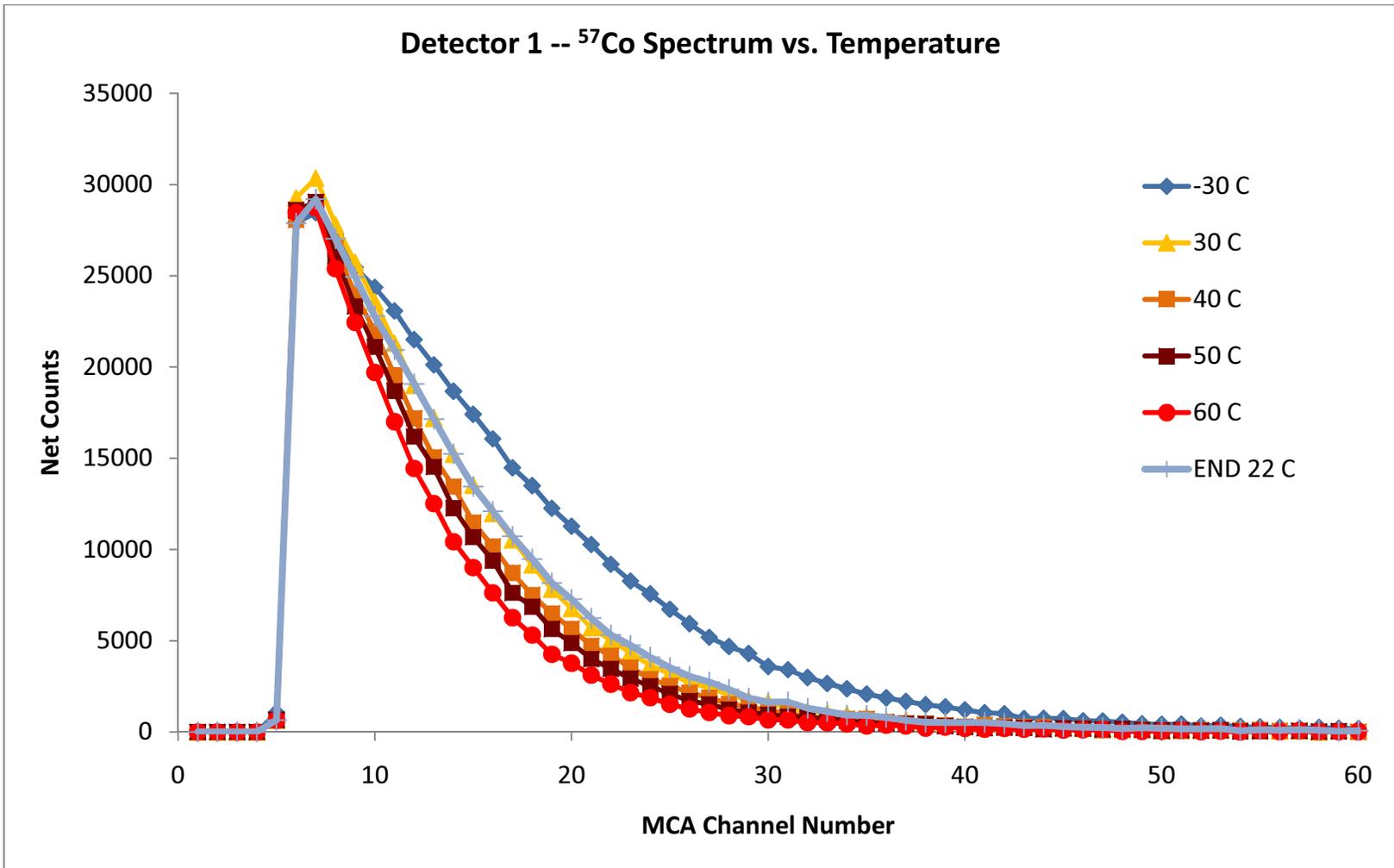
Figure 4.8: Net ^{57}Co spectrum as function of temperature for detector 1.
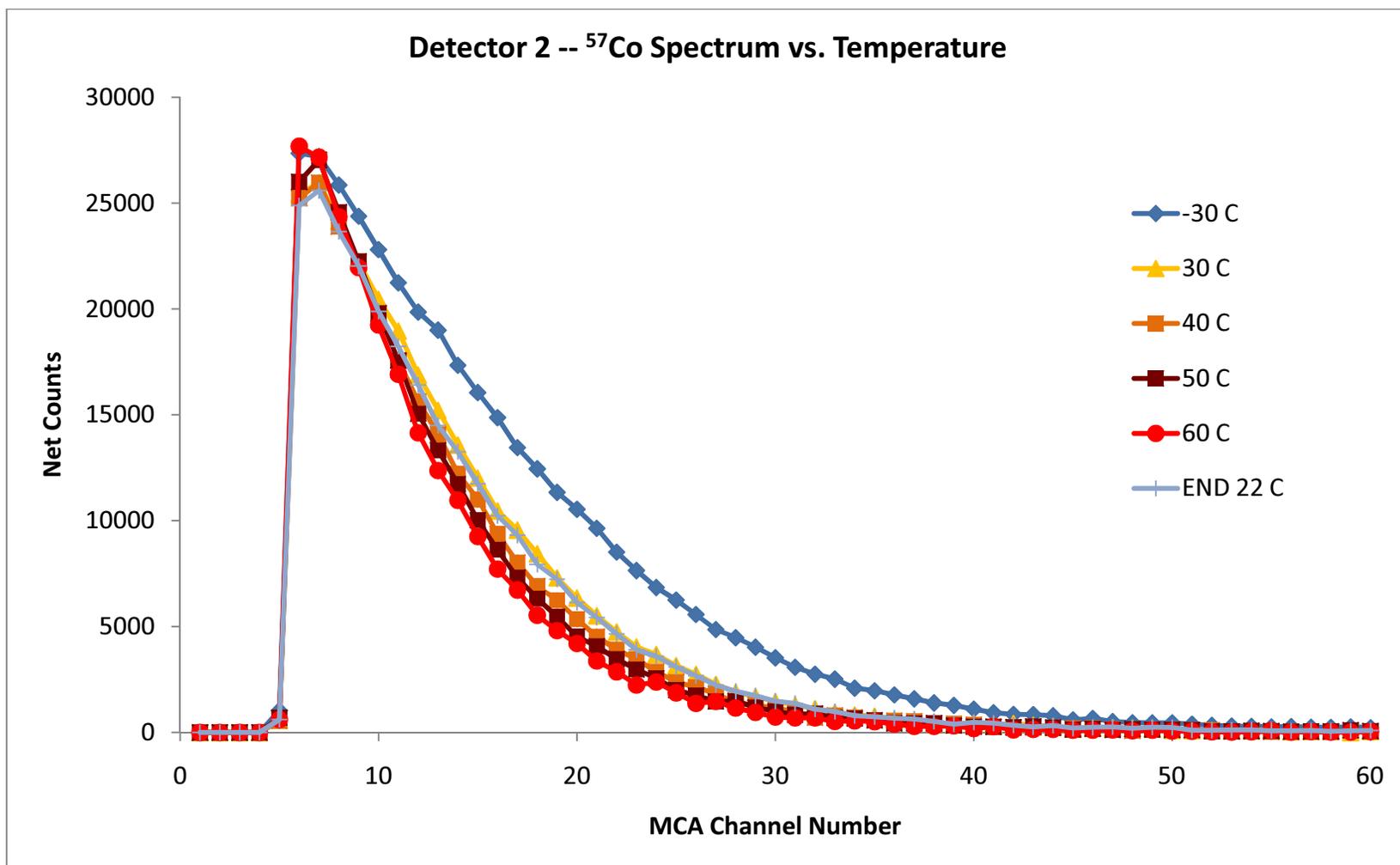
Figure 4.9: Net ^{57}Co spectrum as function of temperature for detector 2.

More detail on the impact that the shifts in the ^{57}Co spectra have on the efficiency is gained by comparing the count rate recorded by the RPM's electronics during the efficiency calculations to an estimated count rate calculated by integrating the spectra over the channels which represent the SCA's discriminator region (channels 6-43). By integrating the ^{57}Co spectra in Figure 4.8 and Figure 4.9, and correcting for an average of 4% SCA dead time, an estimated count rate can be determined which should match the count rate reported by the RPM's electronics. The results of this calculation are shown in Table 4.8.

Table 4.8: Comparison of the net count rate for ^{57}Co source as recorded by the RPM electronics and as calculated from the MCA spectra.

		Detector 1	
Temperature (°C)	Net ^{57}Co Count Rate from RPM Electronics (CPS)	Estimated Net Count Rate from ^{57}Co Net Spectra (CPS)	Percent Difference (%)
-30	1210±30	1170±30	3.49%
22	910±30	910±30	0.47%
30	860±30	900±30	4.81%
40	780±30	800±30	3.30%
50	720±30	750±30	4.79%
60	600±20	570±20	4.04%
		Detector 2	
Temperature (°C)	Net ^{57}Co Count Rate from RPM Electronics (CPS)	Estimated Net Count Rate from ^{57}Co Net Spectra (CPS)	Percent Difference (%)
-30	1120±30	1090±30	1.98%
22	870±30	870±30	0.10%
30	820±30	810±30	1.48%
40	750±30	740±30	1.89%
50	690±30	710±30	3.66%
60	600±20	580±20	2.18%

The results in Table 4.8 show that the count rate calculated from integrating the spectra over a fixed channel window corresponding to the RPM's default discriminator window match the count rate reported by the RPM within a few percent. All but a few of the differences are within one standard deviation of the count rate, and all are within two standard deviations. Given that gamma radiation interactions are expected to follow a Poisson distribution, the difference between the calculated count rate and the recorded count rate is within the expected error associated with gamma radiation counting.

The results of integrating the spectra reiterate that the temperature dependence of the detectors' ^{137}Cs and ^{57}Co efficiencies is clearly a result of the temperature dependent gain shifts associated with these types of detectors. Furthermore, because the energy deposited in the scintillator by ^{57}Co is in the low-energy range (up to approximately 40 keV), this makes the detector's sensitivity to ^{57}Co and other low-energy sources such as highly enriched uranium (HEU) even more susceptible to changes in the sensitive energy window of the RPM that are shown in Table 4.7.

4.1.2 Temperature Dependence of Background Spectra

In addition to spectra collected with gamma sources placed in the detection area of each of the RPM's detectors, a background spectrum was taken for detector 1 and 2 at each temperature interval as well. These background spectra for detector 1 are shown in Figure 4.10 and for detector 2 are shown in Figure 4.11. Note that in the figures, only the first 100 channels of the spectra are shown because everything beyond this range is dominated by system noise when the count rate remains low—as is the case with background count rates.

Both detectors show an increase in low-energy background counts as the temperature increases. Furthermore, the increase for detector 2 is greater than for detector 1 for the spectra collected at 50°C and 60°C, as can be seen in the difference in the vertical axis scale between the two figures corresponding to each detector.

Both the increase in spectrum counts and the extreme nature of the increase for detector 2 in Figure 4.11 are consistent with the increase in the background count rate reported by the RPM and discussed in section 4.1.1. Furthermore, the very-low-energy channels where the most dramatic increases are located suggest that the increases are due to dark current noise being produced by the PMT.   This hypothesis was tested in the second round of temperature tests and will be discussed in section 4.2.5 below.
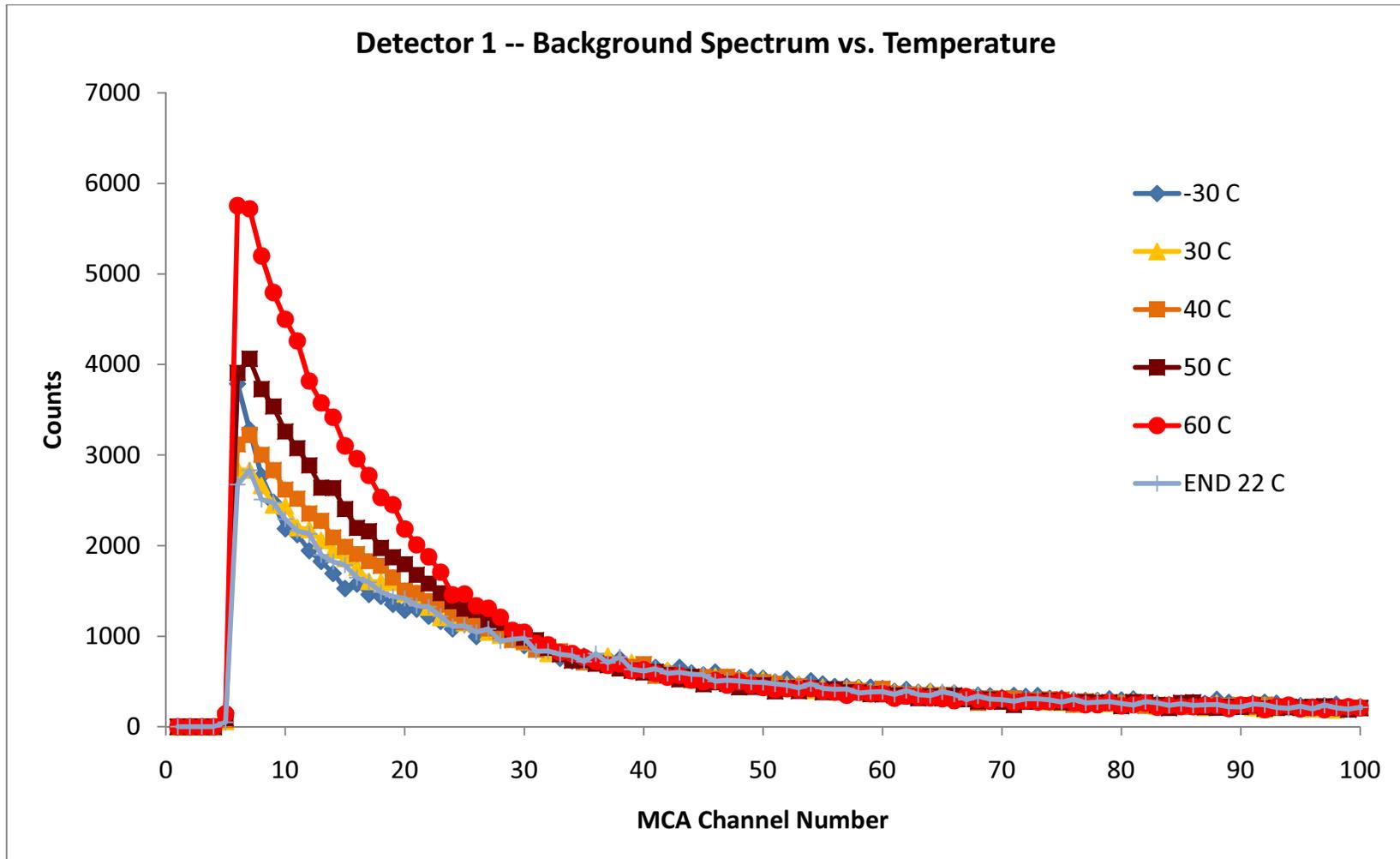
Figure 4.10: Background spectrum at each temperature for detector 1.
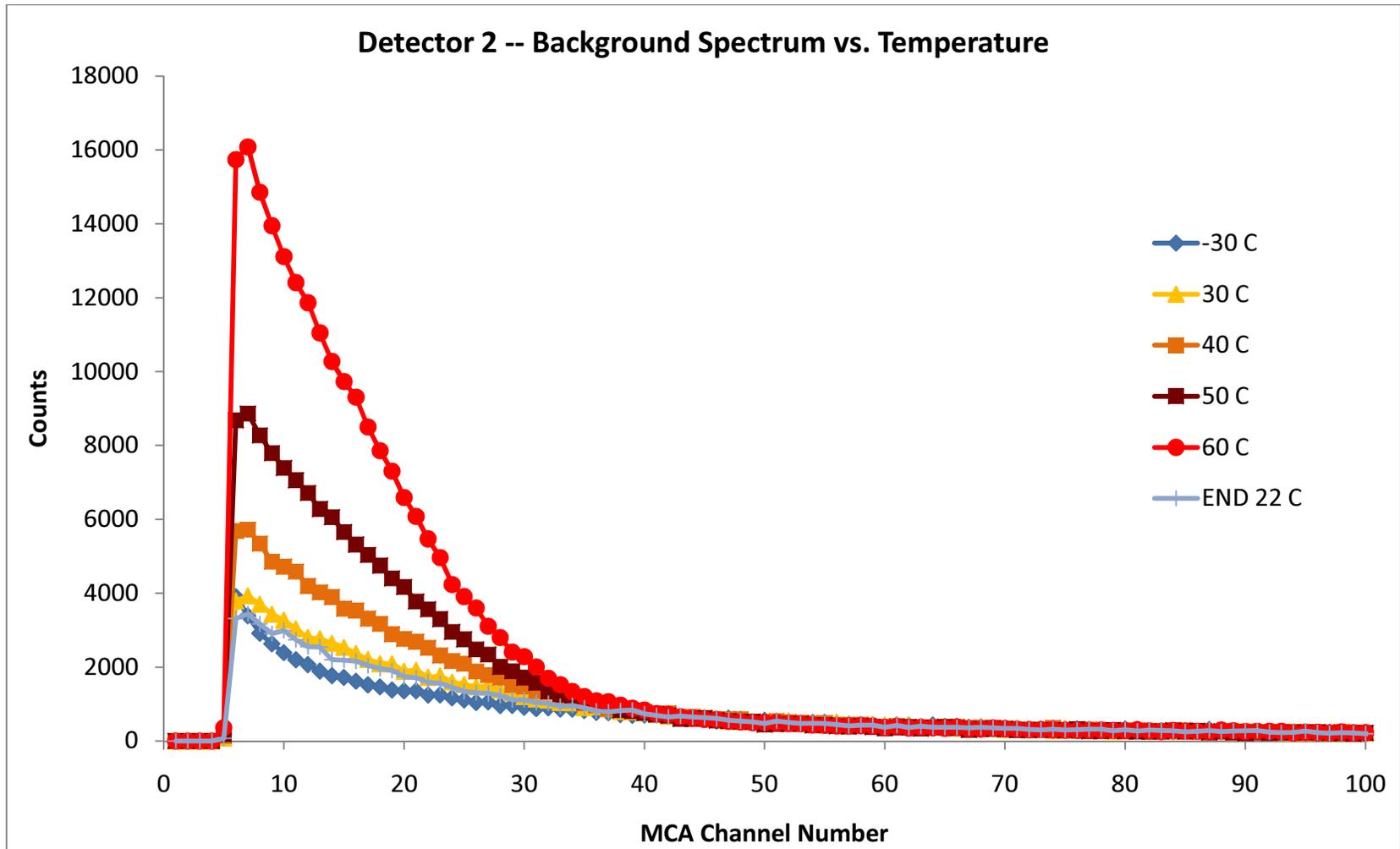
Figure 4.11: Background spectrum at each temperature for detector 2.

4.1.3 Temperature Dependence of the Discriminator Voltages and the High-Voltage Bias

Many of the results discussed in the previous sections are based on the assumption that the discriminator window remained fixed during the temperature cycle. In order to prove that this was the case, the voltages at several critical check points inside the system's SCA were monitored during the tests. Specifically, the voltages which determine the SCA discriminator region were monitored and are shown in Table 4.9 below.

Table 4.9: The lower- and upper- level discriminator voltages as a function of temperature.

	Chamber Temperature (°C)	Gamma LLD (Volts)	Gamma ULD (Volts)
Pre-Test	22	0.063	0.458
Testing Phase	-20	0.061	0.459
	-30	0.061	0.459
	-20	0.062	0.459
	0	0.062	0.459
	20	0.063	0.459
	30	0.063	0.458
	40	0.063	0.458
	50	0.063	0.458
	60	0.063	0.458
Post-Test	22	0.063	0.458

Clearly, the results in Table 4.9 demonstrate that there was no significant drift in the reference voltages for the LLD and ULD, so it can be assumed that there was no drift in the

discriminator region as defined in volts. Since the discriminator examines the voltage of the pulse amplitude coming out of the second stage amplifier, the same range of pulse voltages is counted by the discriminator. However, the gain shifts discussed in section 0 result in shifts in the range of gamma energies necessary to produce a pulse voltage which falls between the LLD and ULD voltages. Thus, even if there is no change the LLD and ULD voltages, there can still be a change in the gamma-energy window corresponding to the discriminator region.

In addition to monitoring the discriminator reference voltages, the high-voltage bias for detectors 4's PMT was also periodically measured at the end of the cycle as the chamber temperature cooled from 60°C to 22°C. Since the high-voltage bias is a factor in determining the gain of the detectors, it is necessary to point out any change in the high voltage which occurs as the temperature changes. The voltage was monitored overnight as the chamber cooled using a DVR, and examined the next morning upon arrival. The results are summarized in Table 4.10. While there was a small decrease of approximately 0.3% in the high-voltage setting, which according to common PMT reference manuals could shift the gain by a small amount, the decrease is not sufficient to be the dominant cause of the gain shifts discussed in the previous sections of this work (Hamamatsu, 2006).

Table 4.10: High-voltage bias for detector 4's PMT as a function of temperature.

Date	Time	Chamber Temperature (°C)	PMT Voltage (V)
6/17/2010	11:37 AM	60	1072.4
	12:23 PM	60	1072.5
	1:30 PM	53	1072.6
	2:00 PM	51.5	1072.9
	2:25 PM	50.6	1072.9
	2:55 PM	49.6	1073
	3:22 PM	48.5	1073.1
	3:36 PM	48.2	1073.2
	4:01 PM	47.3	1073.4
	VOLTAGE AFTER 4:05 PM RECORDED ON VIDEO (DVR)		
6/18/2010	voltage reached stability at approximately 10:30PM		
	8:10 AM	22	1075.5
	10:41 AM	22	1075.5

4.2 Second Round of Testing

The second round of testing performed at ORNL was intended to explore the temperature dependence of the gamma radiation detectors found in RPM systems similar to the pedestrian RPM system tested in the first round of testing. Specifically, the experiments performed during the second round of testing look to explain the temperature dependence of the gamma detectors' count rates. This temperature dependence was identified in the first round of testing and discussed in section 4.1.1 of this research work. In addition, a similar phenomenon was observed in data taken from a deployed rail RPM, providing additional motivation to re-examine the temperature dependence of gamma detectors.

The data collected from the deployed rail RPM revealed oscillations in the gamma background count rates in all four detectors, each having a 24-hour oscillatory period. The maximum count rate for each detector occurred daily in the late afternoon hours, while the minimum count rate for each detector occurred daily in the early morning hours. Given that the warmest and coolest times of the day are generally during the afternoon and early morning respectively, these oscillations appeared consistent with the results discussed in section 4.1.1 of this work. Those results demonstrated that an increase in temperature caused an increase in the gamma background count rate. Furthermore, recall from the Experimental Setup and Procedures chapter of this thesis, that the rail RPM uses the same electronics and the same detector design as the pedestrian RPM tested in round one of the temperature testing. All the results in this section are from temperature testing performed on the actual gamma detectors from the deployed rail RPM system that produced the oscillating background count rate data.

4.2.1 Re-examination of the Temperature Dependence of the Gamma Background Count Rate

The first hypothesis for this set of experiments was that the count rate oscillations observed in field data for these specific gamma detectors were due to the temperature dependence of the background count rate identified in the first round of temperature tests. Furthermore, it was hypothesized that the temperature dependence of the background count rate could be reproduced when only the PVT scintillators and their coupled PMTs were placed inside the cycling temperature and all other electronics were maintained at the

laboratory's room temperature (approximately 22°C). The resulting background count rates

for both detectors during the initial temperature cycle between 22°C and 50°C are shown in

Figure 4.12 below. The average count rates in the figure are referenced to the left vertical

axis and represent the average gamma counts per second (CPS) as recorded by the RPM's

default controller, averaged over successive one minute periods. In addition, the figure also

contains a plot of the chamber temperature in Celsius during the cycle that is referenced to

the right vertical axis.

Clearly the background count rates in Figure 4.12 vary significantly with temperature.

Consistent with the behavior observed in the first round of testing, as the temperature

increases the background count rates for both gamma detectors also increase. Slight increases

in the count rates at temperatures below 40°C are noticeable, but it is during the hold at 40°C

that the background count rate experiences a significant increase, followed by an exaggerated

increase while the temperature rises and holds at 50°C. Furthermore, as the chamber

temperature cycles down from 50°C to 22°C, the background count rates also decrease to

their pre-cycle values.
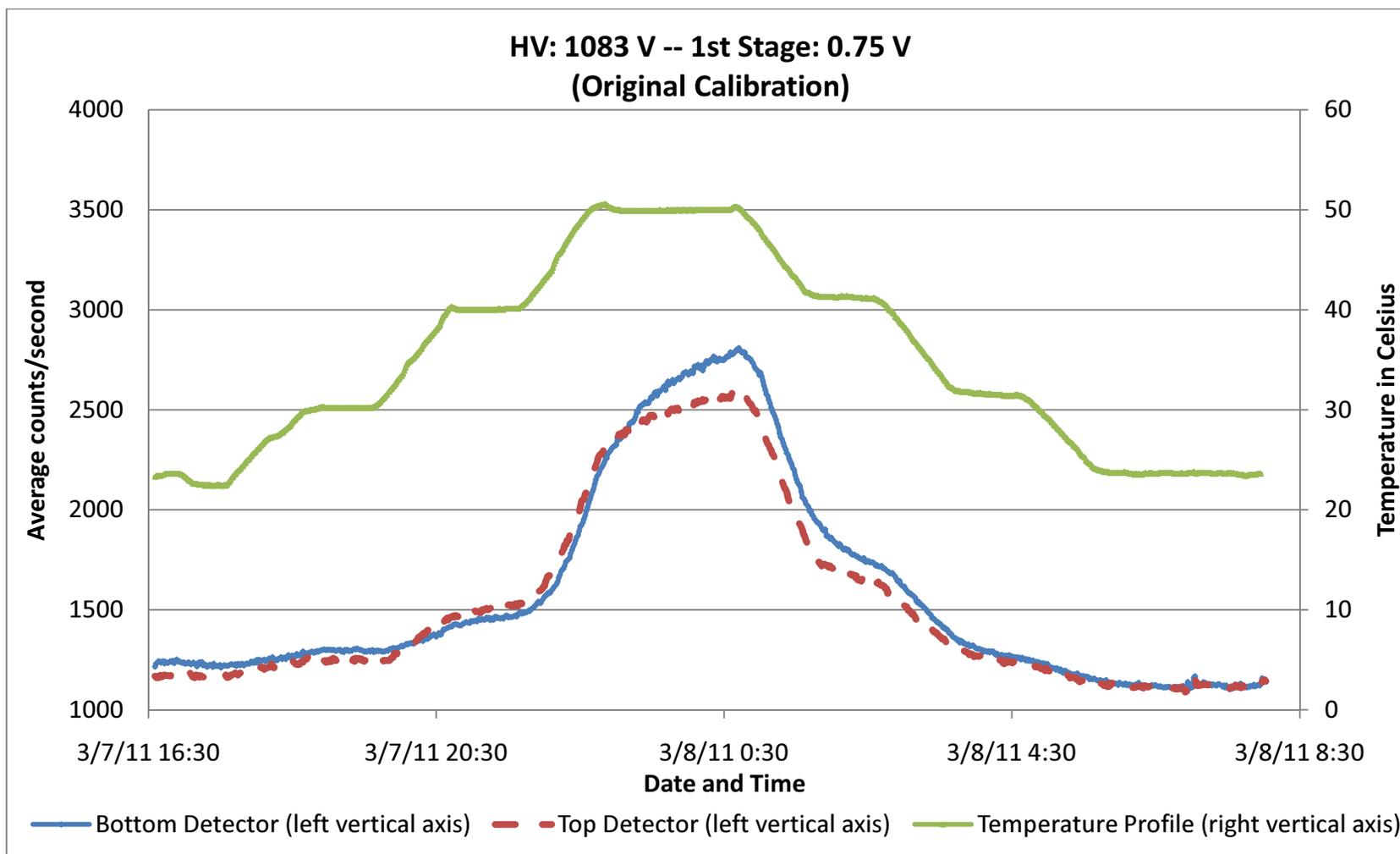
Figure 4.12: Average background count rate during the initial temperature cycle.

One additional observation from Figure 4.12 above is sthat at the end of the temperature hold at 50°C, the count rates have not leveled off but are still increasing. This suggests that the gamma detectors did not reach thermal equilibrium even after 2 hours at 50°C and that the values of the background count rate would have continued to increase if the temperature had not begun to decrease. Therefore, the fifth temperature cycle, which occurred over a weekend, utilized a much slower cycle. Using the nominal calibration procedure again, the temperature was first cycled very slowly from 22°C to 50°C and back to 22°C. The temperature then ramped back up to 50°C with five hour holds at each 10°C interval. The results from the first part of this cycle are shown in Figure 4.13, while the results for the ramp back to 50°C are shown in Figure 4.14.

Figure 4.14 clearly demonstrates that the count rate does not reach an equilibrium value during the two hour temperature hold at 50°C which was used not only in the initial cycle, but also in the other cycles completed before fifth cycle. In fact, it is clear from the figure that the count rate does not begin to level off until well into the five hour hold at each temperature interval. The results from this experiment prompted the decision to extend the temperature hold at 50°C from two hours to five hours during the cycles following this experiment.
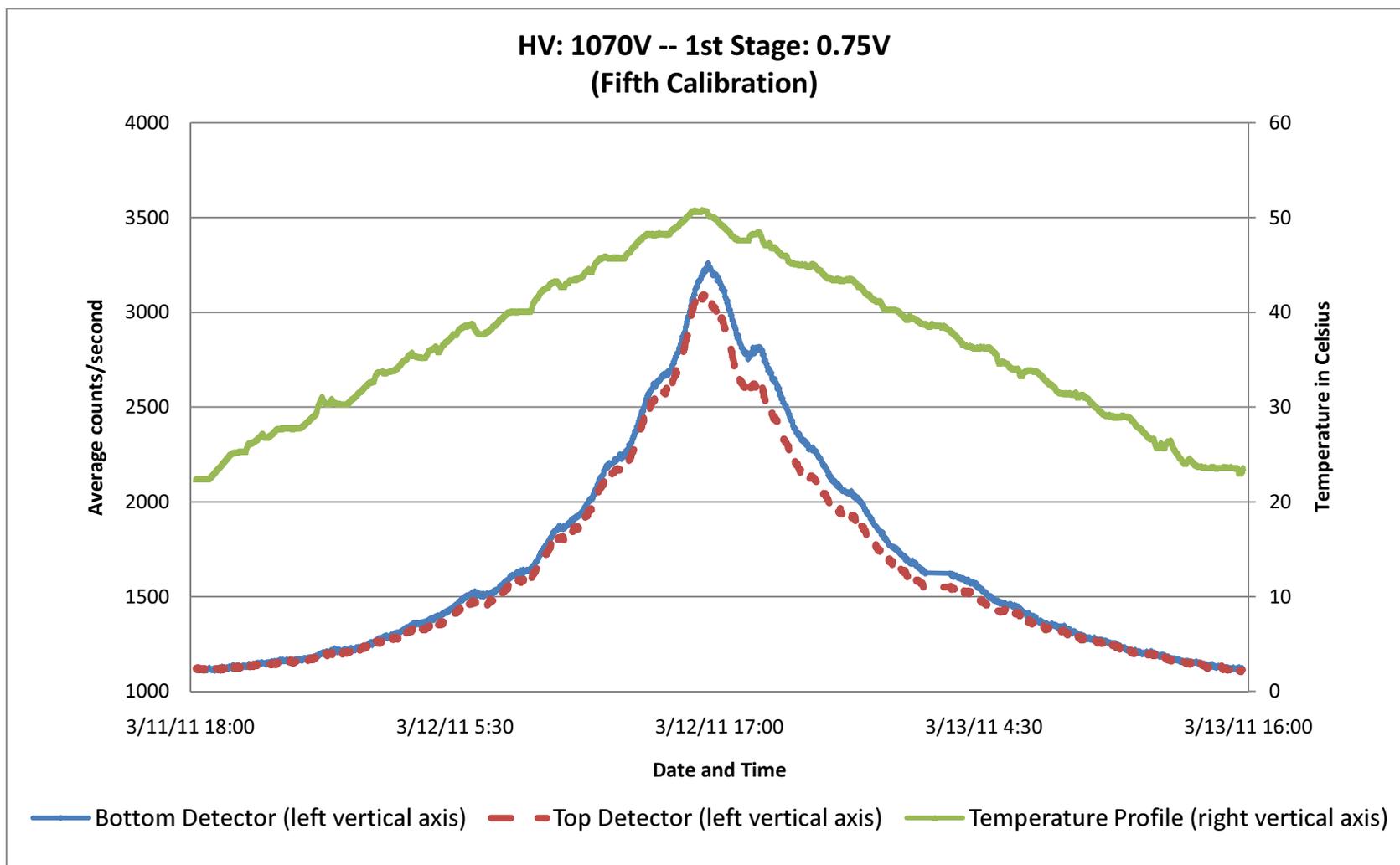
Figure 4.13: Average background count rate of the detectors during the fifth temperature cycle (first half).
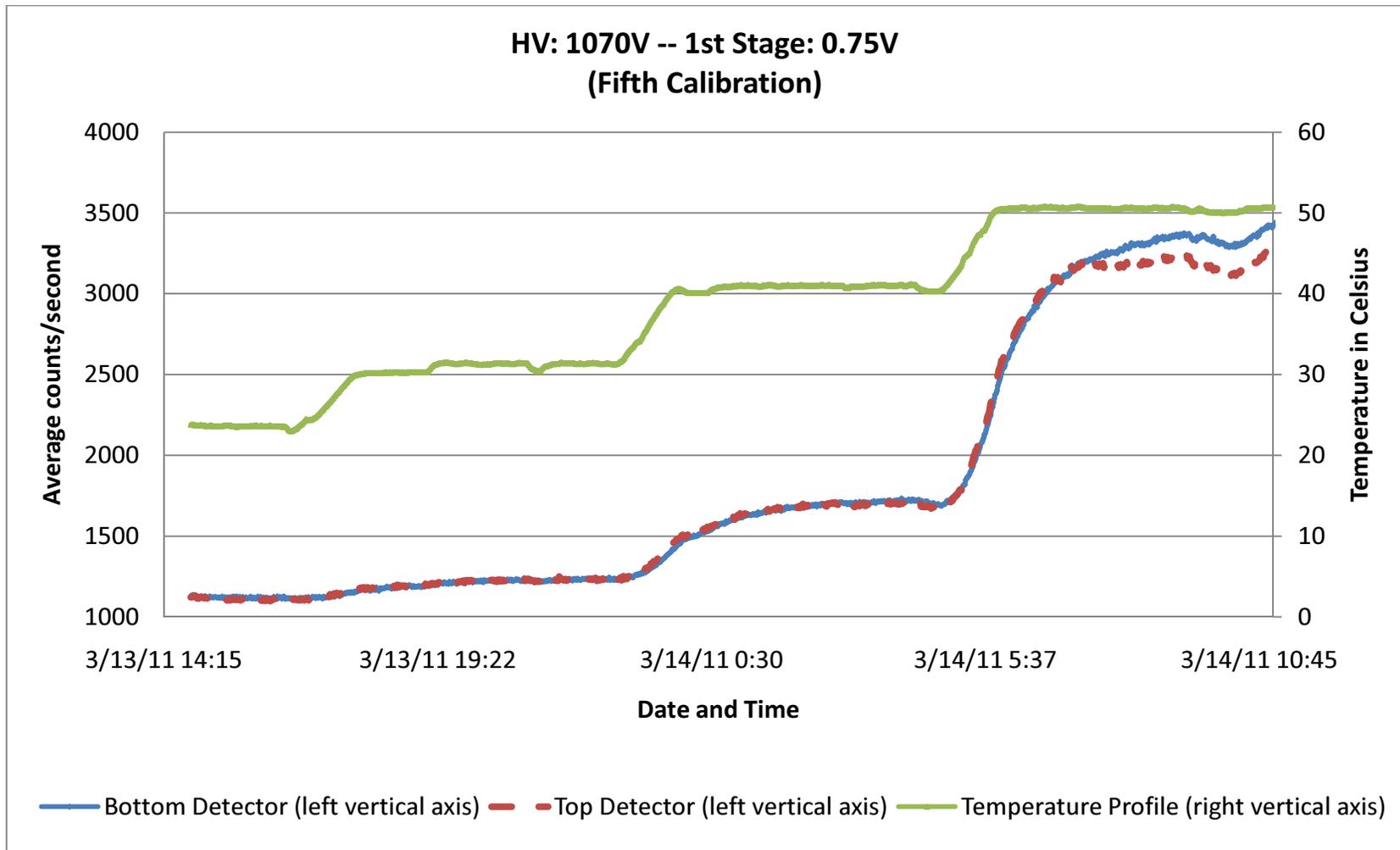
Figure 4.14: Average background count rate of the detectors during the fifth temperature cycle (second half).

The results presented in Figure 4.13 provide a detailed picture of the effect that increasing temperature has on the count rate. By increasing the temperature very slowly—at an average rate of 1°C per hour—the influence that temperature has on the background count rate is shown to be exponentially shaped. Specifically, the slow cycle shows that the rate of increase in the background count rate reaches a critical point as the temperature increases past 40°C. After this point, even the smallest fluctuation in temperature has a dramatic effect on the count rate, an effect that is clearly seen as the temperature decreases from 50°C. During this temperature decrease, the chamber temperature seems to experience a small and short-lived increase (seen as a slight bump in the curve) that results in an exaggerated spike in the background count rates for both detectors. A two-way ANOVA test showed with high confidence that each detector's count rate was dependent on both the detector characteristics and the temperature, proving the statistical significance of the data.

A closer examination of the slow increase from 22°C to 50°C in cycle five is shown in Figure 4.15. This figure shows the counts as a function of temperature during the slow increase on a log scale plot. Since the data does not form a flat line when the vertical axis is log scaled, it is clear that the count rate as a function of temperature is actually super exponential. Recalling that both Knoll (2000) and the Hamamatsu PMT handbook (2006) suggest that the PMT noise should increase exponentially in theory, the super exponential behavior of the count rate suggested that the system noise is increasing at a rate which exceeds the manufacturer's specified rate of noise production in the PMT. Therefore, this phenomenon should be reexamined by future work which explores the same procedure for a

larger sample size of gamma detectors. From this larger data set, a more generalized model

for the increase in the noise as a function of temperature could be developed.
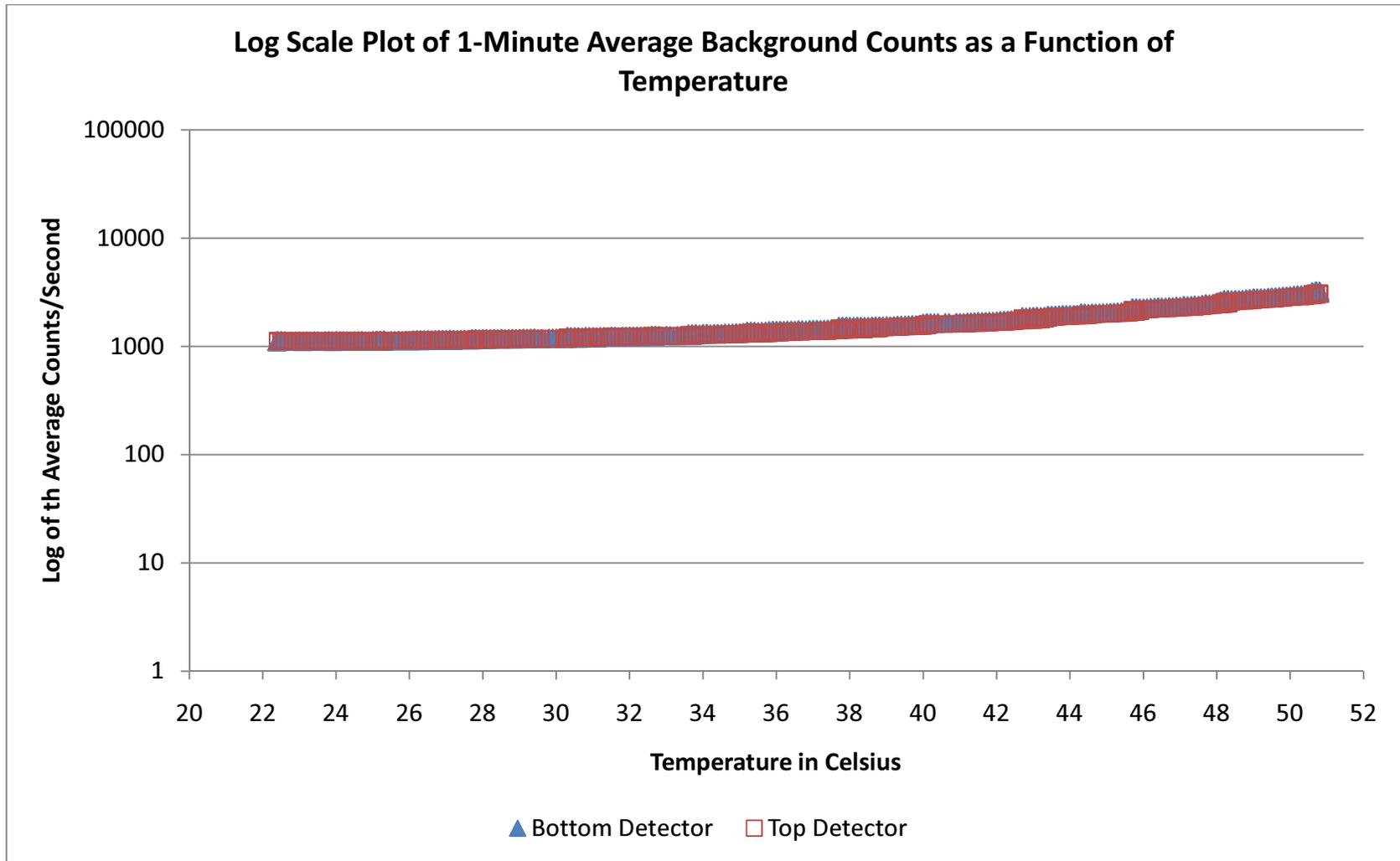
Figure 4.15: Background count rate for both detectors as a function of temperature.

4.2.2 Examination of the Effect of the SCA on the Temperature Dependence

Following the determination that the count rate oscillations observed in the field could be reproduced by varying the ambient temperature experienced by the radiation detectors, the temperature tests sought to examine the effect that the specific SCA chosen for this round of experiments had on the temperature dependence of the count rates. Specifically, this experiment explored whether the count rate oscillations were unique to the original SCA used in the initial cycle. In addition, this experiment sought to examine whether the temperature dependence of the SCA's internal electronics had any effect on the magnitude of the count rate oscillations. While an ideal testing schedule would have allowed these two hypotheses to be tested in two separate tests, time constraints dictated that these two tests be performed as one. Therefore, the original SCA was replaced by a recently purchased SCA from the same manufacturer, and the new SCA was placed in the climate chamber with the gamma detectors—meaning that the new SCA experienced the same temperature cycles as the plastic scintillators and PMTs. The results from the temperature cycle with the new SCA connected are presented in Figure 4.17 and can be compared to the cycle with the original SCA in Figure 4.16. Also, since the new SCA's temperature cycle occurred after cycle five, the temperature hold at 50°C was three hours longer than the temperature cycle for the original SCA.
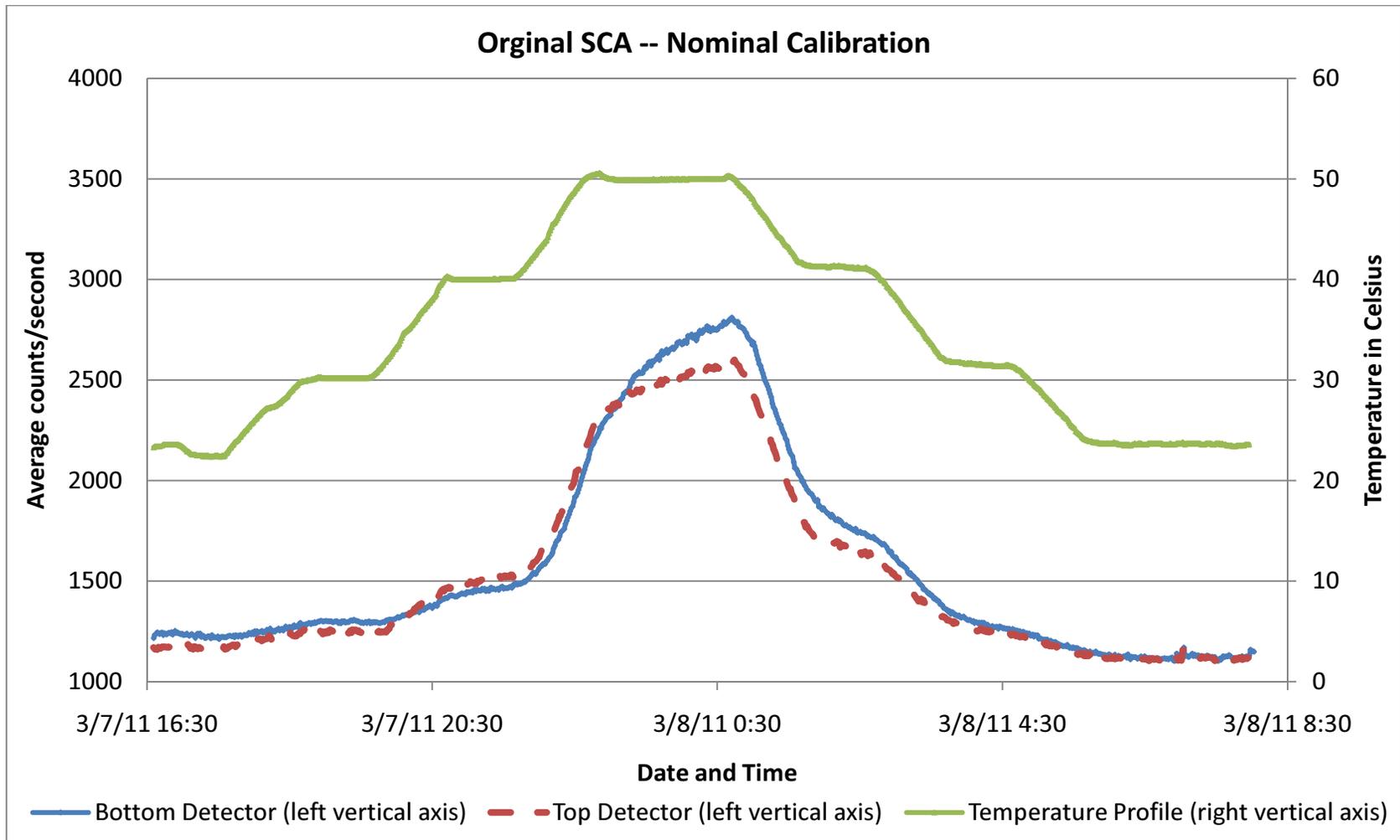
Figure 4.16: Gamma background count rates for the original SCA during temperature cycle.
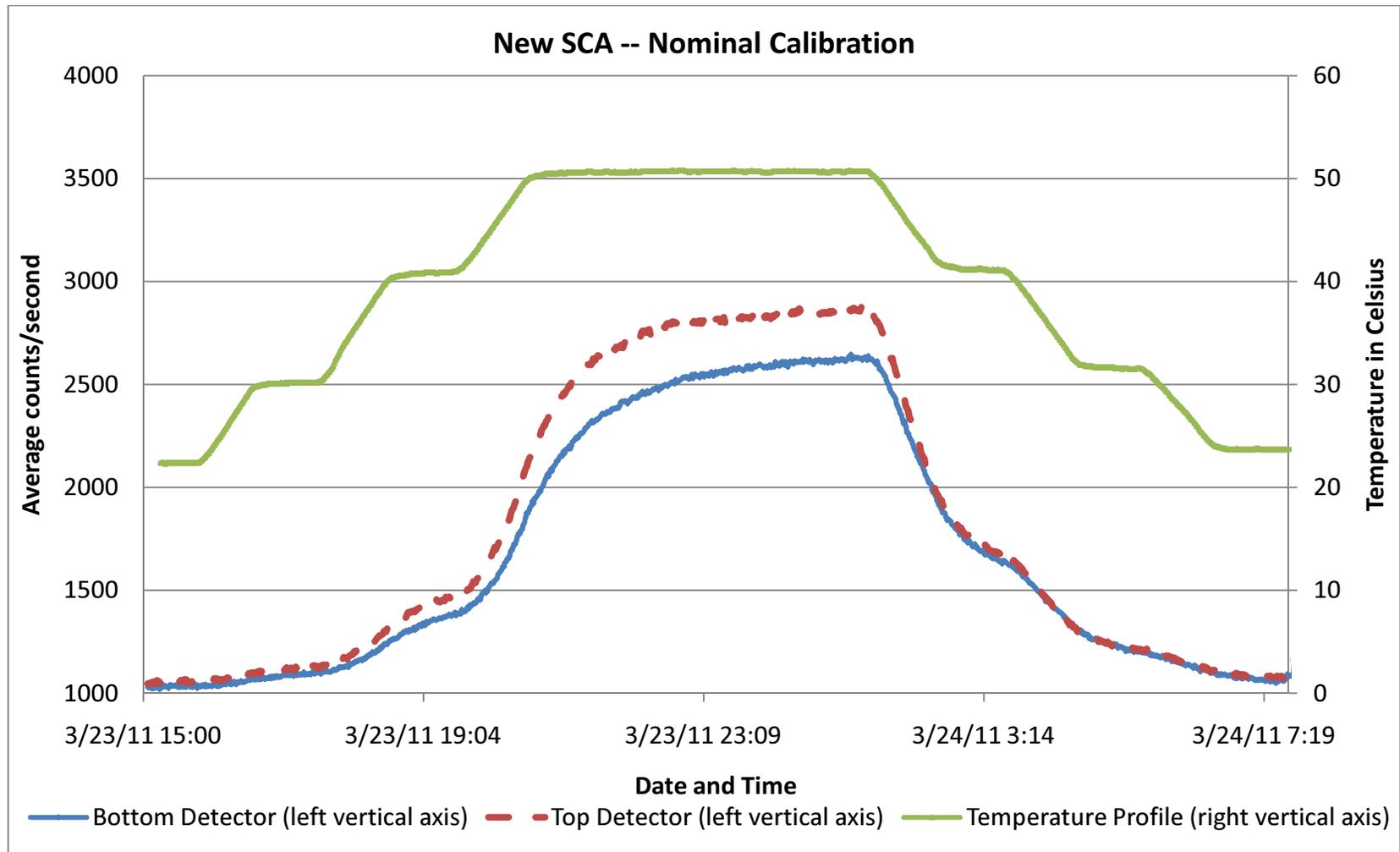
Figure 4.17: Gamma background count rates for the new SCA during temperature cycle.

A comparison of Figure 4.16 and Figure 4.17 demonstrates that the magnitude of the background count rate oscillations does not vary significantly between the two cycles. This suggests that the temperature dependence of the background count rate is not significantly affected by variations between individual SCAs or by the temperature dependence of the electronics of the manufacturer's default SCA. Furthermore, the difference in which detector exhibits the maximum increase in count rate and the differences between each detector's maximum amplitude during the two cycles are due to the inherent uncertainties in the standard calibration procedure.

Another comparison between the two cycles is shown below in Table 4.11. The table compares the minimum count rate of each detector at 22°C to the maximum count rate of each detector at 50°C for both the original SCA and the replacement SCA. Also included is the ratio of the maximum counts to the minimum counts, which quantifies the magnitude of the increases with temperature. The results in this table reiterate that there was no significant difference between the count rate oscillations for the cycle utilizing the original SCA and the cycle utilizing the replacement SCA.

Table 4.11: Results comparing the difference between cycles utilizing different SCAs.

Comparison of the Minimum and Maximum Count Rates for Old SCA versus New SCA Inside Chamber								
Calibration	HV:	Bottom Detector			Top Detector			
		22C	50C	50C to 22C Ratio	22C	50C	50C to 22C Ratio	
Original	1083	1103	2810	2.55	1089	2600	2.39	
New SCA Inside	1060	1020	2646	2.59	1043	2876	2.76	

4.2.3 Exploration of Alternative High Voltage Settings

Based on expert opinion from senior technical staff at ORNL, a series of experiments was performed in order to find an alternative high-voltage bias which would provide more temperature stability for the gamma count rates. The hypothesis that the high-voltage bias for the PMTs could affect the temperature dependent noise stems from the consensus among experts at ORNL that dark current, possibly in the form of thermionic emissions, was the cause of the increase in count rates at high temperatures. This hypothesis is consistent with some of the existing literature in the Literature Review of this work.

To test this hypothesis, temperature cycles similar to the initial cycle were repeated six times, each with a different PMT high-voltage (HV) bias. Only the PVT scintillators and the coupled PMTs were placed in the cycling temperature chamber for these tests, which is consistent with the initial cycle set-up, so that the only perturbation for each cycle was the HV setting. Each alternative HV setting was in the range of 870 V to 1300 V, and for all settings except the 1300 V setting, the second stage amplifier was aligned so that a ^{137}Cs on

the face of the detector produced a 2.0 V pulse height. By maintaining the 2.0 V pulse height, the proper energy-to-voltage ratio for nominal temperatures was ensured, and no adjustments had to be made to the discriminator settings. For the 1300 V setting, the second stage pulse height was 3.0 V, corresponding to a unity amplification of the 3.0 V first stage pulse height. Since the 3.0 V pulse height was three-halves the nominal height of 2.0 V, the LLD and ULD voltages were increased to three-halves their default values.

4.2.3.1 Reduced High Voltage Settings

Three of the alternative HV settings, specifically cycles 2, 4, and 7, represented a lower-than-nominal HV setting. This resulted in a sub-nominal pulse height coming out of the PMT, and thus a sub-optimal pulse height after the fixed gain first stage amplifier. Therefore, these settings required an increase in the amplification of the second stage amplifier in order to maintain the 2.0 V second stage pulse height for ^{137}Cs. The results for these three lower-than-nominal HV settings are shown the following: Figure 4.18 for cycle 2, Figure 4.19 for cycle 4, and Figure 4.20 for cycle 7.
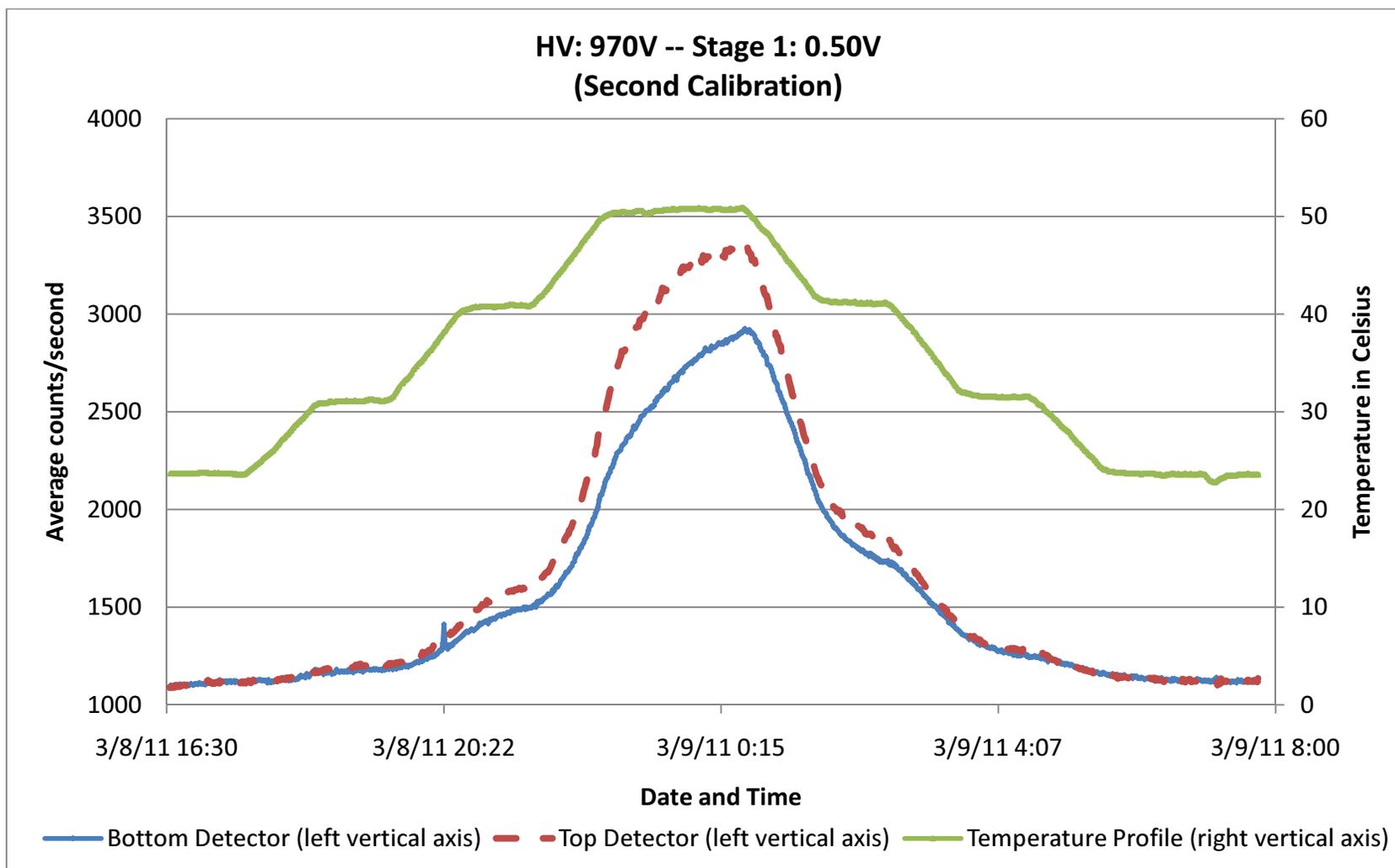
Figure 4.18: Average background count rate during the second temperature cycle.
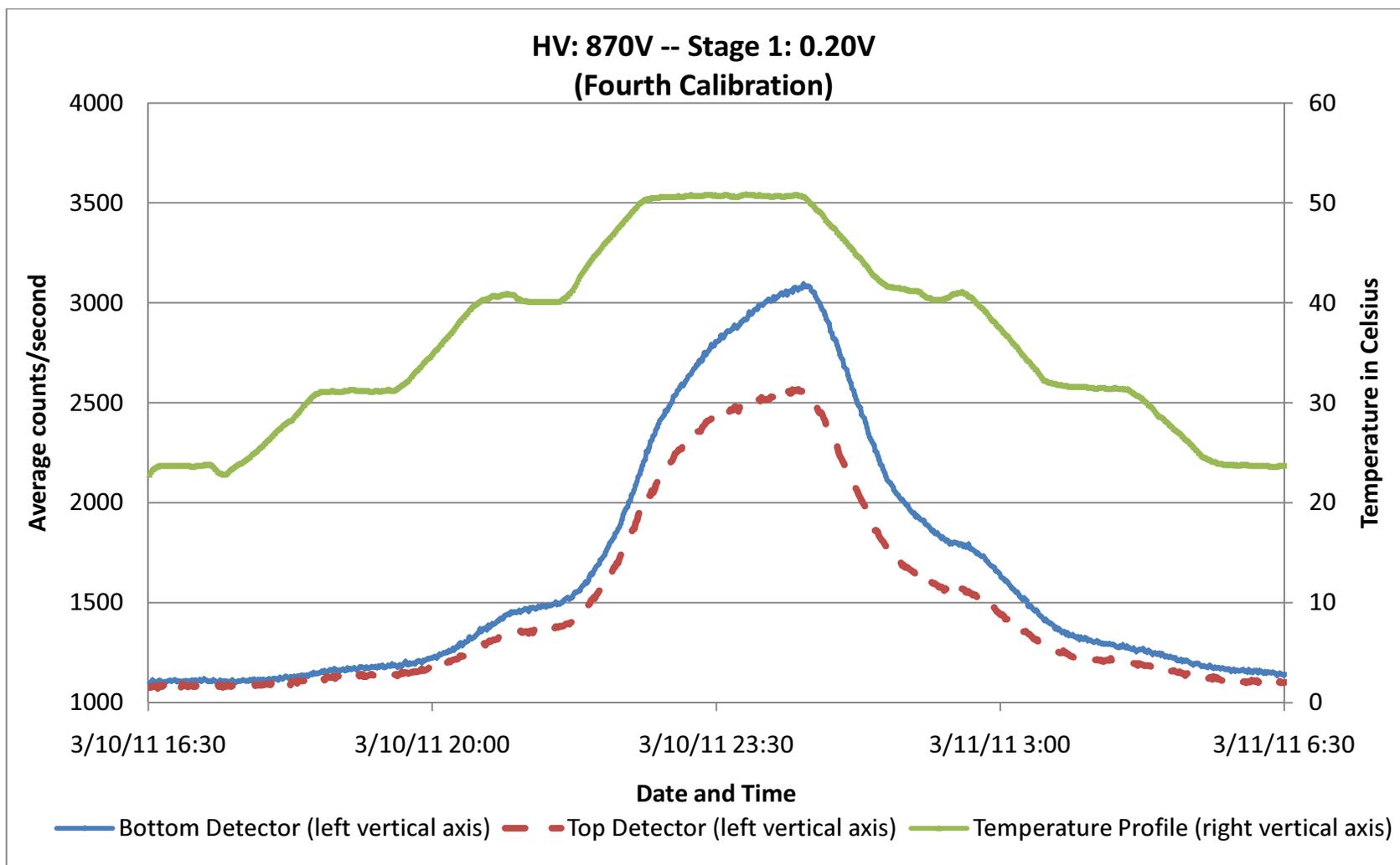
Figure 4.19: Average background count rate during the fourth temperature cycle.
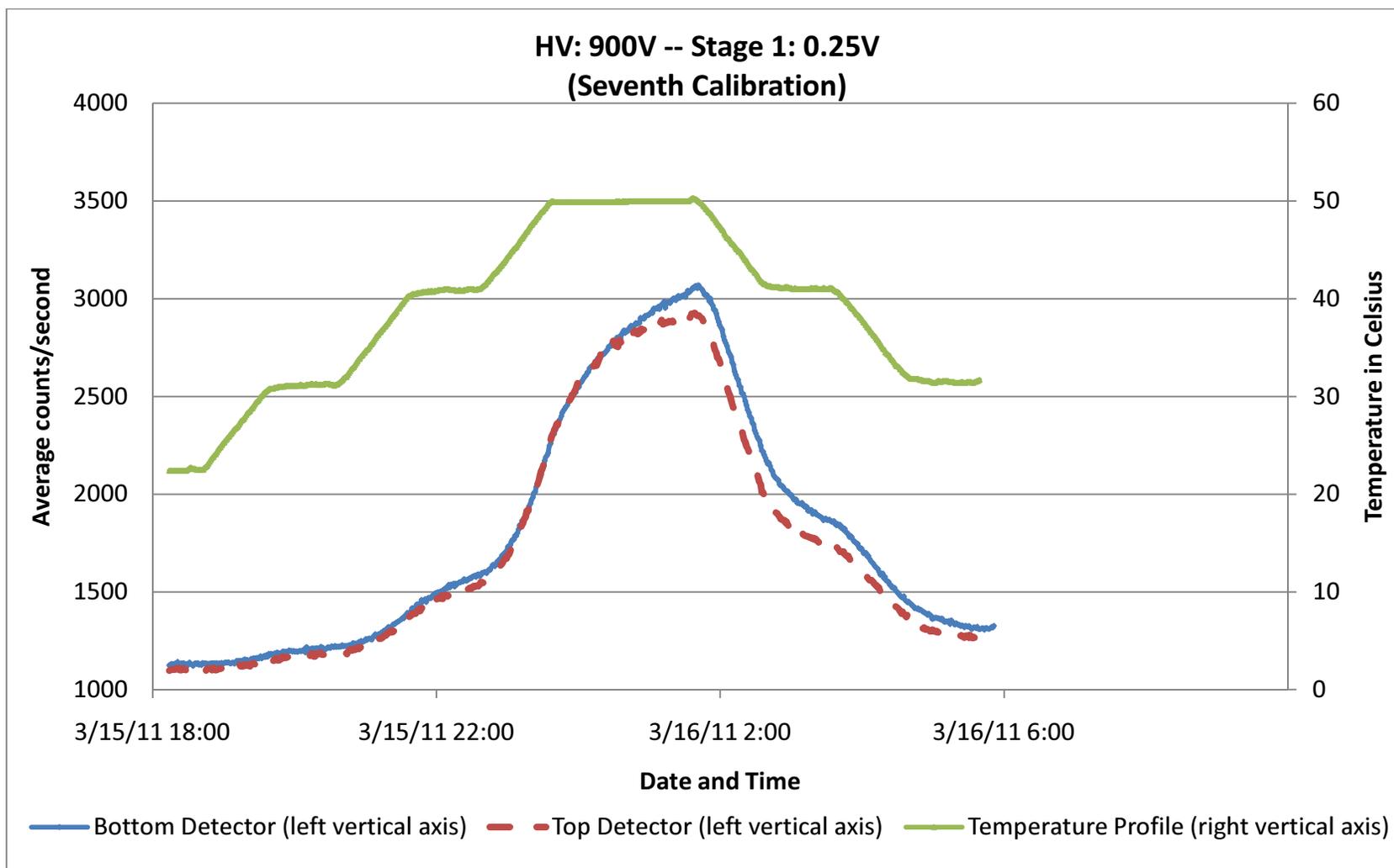
Figure 4.20: Average background count rate during the seventh temperature cycle.

The results in Figure 4.18 through Figure 4.20 reveal that no significant improvement in the temperature dependence of the background count rate was achieved by lowering the HV settings to values below nominal. In fact, it appears that the nominal setting seems to result in better performance than any of the three below-nominal HV settings. In addition, the magnitudes of the increase in background count rates at 50°C relative to the count rates at 22°C for each cycle are compared in Table 4.12. The table also includes the same information for the original cycle, along with the ratio of the maximum count rate at 50°C to the minimum count rate at 22°C for each detector. The data in Table 4.12 confirms that the nominal calibration of the original cycle resulted in the smallest ratio of maximum count rate to minimum count rate for both detectors.

Table 4.12: Comparison of the background count rate increase for the nominal HV setting to the background count rate increase for below nominal HV settings

Comparison of the Minimum and Maximum Count Rate for HV Settings Below Nominal							
		Bottom Detector			Top Detector		
Calibration	HV:	22C	50C	50C to 22C Ratio	22C	50C	50C to 22C Ratio
Original	1083	1103	2810	2.55	1089	2600	2.39
Second	970	1086	2926	2.69	1089	3355	3.08
Seventh	900	1121	3069	2.74	1097	2926	2.67
Fourth	870	1098	3095	2.82	1070	2567	2.40

4.2.3.2 Increased High Voltage Settings

In addition to exploring lower-than-nominal HV settings, two alternative HV settings were tested in cycles 3 and 6 in which the HV was increased to above the nominal value. These higher-than-nominal HV settings resulted in a first stage pulse height which was greater than the nominal 0.75 V. Therefore, the second stage amplification was decreased for these settings. For cycle 3, the second stage amplifier was set to maintain the normal 2.0 V second stage pulse height, ensuring the recommended energy-to-voltage ratio was maintained. After discussions with the expert technical staff at ORNL, it was decided that since a small HV change resulted in large gain increases, cycle 6 should be run with the HV set to 1300 V, providing a 3.0 V first stage pulse height. For this setting, the second stage amplifier was set for a unity gain and the discriminator voltages were increased by 50% to ensure the detectors were sensitive to the desired gamma energies. The results are shown for cycle 3 in Figure 4.21 and for cycle 6 in Figure 4.22.

It is clear from Figure 4.22 that the 1300 V HV setting resulted in temperature dependent count rate increases which were far worse than any other setting explored. Furthermore, it is likely that the second stage amplifier was saturated since the first stage peak pulse amplitude was 2.0 V, resulting in a distorted pulse shape. It is unclear whether the distorted pulse shape would provide true physical results. By contrast, the HV setting of 1101 V showed slightly positive results compared to the nominal setting. The magnitude of the temperature dependent count rate increase appears to have improved slightly for the bottom detector. However, this small improvement is negated by the slight exacerbation of the top detector's count rate increase.

Table 4.13 summarizes the results shown in Figure 4.21 and Figure 4.22 by comparing the maximum count rate at 50°C to the minimum count rate at 22°C. The ratio of counts at 50°C to 22°C provides insight as to the magnitude of the count rate increase as the temperature increased from 22°C to 50°C.
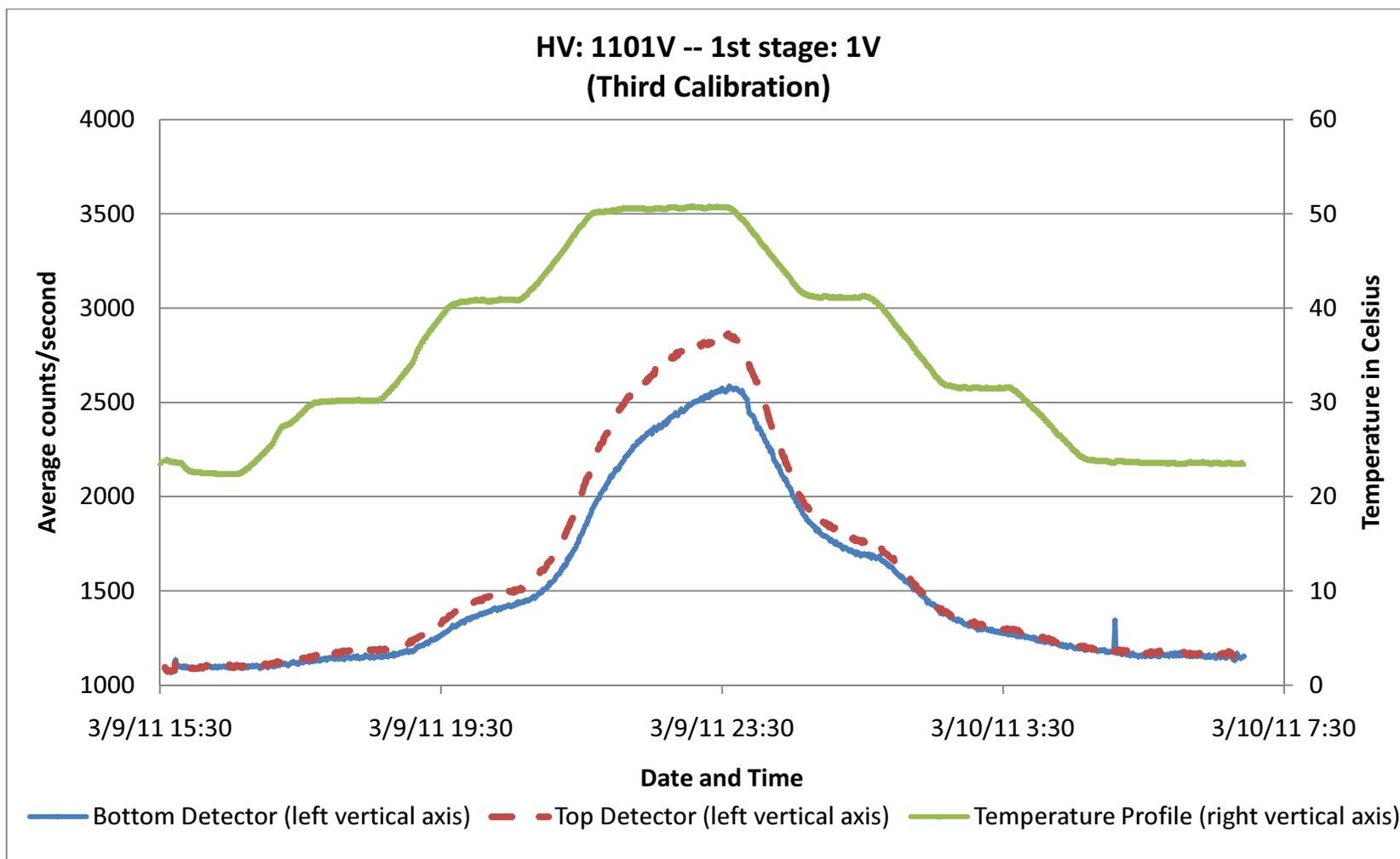
Figure 4.21: Average background count rate during the third temperature cycle.
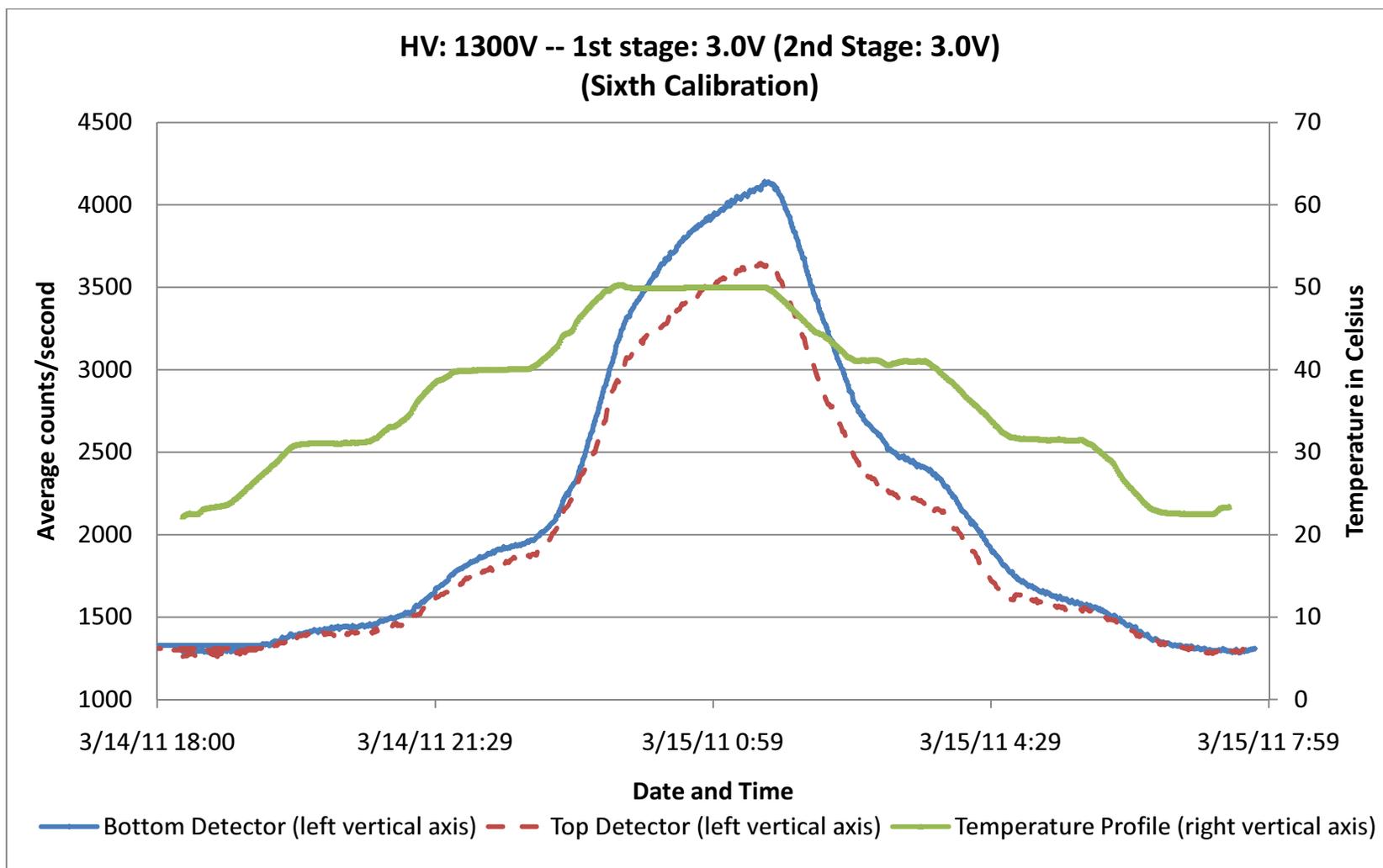
Figure 4.22: Average background count rate during the sixth temperature cycle.

Table 4.13: Comparison of the background count rate increase for the nominal HV setting to the background count rate increase for above nominal HV settings.

Comparison of the Minimum and Maximum Count Rates for HV Settings Above Nominal							
		Bottom Detector			Top Detector		
Calibration	HV:	22C	50C	50C to 22C Ratio	22C	50C	50C to 22C Ratio
Original	1083	1103	2810	2.55	1089	2600	2.39
Third	1101	1072	2586	2.41	1071	2864	2.67
Sixth	1300	1285	4141	3.22	1260	3649	2.90

The results of this section and of section 4.2.3.1 demonstrate that the high voltage setting had an inconsistent effect on the performance of the gamma detectors which were tested. In addition, the results reveal that none of the alternative high voltage settings tested provided a significant improvement in the temperature dependent count rate increases during the cycles. Following the failure to find an optimal high voltage setting which solved the temperature dependence of the count rate, the non-conventional hypothesis that the photocathode could be cleaned using an extremely high HV setting was tested. The results of this hypothesis are presented in the following section.

4.2.4 Attempt to Clear Impurities in the PMT

As discussed in the Literature Review, a known issue that can create spurious pulses in the PMT and lead to the formation of dark current is the build-up of impurities on the photocathode. In addition, since it thermionic emissions are the result of the thermal excitation of conductance electrons, it was thought that a particular noisy PMT could be the

result of an increased number of conductance electrons which were near the surface of the photocathode. After discussion with technical staff both at ORNL and the manufacturer, it was decided that a method intended to clean any impurities in the PMT would be tested. The proposed method set the HV to the maximum rated voltage (1500 V) and allowed the detectors to sit overnight at this voltage while at room temperature (22°C). By setting the voltage to the maximum rated voltage, it was hypothesized that the impurities would be driven off the surface of the photocathode by the increased voltage, and that any unusually high-energy conductance electrons which were near enough to the surface would be forced out of the photocathode. The result would be a temporary increase in the noise of the PMT during the soak, but once all or most of the impurities and over-energetic electrons were cleared from the photocathode, the PMT would be quieted.

No data was collected during this high-voltage soak. The next morning, the system was recalibrated to the nominal setting, mirroring the initial calibration. After recalibration, the typical temperature cycle used in this set of experiments was initiated. The count rates recorded during the cycle were normalized to the average count rate at 22°C and are presented in Figure 4.23. Also in Figure 4.23, the background count rates from the first cycle are presented as well, normalized to the average count rate at 22°C during the first cycle. The normalized results in the figure allow for the comparison of the count rates for both detectors, when calibrated nominally, before and after the cathode "bake" at 1500 V. The chamber temperature for both cycles is presented in the figure as well, showing that the temperatures experienced in each cycle were very similar.

The results in Figure 4.23 reveal that the increase in the background count rate as the temperature increased was worse after the detector sat overnight at 1500 V. Because the count rate still increased after sitting at 1500 V, the decision was made to stop the cycle and the data acquisition after the hold at 50°C; therefore Figure 4.23 only includes the increasing part of the temperature cycle.

A closer examination of how the detectors respond to similar increases in the high-voltage setting should be performed since the temperature dependent count rate increase was worse after the detectors were exposed to the 1500 V setting. In addition, anecdotal evidence from the field suggests that detectors which previously did not exhibit any background count oscillations were made to oscillate following a botched calibration which set the high-voltage bias well above nominal. The botched calibration resulted in an extreme increase in the background count rates for the affected detectors, but once the calibration was corrected, this behavior disappeared. Further questions for study include: Does the PMT recover from the high voltage soak and return to the same magnitude of oscillations observed before the soak? Can the background count oscillations be induced in detectors which previously did not show evidence of count rate oscillations by a similar increase in high voltage bias?
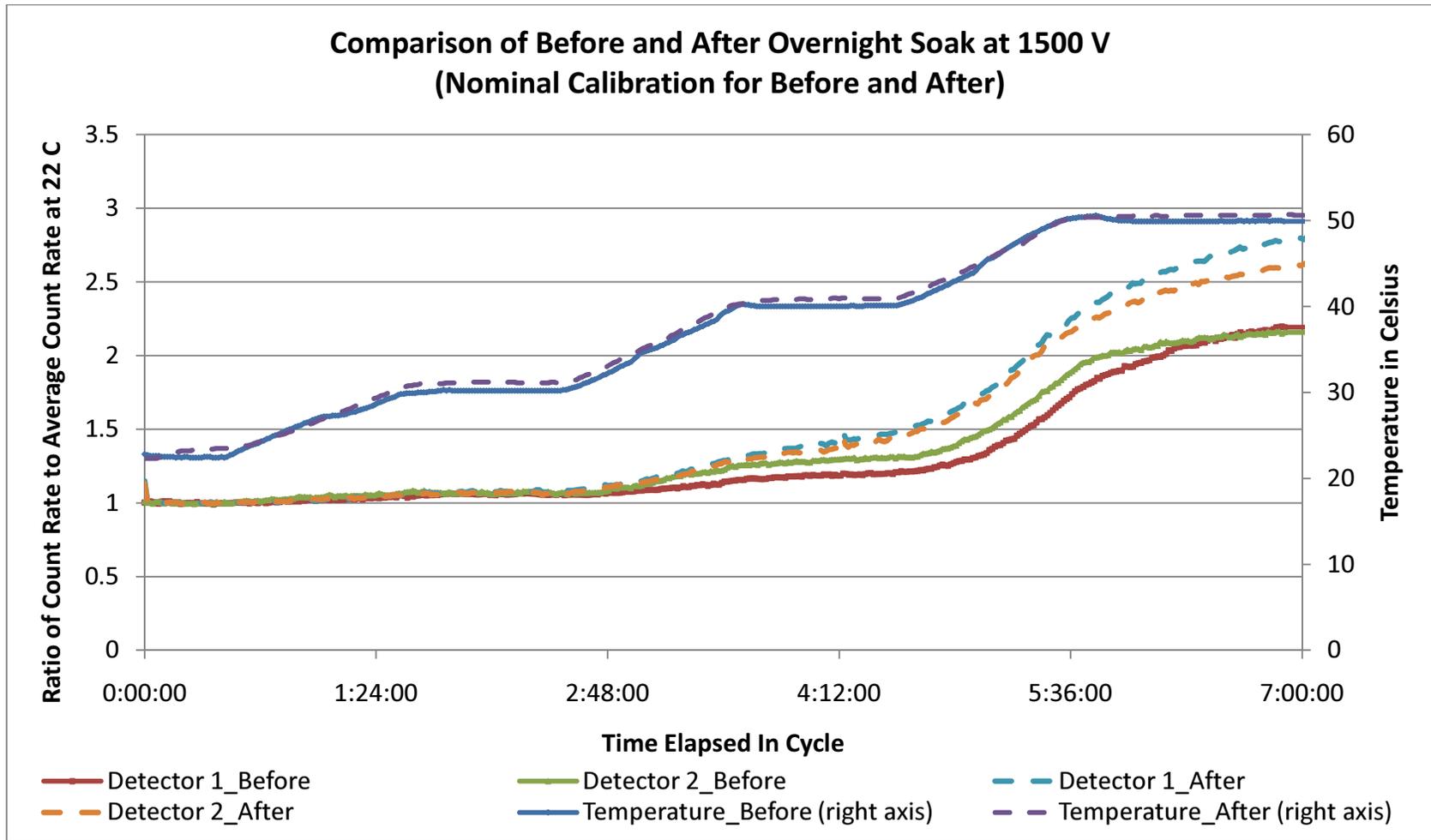
Figure 4.23: Comparison of the average count rates for both detectors before and after the HV was left at 1500V overnight. All count rates are normalized to their respective average count rate at 22°C.

4.2.5 Identification of Component Responsible for Temperature Dependence

The results of the second round of testing discussed so far determine that the cause of the temperature dependence of the background count rates was either the scintillator or its coupled PMT. In order to examine which of these two components was responsible for the temperature oscillations, it was decided that the top detector's scintillator should be removed from its coupled PMT. Before the scintillator was cut off, the system was calibrated to the factory recommended (nominal) settings. In order to maintain this calibration, the system was not powered off and no further adjustments were made after the recalibration to nominal. The top detector was then disconnected from the system, and the PVT scintillator was separated from the PMT. After the scintillator was removed, the cut-off PMT was reconnected to the system and placed in a light-tight covering inside the temperature chamber, along with the intact bottom detector. The average background count rate recorded from both the intact detector and the cut-off PMT during the typical temperature cycle used in these tests is shown in Figure 4.24.

Since the cut-off PMT was isolated from all light sources via removal of the scintillator and placement in a light-tight covering, the count rate reported from the cut-off PMT is assumed to be due to dark current which originated in the tube itself. It is clear from Figure 4.24 that both the intact detector and the cut-off PMT follow the same trend during the temperature cycle, suggesting that the temperature dependence of the gamma detector's background count rate is likely due to the temperature dependence of the PMT. The difference between the two curves in Figure 4.24 was calculated in order to provide a simplified measurement of the contribution that the PVT scintillator made to the temperature

dependent count rate oscillations. Figure 4.25 shows the results of this calculation. Figure 4.26 shows the difference between the curves during the cycle normalized to the average difference at 22°C.
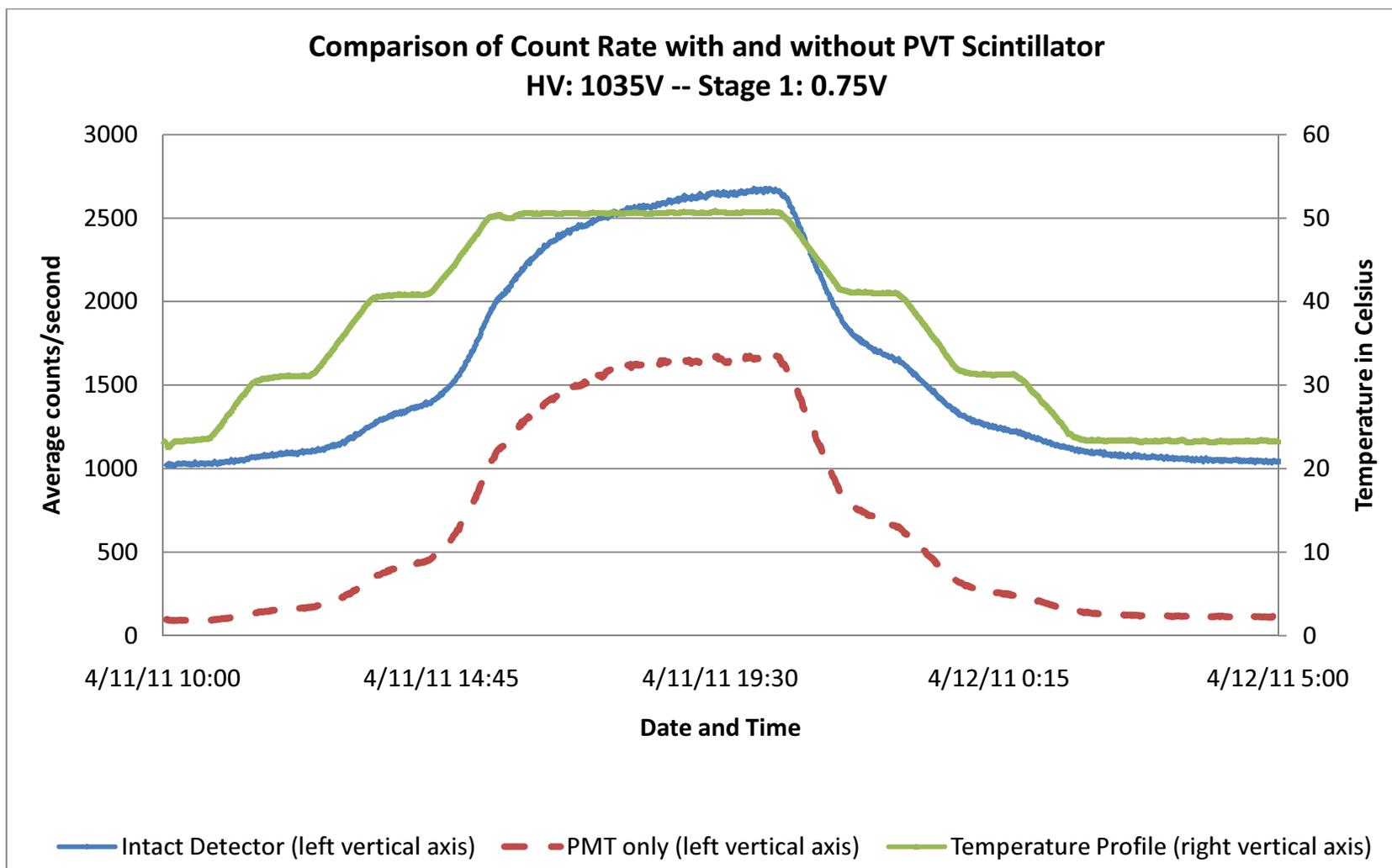
Figure 4.24: Comparison of the average background count rate for the intact detector and the PMT with no PVT scintillator.
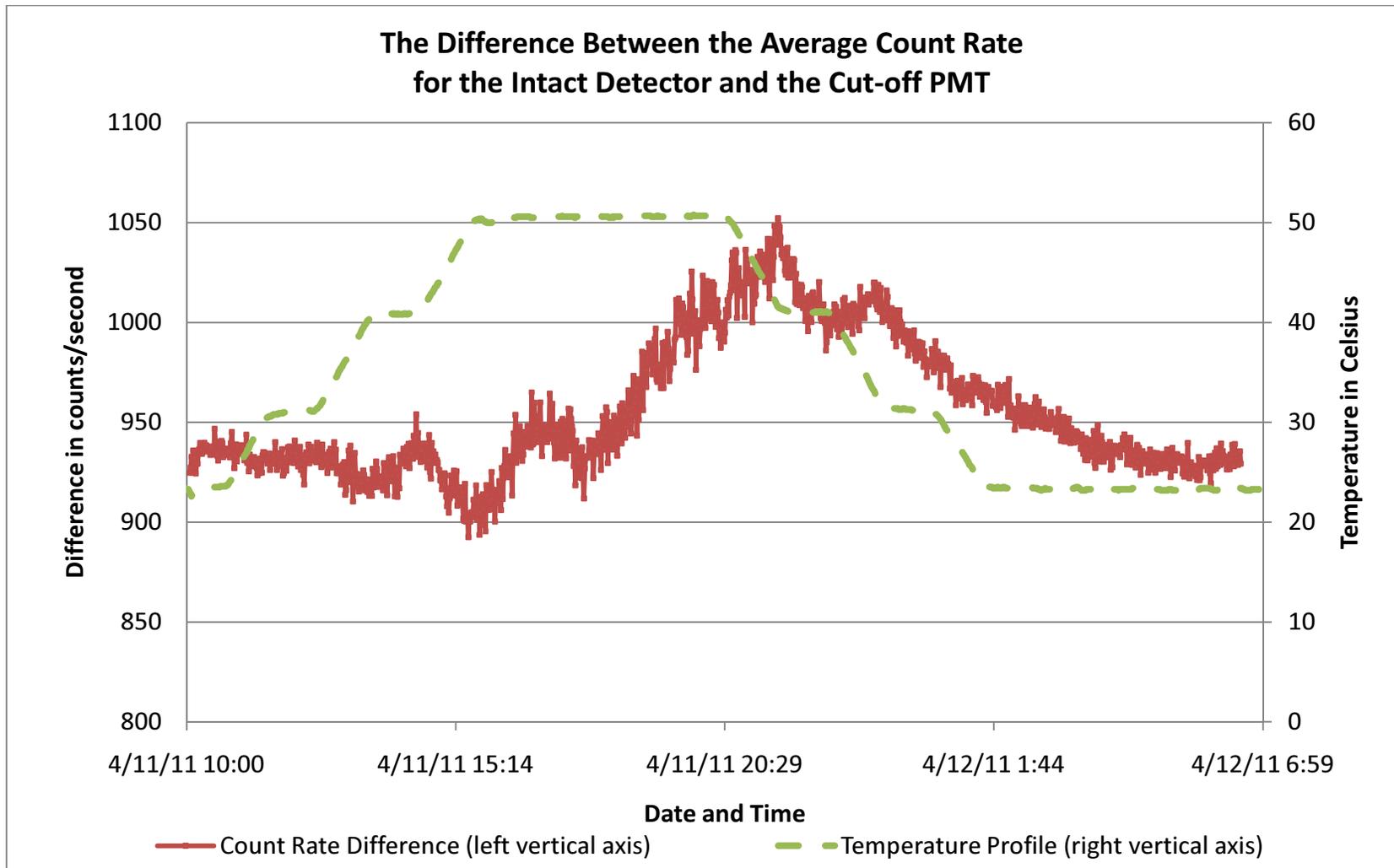
Figure 4.25: The difference in the count rate for the intact detector and the count rate for the cut-off PMT.
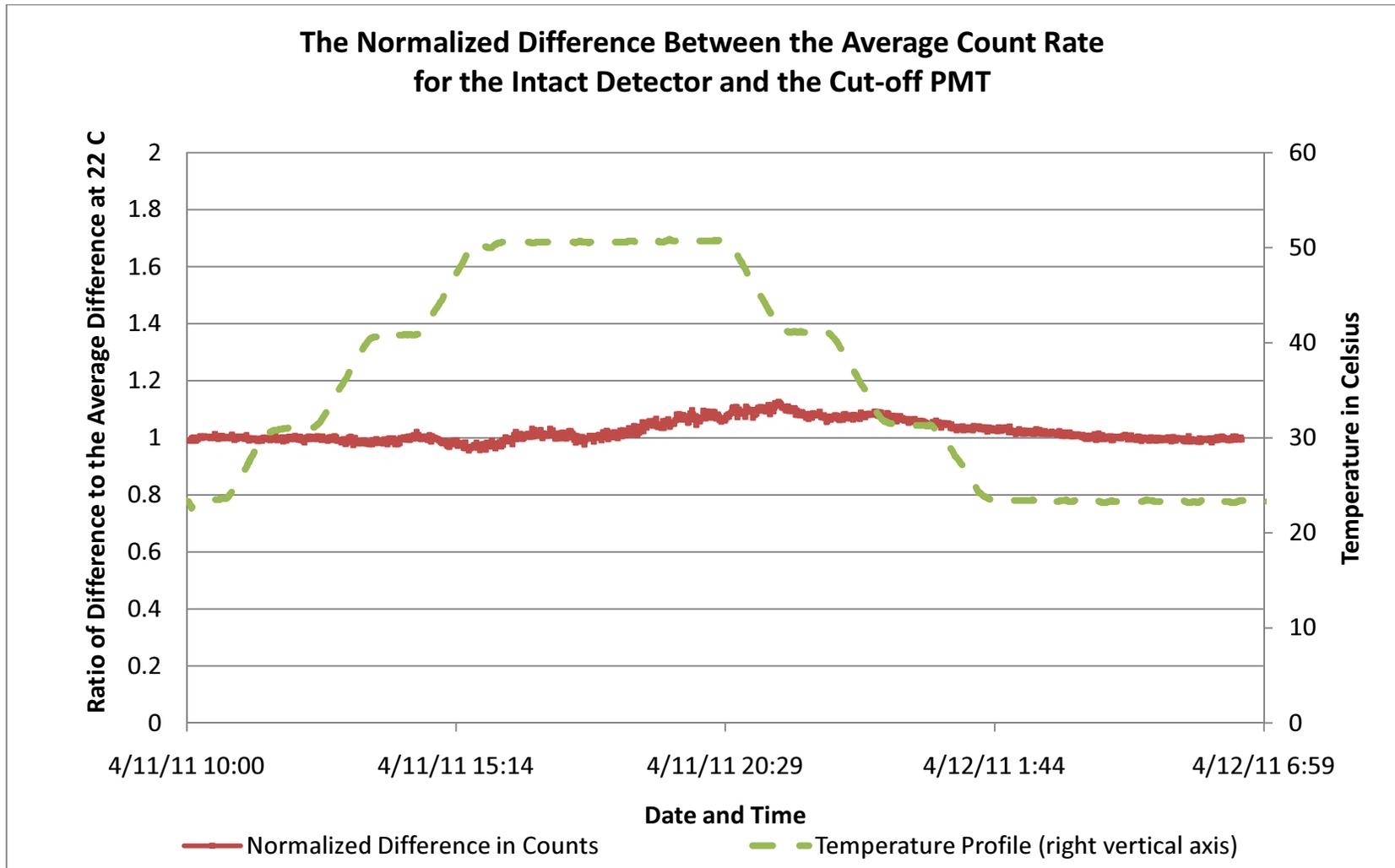
Figure 4.26: Normalized difference in the count rate for the intact detector and the count rate for the cut-off PMT.

The absolute difference between the count rate reported from the intact gamma detector and the cut-off PMT, shown in Figure 4.25, reveal that the intact gamma detector's count rate begins between 900 and 950 counts per second higher than the cut-off PMT's count rate, and eventually reaches a peak at approximately 1050 counts per second higher than the cut-off PMT's count rate. Combined with the actual count rate data for both the intact detector and the cut-off PMT which was shown in Figure 4.24, the difference in the count rate at 22°C reveals that the cut-off PMT's count rate was less than 100 counts per second at the nominal temperature. This low count rate is consistent with minimal amounts of light being able to reach the cut-off PMT inside its covering and demonstrates that any dark current creation at 22°C accounts for less than 10% of the count rate when compared to the average count rate of the intact detector at 22°C in Figure 4.24.

Furthermore, Figure 4.25 reveals that the difference between the count rates at the end of the temperature hold at 50°C is approximately 1025 counts per second. Using this difference and the average count rate data in Figure 4.24, the count rate from the PMT is approximately 62% of the count rate from the intact detector. It is a reasonable assumption that the same amount of light reached the cut-off PMT at 50°C. Therefore, this data suggests that dark current accounts for approximately 62% of the total count rate at 50°C and that the PVT scintillator accounts for only 38% of the total count rate at this temperature. The change in the percent contribution of the individual components at 22°C and 50°C is shown in Table 4.14.

Table 4.14: The PMT and scintillator's relative contributions to the expected count rate of an intact detector for 22°C and 50°C.

Chamber Temperature (°C)	PMT Contribution (%)	Scintillator Contribution (%)
22	10%	90%
50	62%	38%

The behavior of the curve in Figure 4.25 also reveals that there is a lag between when the temperature increases and when the difference between the counts begins to increase. This behavior is most evident during the temperature hold at 50°C. The difference between the count rates actually decreases as the temperature ramps up to 50°C. This decrease means that the count rate for the cut-off PMT is increasing faster as the temperature ramps up than the intact detector's count rate. However, once the system begins to hold at 50°C, the gap between the two count rates increases and continues to do so during the remainder of the hold. Furthermore, even after the soak ended and the temperature began to decrease, the difference between the count rates continued to increase. This behavior demonstrates that the count rate for the cut-off PMT reaches its maximum before the intact detector does, suggesting that the cut-off PMT reaches thermal equilibrium before the intact detector. Consistent with this conclusion, each time the temperature begins to change, the count rate of the cut-off PMT responds faster than that of the intact detector. When one considers the

mass difference between the intact detector and the PMT with no scintillator, the difference in the time to reach thermal equilibrium is a reasonable conclusion.

While the information in Figure 4.25 presents the absolute difference in the count rates and allows for analysis of the overall behavior of the difference, Figure 4.26 shows the difference in count rates normalized to the average difference between the two count rates at 22°C. By normalizing the data, the change in the absolute difference between the intact detector's count rate and the cut-off PMT's count rate as the cycle progresses can easily be compared to its initial value at 22°C since the ratio at the initial 22°C hold is equal to one. The normalized data can also be interpreted as the ratio of the count rate difference as the temperature changes to the count rate difference at 22°C. By examining this normalized data, it is clear that the peak difference in counts is about 10% higher than the difference in counts when the system is at thermal equilibrium at 22°C. This result strengthens the hypothesis that the PMT is the driving component for the temperature dependent count rate oscillations, while the PVT scintillator superimposes actual gamma counts on top of the inherent dark counts in the PMT and has little effect on the temperature dependent trends of the count rate. The result of this additive factor is a higher background count rate but one whose temperature dependent trends are dictated by the temperature dependence of the PMT.

Spectra were also collected from the cut-off PMT every 30 minutes during the test. A sampling of the spectra collected is displayed in Figure 4.27, showing the spectrum at each 10°C step as the temperature increases, during the beginning, middle, and end of the hold at 50°C, and again at each 10°C step as the temperature decreases to 22°C. One caveat for this result is that a misalignment of the MCA's lower level discriminator (LLD) appears to result

in a non-physical shape of the left edge of each spectrum. However, the spectra still provide

some important insights which are discussed after the figure.
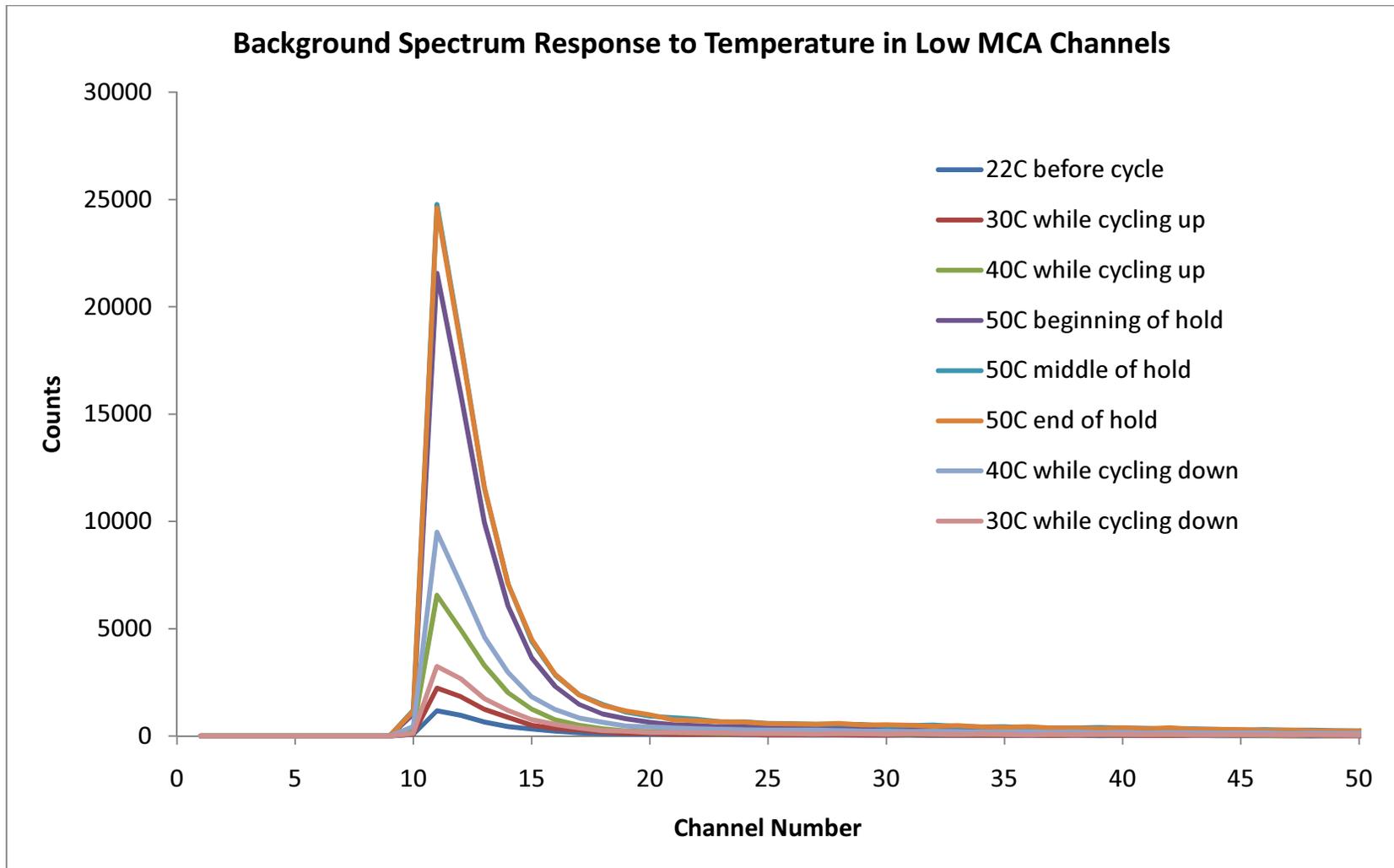
Figure 4.27: Spectra collected from the cut-off PMT as the temperature increases to 50°C, holds at 50°C, and returns to 22°C.

The results in Figure 4.27 reveal that the amplitude of the spectrum at each 10°C step rises as the temperature increases from 22°C to 50°C. Furthermore, as the temperature holds at 50°C and the PMT reaches equilibrium, the amplitude of the spectrum continues to increase. While the spectrum amplitude begins to decrease again as the temperature decreases, the spectrum at each 10°C step following the hold at 50°C has a higher amplitude than it did at the same temperature before the hold at 50°C. This is because the PMT does not have time to reach thermal equilibrium during the temperature ramps and is therefore cooler than the chamber temperature during the cycle up to 50°C and warmer than the chamber temperature during the cycle down from 50°C. The most important observation is that the change in the spectrum's counts is clearly in the low-energy channels, suggesting that the counts from the cut-off PMT are dominated by dark current due to thermionic emissions (Knoll, 2000). If the MCA's LLD had been properly aligned, it is assumed that the spectra would show real counts in channels below channel 10. However, since the right edges of the spectra are unaffected by the misalignment, it is not expected that more counts would fall in higher-energy channels. Therefore, it is a reasonable conclusion that the spectra shapes indicate the source of the increase in counts is due to a mechanism consistent with thermionic emissions.

4.2.6 Replacement of the Default SCA

An additional experiment attempted to rule out the possibility that a poor design in the manufacturer's default SCA exacerbated the temperature sensitivity of the RPM detectors by replacing the default SCA with the following Nuclear Instrumentation Module (NIM)

standard equipment: pre-amplifier, amplifier, and single-channel analyzer. Because there are

several unexplained phenomena associated with the results of this test, they are not presented

in this research and cannot be used to draw any meaningful conclusions. However, these

tests should be repeated with greater care and include the following:

a. Examination of the pulse shape using an oscilloscope to ensure that the pulse has

   physical meaning.

b. Continued examination of the pulse shape as the temperature is cycled by

   recording the oscilloscope viewing screen with a DVR or a digital camera used at

   incremental temperatures.

c. Measurement of the ^{57}Co efficiency using both the manufacturer's SCA and the

   NIM standard equipment to determine if the discriminator window is the same for

   both. If not, then find the discriminator window necessary to give efficiency

   measurements for the NIM standard equipment that are consistent with those

   measured by the manufacturer's SCA.

4.3 Summary of Results

The results presented in this research work clearly demonstrate that the performance

of PVT scintillator based gamma detectors used in common RPM systems is temperature

dependent. Specifically, it has been shown that the background count rate reported by the

RPM increases with increasing temperature. The magnitude of these increases is detector

dependent and can, in some cases, be extremely significant. Furthermore, the first set of

temperature experiments, performed on a pedestrian RPM identified the temperature

dependence of the gamma detectors' sensitivities to both ^{57}Co and ^{137}Cs, and also showed that the cause of this was temperature dependent gain shifts. Examination of spectra collected from the RPM system revealed that the gain decreases with increasing temperature, as evident in the MCA channel position of the Compton edge of ^{137}Cs. Crude models of the temperature dependent changes in the ^{57}Co efficiency and in the MCA channel position of the Compton edge of ^{137}Cs were also presented.

Follow-up experiments in the second set of temperature tests confirmed that the increases in the RPM count rates could be recreated in a separate set of PVT scintillation based gamma detectors. The new experiments revealed that the temperature dependence of the count rates becomes very significant as the ambient temperature experienced by the PVT scintillator and PMT exceeds 40°C. The second round of temperature tests also demonstrated that the gamma detectors' supporting electronics do not contribute significantly to the temperature dependence of the count rates and that there is no "operational sweet spot" for the high-voltage bias which decreases the magnitude of the count rate increases with rising temperature. Furthermore, an attempt to quiet the thermionic emissions in the PMT by soaking the tube at its maximum rated voltage was unsuccessful.

The most promising results of this research demonstrated that the PMT is most likely responsible for the temperature dependence of the RPM's gamma detectors. Furthermore, the results showed with high confidence that the increases in the count rate at high temperatures is due to temperature dependent dark current, consistent with thermionic emissions, produced in the PMT. In addition, the gain shifts identified in the first set of

temperature experiments are also consistent with known PMT responses to temperature as discussed in the Literature Review of this research work.

Chapter 5: Conclusions and Future Work

5.1 Conclusions

The experimental investigation of the effect of temperature on radiation portal monitor (RPM) performance demonstrates that the gross count detectors used in many RPM systems exhibit temperature dependent behavior. Specifically, it has been shown in this research that the recorded gamma background count rates, gamma efficiencies, and each detector's gain are all dependent on the ambient temperature of the RPM's environment. While several potential fixes for the temperature dependent RPM behavior were explored during this research, none provided an operational solution. Furthermore, this research identifies that the temperature dependence of these RPM systems exists primarily in the coupled PMT and PVT scintillator detectors and is not significantly influenced by the temperature dependence of the other electrical components of the RPM system.

It is clear from the investigation that increases in the background count rates with increasing temperature are driven by the temperature dependence of the PMT. The investigation concludes with high confidence that as the temperature of the PMT increases, the dark current created in the PMT begins to drive the increase in gamma count rates. This conclusion is consistent with existing literature discussed in the Literature Review of this research work. The result is a false elevation of the gamma background counts. Thus, since the typical RPM alarm algorithm is based on a count rate threshold above the average background count rate, the false elevation of the average background count rate leads to an increase in the source activity necessary to trigger an alarm.

Both the temperature dependence of the gamma efficiencies and the gain of the gamma detectors used in RPM systems were shown to be interrelated during this experimental study. Results presented in this research and in existing literature point to the temperature dependence of PVT scintillators and common PMTs as the cause for the efficiency and gain's dependence on temperature.

The combination of decreases in sensitivity to sources of low-energy gamma radiation, such as ^{57}Co, and increases in the background count rates as the temperature increases leads to decreased performance in the detection of special nuclear material (SNM) at high temperatures. Since detection of SNM is the primary goal in many RPM deployments, the results of these experiments help to identify a potential vulnerability in the RPM's performance in high temperature climates.

In the Introduction of this research work, three hypotheses were presented which summarized the intentions of these experiments. The discussion of the results from these experiments provides the answers to these hypotheses. Namely, the answers to the three hypotheses are as follows: the behavior of the gamma detectors is temperature dependent; the magnitude of the temperature dependence could not be decreased by operational solutions tested in this research; and the PMT is most likely the detector component which contributes the most to the temperature dependent behavior of the RPM detectors.

While this research work identifies many temperature sensitivities in the performance of RPMs, it is unable to present a solution to the temperature dependence of the system components and to the potential vulnerabilities which result from these dependencies. However, the importance of indentifying these sensitivities cannot be overlooked, and this

study offers justification for the continued exploration of the temperature dependence of the detectors' behavior. Some important questions which should be examined in future testing will be presented in the following section.

Until these questions can be addressed and more meaningful solutions to the vulnerabilities can be developed, a temporary solution which circumvents the temperature dependence is to minimize the maximum temperature experienced by the RPM detectors and particularly the PMTs. A simple implementation of this solution is to provide shade to the RPM systems. By limiting direct exposure of the sealed RPM pillars to sunlight, the amount of solar heating can be minimized. Limiting the solar heating would prevent the maximum internal temperature of the RPM pillars from exceeding that of the ambient air temperature and would cause the pillar's internal temperature to warm at a much slower rate. A more complex solution involves active cooling systems, similar to those used in many high-resolution detectors, which keep the detector at a low temperature regardless of the environmental temperature (Knoll, 2000).

While this study focuses solely on RPM systems, the results identify temperature dependent behaviors of the gamma detectors used in both these and other systems. Therefore, the results and conclusions presented in this research are applicable to many other gross-count detector systems which employ similar detection schemes.

5.2 Future Work

Some of the experiments performed for this investigation should be repeated and more thoroughly examined. In particular, the tests involving the replacement of the

manufacturer's default SCA with Nuclear Instrumentation Module (NIM) standard

equipment as discussed in section 4.2.6of the results should be reexamined. The tests

outlined at the end of that section are currently in discussion at Oak Ridge National

Laboratory (ORNL) and will potentially be explored by either the author of this research

work or by a researcher already at ORNL.

Similarly, the attempt to clean the photocathode which was discussed in 4.2.4is also

being discussed as a potential for repeat experiments. The purpose of repeating the

measurement would be to examine the effect that exposing a quiet PMT to extremely high

voltages would have on the PMTs noise level and to determine whether or not the previously

quiet PMT would become noisy after exposure to the very high voltage.

Regardless of whether or not any tests from this investigation are repeated, the results

and conclusions presented in this research work provide justification for the continued

exploration of the temperature dependent behavior of detectors used in RPM applications.

Such exploration should continue to search for an operational solution to the temperature

dependent behavior of the detectors. A promising solution involves shifting the

discriminator region to compensate for the change in the system's gain as the temperature

changes. By performing a more thorough examination of changes in the Compton edge

position with changing temperature, a more accurate equation than the one presented in this

work could be developed to identify the position of the Compton edge for a given

temperature. Using this equation and thermocouples placed inside the RPM pillars, the

Compton edge, and thus the gain of the system, could be determined as the temperature

changed during the day. The identification of the new Compton edge would determine the

new energy-to-channel and energy-to-voltage ratios. With this new energy-to-voltage ratio known, the discriminators could be adjusted to maintain sensitivity to the same range of gamma energies. The implementation of this solution would require more advanced electronics in the RPM system than those used in the system tested for this research work.

In addition, future experiments should also seek to build upon the knowledge added by this research work and to answer some of the questions left unanswered in this research. Important questions to consider in future investigations include: Operationally, why do some detectors exhibit significant temperature dependence while others do not? Can the background count oscillations be induced in detectors which previously did not show evidence of count rate oscillations? Are there any settings not explored in this study which can alleviate the oscillations in detectors which do exhibit this behavior? Can more advanced models of the detectors' behavior be developed which better predict the general response of the detectors to changing temperature, and if so, can more advanced electronics measure changes in the ambient temperature and compensate for the change in gain?

Following any repeated experiments and further investigation of the questions presented above, a more complete solution can be developed to alleviate the effect that temperature has on radiation portal monitor performance.

REFERENCES

Addington, D., Baird, K., & Chiaro, P.*Temperature test report for a pedestrian radiation portal monitor used in nuclear security applications.* (OUO No. ORNL/TM-2011/128). Oak Ridge, TN: Oak Ridge National Laboratory.

American national standard for evaluation and performance of radiation detection portal monitors for use in homeland security (2004).

Ball, W. P., Booth, R., & Macgregor, M. (1957). Temperature coefficients of scintillating systems. *Nuclear Instruments, 1*(2), 71-74. doi:DOI: 10.1016/0369-643X(57)90052-X

Ely, J., Kouzes, R., Schweppe, J., Siciliano, E., Strachan, D., & Weier, D. (2006). The use of energy windowing to discriminate SNM from NORM in radiation portal monitors. *Nuclear Instruments and Methods in Physics Research Section A: Accelerators, Spectrometers, Detectors and Associated Equipment, 560*(2), 373-387. doi:DOI: 10.1016/j.nima.2006.01.053

Fehlau, P. E. (1987). *An applications guide to pedestrian SNM monitors.* No. LA-10912-MS). Los Alamos, NM: Los Alamos National Laboratory.

Hamamatsu. (2006). *Photomultiplier tubes: Basics and Applications* (Third ed.) Hamamatsu Photonics K.K., Electronic Tube Division.

Kawada, Y., Ito, J., & Wang, Q. (2004). Temperature dependence of spurious pulses in use of plastic scintillation detectors. *Applied Radiation and Isotopes, 60*(2-4), 403-407. doi:DOI: 10.1016/j.apradiso.2003.11.049

Kinard, F. E. (1957). Temperature dependence of photomultiplier gain. *Nucleonics, 15*(Number 4), 92-92-97.

Knoll, G. F. (2000). *Radiation detection and measurement / glenn F. knoll*. New York: J. Wiley. Retrieved from http://www2.lib.ncsu.edu/catalog/record/DUKE002686169

Kouzes, R. T., Ely, J. H., Milbrath, B. D., Schweppe, J. E., Siciliano, E. R., & Stromswold, D. C. (2005). Spectroscopic and non-spectroscopic radiation portal applications to border security. Paper presented at the *Nuclear Science Symposium Conference Record, 2005 IEEE, , 1* 321-325.

Kouzes, R. T., Siciliano, E. R., Ely, J. H., Keller, P. E., & McConn, R. J. (2008). Passive neutron detection for interdiction of nuclear material at borders. *Nuclear Instruments and Methods in Physics Research Section A: Accelerators, Spectrometers, Detectors and Associated Equipment, 584*(2-3), 383-400. doi:DOI: 10.1016/j.nima.2007.10.026

Leo, W. R., 1948-. (1994). *Techniques for nuclear and particle physics experiments : A how-to approach*. Berlin ; New York: Springer. Retrieved from http://www2.lib.ncsu.edu/catalog/record/DUKE001850973

Pausch, G., Stein, J., & Teofilov, N. (2005). Stabilizing scintillation detector systems by

    exploiting the temperature dependence of the light pulse decay time. *Nuclear Science,*

    IEEE Transactions on, 52(5), 1849-1855.

Siciliano, E. R., Ely, J. H., Kouzes, R. T., Milbrath, B. D., Schweppe, J. E., & Stromswold,

    D. C. (2005). Comparison of PVT and NaI(tl) scintillators for vehicle portal monitor

    applications. *Nuclear Instruments and Methods in Physics Research Section A:*

    Accelerators, Spectrometers, Detectors and Associated Equipment, 550(3), 647-674.

    doi:DOI: 10.1016/j.nima.2005.05.056

Singh, A. S., & Wright, A. G. (1987). The determination of photomultiplier temperature

    coefficients for gain and spectral sensitivity using the photon counting technique.

    Nuclear Science, IEEE Transactions on, 34(1), 434-437.

Wahl, C. G., Alderson, D., & Pibida, L. (2007). Studies for software optimization for gross

    counting portal monitors. *Nuclear Instruments and Methods in Physics Research*

    Section A: Accelerators, Spectrometers, Detectors and Associated Equipment, 574(1),

    185-191. doi:DOI: 10.1016/j.nima.2007.01.165